Neurological Modelling of the Vision System with Relevance to an Application for Improved Detection of Early Breast Cancer

Thesis submitted for the degree of

Doctor of Philosophy

By

Elysia Thornton-Benko BSc (Biol/Maths) MB BS (Hons)

Faculty of Science

University of Technology, Sydney

January, 2005

Engineers often view the eye as a kind of television camera with a certain bandwidth and dynamic range. Conversely, it is more natural for a biologist to see the visual system as an active synthesiser of the world we see. . . The visual system is dedicated to synthesising a world from inchoate patterns of light that reach the retina. Its ability to find order in a multitude of perceptual dimensions does, indeed, sometimes seem magical.

Friedhoff & Kiely

Computer Graphics World 1990

Certificate of Authorship / Originality

I certify that the work in this thesis has not previously been submitted for a degree nor has it been submitted as part of requirements for a degree except as fully acknowledged within the text.

I also certify that the thesis has been written by me. Any help that I have received in my research work and the preparation of the thesis itself has been acknowledged. In addition, I certify that all information sources and literature used are indicated in the thesis.

Signature of Candidate

Production Note:
Signature removed prior to publication.

ACKNOWLEDGEMENTS

As with any PhD, a variety of people have contributed in some way whether it be providing necessary equipment, offering helpful suggestions, aiding with subject specific specialty knowledge. I feel honoured to have worked with many experienced people during this project and sincerely thank you all. Special mention must be made for the following:-

Professor Hung Nguyen, Principal Supervisor, provided the computer system, program and servo for the computer controlled polaroid motion in the experimental system and gave valuable information and references from his previous experience in microcalcification studies and computer based methods of assessment.

Associate Professor Loraine Holley, Co-Supervisor, provided important advice on experimental design and procedures, especially in regard to the methods for observers in the first and second series of observer trials. Her careful attention to project details was greatly appreciated.

Dr Arthur Hung as a Co-Supervisor externally, devoted considerable time assisting with computer programming for the model as well as assistance in the early years of the project regarding microcalcification characteristics and imaging. His statistical expertise was very valuable in the assessment of the experimental results.

The writer thanks all three supervisors for their patience and encouragement during the project especially towards the final stages while working full time as a hospital medical doctor.

The sets of unidentified mammograms for our tests were provided by Breast Screen NSW – Western Sydney, courtesy of Dr Warwick Lee, Deputy Chief Radiologist.

Mr Philip Ciddor, a Principal Research Officer at the National Measurement Laboratory, CSIRO, provided sets of polaroid sheets for use in the experimental system and also provided several reference papers on optical matters.

Dr Thomas Lee, Department of Statistics, University of Chicago, provided results from his program for segmentation for some of our microcalcification deposits in the initial stages of our study of calcifications.

Mr Paul Newman, a Project Manager with the National Health and Medical Research Council (NHMRC), Clinical Trials Unit, University of Sydney, provided helpful information on some practical aspects of trials in relation to the project.

Thanks are also due to the two groups of observers who gave their time generously for the sequences of experiments involved in the tests conducted in the Biomedical Laboratory at the University of Technology, Sydney (UTS). The cooperation from Mr Geoff Stockton in the Department of Physics (UTS) in obtaining the spectral data plots for the colour filters tested at several stages is appreciated. The writer also thanks Dr Peter Petocz of the School of Mathematical Sciences (UTS) for his interest in the experimental results and additional statistical calculations which may be avenues for future work.

In addition much thanks goes to Fae Thornton for greatly assisting with the typing of the thesis as well as to Em. Professor Barry Thornton for his experience, support and guidance from the commencement of the project and especially later with regards to the mathematical modelling. I also am grateful to my husband Ivan Benko for his support and encouragement.

TABLE OF CONTENTS

Structure and Flowchart

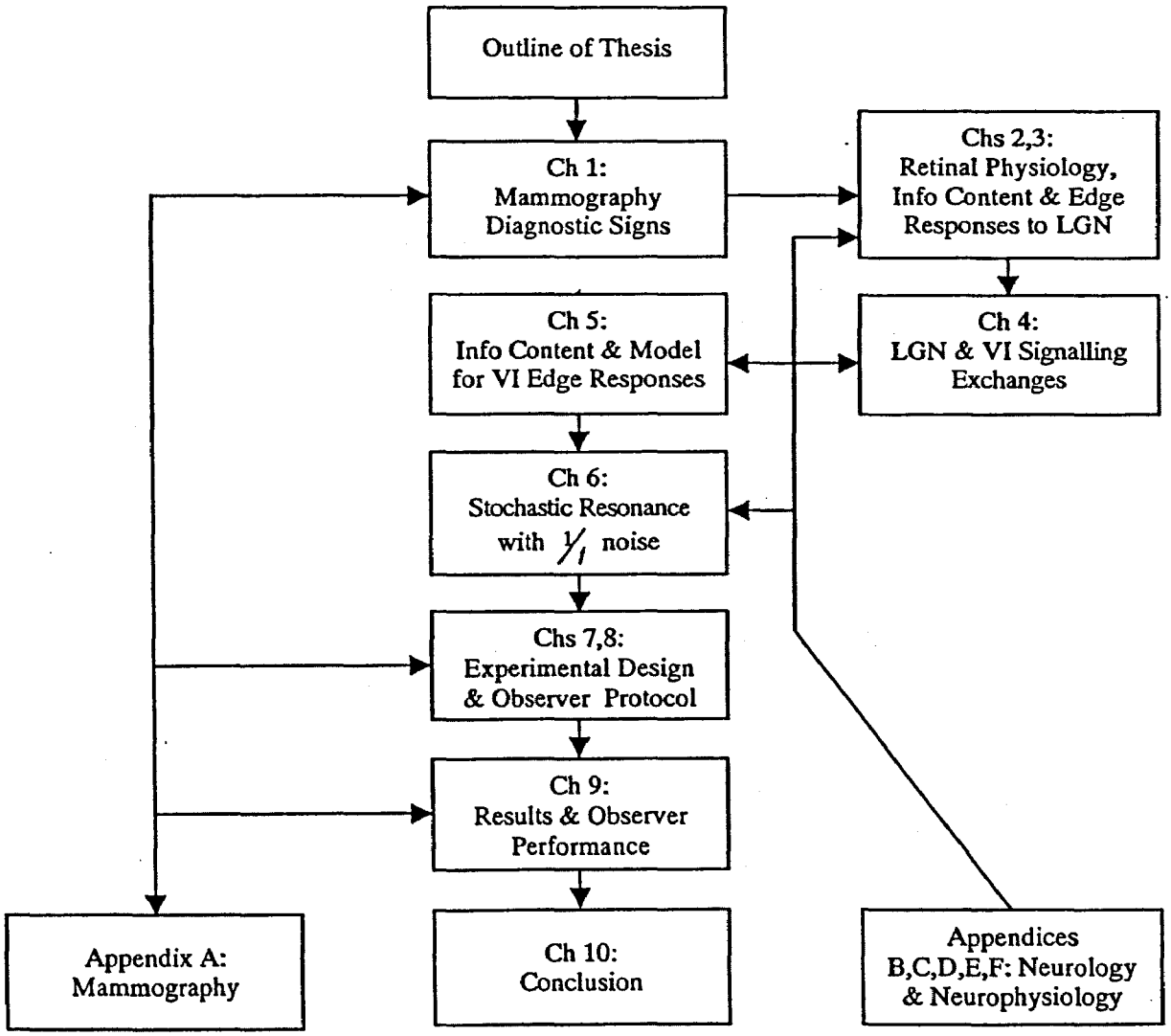

LIST OF FIGURES AND ACKNOWLEDGEMENT OF SOURCES

Figures are listed below together with acknowledgement of sources (shown in brackets when obtained from the publications in the Reference List in the thesis. The sources are also acknowledged on the Figures themselves).

Note Regarding Figures in the Chapters
There is a large number of figures in this thesis. To avoid discontinuity in reading the text, the figures are placed at the end of each chapter.

LIST OF TABLES

ABSTRACT

Detection and recognition of early signs of breast cancer when represented by cancer-related types of microcalcifications, are key requirements in breast screening mammography. Edge detection plays a vital role not only in observing detail in lesions with microcalcifications but also for the perception of often weakly defined stellate tumours. Mammograms are read at around 60 to 80 per hour.

We develop a neurological based functional model for edge responses of on-centre (C_L) and off-centre (C_D) groups of neurons in the early vision physiology, from the retina to the striate visual cortex V1. It is shown that the responses of the resulting differential equations at the retina and at V1 are of the Lotka-Volterra (LV) type. They display two important properties: consistency with the retinotopic property of early vision physiology and susceptibility to the $1/f$ type noise for a stochastic resonance (SR) effect on the edge responses based on C_L and C_D interactions. Computer simulations of repeated cycles of the LV responses when $1/f$ noise was incorporated into the interaction terms of the equations, showed an increased probability of occurrences of closely coupled small values of C_L and C_D. This indicated an underlying stochastic resonance effect. Such occurrences suggested a method for improved edge detection for "low observables" and improved detail in microcalcification regions in mammograms.

An experimental viewing system using a dynamic polaroid and eyepieces with colour filters was developed to provide $1/f$ noise to test this hypothesis. It provided for the resulting C_L and C_D inputs from the left and right eye of an observer to interact in the V1 laminae. Using a set of 30 microcalcification region of interest images, tests were conducted in real-time readings with five observers, each at two different times. There was double blind randomisation of the sequence of images in addition to the order of presentation of "with" and "without noise". The experience levels of the observers ranged from a low level working with technical images (not mammograms) to a high level experienced radiologist. An initial series of 300 observations using ratings of detail

quality (1 to 5) showed significance for an improved effect $(p<0.05)$. A second series of 300 observations for a more stringent test with improved symmetrical experimental design of the equipment and alternative-forced-choice for observers to reduce subjectivity, showed a "trend to significance" $(p<0.1)$. Observers with more experience had better performance in the tests $(p\sim0.07)$. Intra-observer variability was consistently good compared with inter-observer results. A parameter in the L-V equations which is related to observer attention, coupled with a spatial search requirement, may be part of the inter-observer variability. The findings also have implications for the training of radiologists in reading mammograms in real-time screening. Recent developments in spectral properties of photonics materials may provide a simple implementation of the principles developed in the thesis.

Brief Outline of Thesis and its Significance

The project deals with the early signs of breast cancer (details in lesions) with relevance to their visual detection in the breast screening process. Mammograms from screening are typically read at 60 to 80 per hour. Because only about 0.5% of these cases will have breast cancer, care and experience is required to find the often subtle indications of malignancy on a mammogram. Depending on the various data sources somewhere between 5% and 30% of women who do have breast cancer and have a mammogram are diagnosed as normal. Therefore any aid for detection of detail in real-time would be desirable. We develop a model for edge responses which allows us to test the ability of stochastic resonance to improve detection of stealthy edges and image details. Since microcalcifications are considered the earliest visible, non palpable features in nearly 25% of mammograms, attention will be given to them for our observer tests.. Also such deposits are easier to see than early stellate tumours by inexperienced observers used in our test for improvement of detail in lesions. Although only about 15% of cancers are detected solely on the basis of microcalcifications, other cases which are biopsied often exhibit microcalcifications which were not detected on initial screening. (This can relate to the extent of surgical margin required). Microcalcifications (Fig 1) are byproducts of a lesion and are "signs" in detection whereas masses need direct detection. The model developed for improving the visual detection by adding a type of noise can apply to both since both involve the need for acutance and acuity for recognition of edges and detail in real-time breast screening. In mammography, contrasts are inherently low due to small differences in the X-ray attenuation coefficients.

The thesis begins with an introduction to breast screening mammography and the nature and properties of microcalcifications which are used by radiologists when searching a mammogram. A good review of detection of microcalcifications is by Nishikawa (2002). We then proceed to the problem of actual edge detection. A seminal paper on the theory of edge detection by Marr & Hildreth (1980) developed a mathematical expression (not a model) to represent the "Mexican Hat" shaped response of an edge in the visual cortex

(Fig 2). They briefly commented on neurological and psychophysical implications but it was not intended as a physiological mechanism. Our project requires a model for edge responses in the early vision system. We develop it from the on-centre C_L and off-centre C_D neurons in early vision. The model allows us to investigate if our proposed addition of coloured $1/f$ type noise might cause stochastic resonance with small objects such as microcalcifications close to the visual threshold. Such noise has correlations over most frequencies f in its power spectrum which declines as $1/f$ and these characteristics can be of value regarding possible resonances for size and cluster distribution.

The primary visual pathway begins at the retina and involves the lateral geniculate nucleus (LGN) and the visual cortex V1. A greatly simplified illustration of the visual pathways is shown in Fig 3a (Kulikowski, 1979). The LGN is a small but very important part ($\approx$ 1.5 million cells) of the thalamus in the pathway for each eye. Retinal ganglions receive spatial information in the form of excitatory ("light") and inhibitory ("dark") signals and transmit this information via action potential spike pulses to the separate layers of the LGN. Each LGN relays signals to the visual cortex V1 but it also is involved with extensive signals back-projected from the cortex and associated neurological processes, not all of which are known in their exact functions.

The striate cortex V1 has six laminae due to many myelinated axons running roughly parallel to the cortical sheet, (Fig 3b). Its network of neurons performs extensive interactions of visual information originating from both eyes and sends rapid messages to many other parts of the brain.

The shape of the retinal image is conformally preserved in its general spatial relationships in the transmission from the retina to the LGN and on to the striate cortex. This is the primary "retinotopic" map of early vision illustrated in Fig 4 (Cook, 1986). At the visual cortex on-responses and off-responses interact by processes indicated in Fig 5 (Crick, 1994). The results of these interactions may be achieved in our model by a simple convolution process using the versatile properties of neurons. By using such processes

the cortical area can communicate its messages very rapidly because it is believed that it performs very few iterations before doing so. Therefore the usual concept of computations requiring many iterations probably does not apply (Crick, 1994). This is supported by the absence of extensive inhibitory neurons which would be needed for extensive computation.

Much of our knowledge of the neurological structure and properties of cell types in the vision system comes from the extensive work of Hubel and Wiesel in the 1960's and 70's (eg see Hubel and Wiesel, 1977). (Nobel Prize in Medicine awarded 1981). Their work is still the basis of much research in vision. The two main information pathways in the vision system are for the on-centre and off-centre neuron responses which are initially generated at the receptive fields of retinal neurons. This is an efficient method used by the vision system for eventual contrast detection in the visual cortex of the observer. The important on- and off-spatial response gradients determine the "zero crossings"(ie light $\leftrightarrow$dark) corresponding to the arrows in Fig 2 at the inflexions of the edge intensity response. A surprising theorem of Logan (1977) shows that this information at zero crossings contains all that is required to define the response. We utilise this fact and designate the respective information content of on-centre and off-centre groups of cells involved for edge transition from dark(D) to light(L) as C_L and C_D. These respond antagonistically in excitatory or inhibitory mode depending on the light or dark regions of the image component presented at the particular spatial retinal receptors which are associated with subsequent convergence of signals on to a particular retinal ganglion. Signals from groups of ganglions are then responsible for the coded image messages sent into the optic nerve channels to the LGN.

The two separated on- and off-pathways from the retinal ganglions undergo a division at the LGN into a magno (M, large cell) and parvo (P, small cell) path. There is also some individual "sharpening" of responses at the LGN in addition to psychophysical feedback from the reticular formation at the top of the brainstem via the inferior temporal cortex (ITC). By this stage the pathways carry spatio-temporal, size, and colour information as well as spatial frequency components of the image. Our experimental arrangement in

which $1/f$ "coloured" noise is added, results in the effect being registered in the cortex V1 in liaison with the cortex region V4 (for any colour perception).

We use the visual system's development of "information content" from Information Theory to allow us to compare the spatial information of C_L and C_D at V1 and that which is input from the previous LGN level. The algebraic difference between results of processes at C_L and C_D for spatial gradient at LGN and V1 must be due to the processes for the result at V1. This yields a differential equation for each of C_L and C_D from which their spatial response at V1 can be formulated. The spatial gradients of C_L and C_D directly effect the intensity contrast for the actual perception by the observer at higher cortical levels.

We show that a class of Lotka-Volterra differential equations can describe the retinal ganglions output and that similar equations also arise in the V1 striate cortex where the on-centre and off-centre responses are interactively combined. This similar class of equations at both locations is supported by the known retinotopic property of early vision. We then suggest that a property of the L-V differential equations in regard to responses from the addition of $1/f$ noise injected into the interaction process of our model at V1 can produce a type of selective stochastic resonance (SR) in the cortex to improve contrast. This arises as follows: the brain, and neurons generally, are noisy but this random noise does not affect normal vision. However, published research has shown that other classes of noise including $1/f$ type noise, can produce resonance solutions to L-V equations. Our hypothesis is that in the physical system of our experiment, in which we can internally introduce $(1/f)$ noise to V1 of the observer, resonances in the on-responses and off-responses can occur for edges and associated details.

The results from 300 observations is an initial set of observations from two groups of observers indicate that the effect is present $(p<0.05)$. In a subsequent second set of 300 observations with more stringent conditions the significance value was $p<0.1$. Values

of $p \sim 0.07$ occurred for observers who have had some experience in viewing detail in images (not necessarily mammograms). The probable reasons appear to be associated with observer-related parameters in the L-V equations. Implications for breast screening are discussed in relation to attention and search methods used by observers.

We note that a recent report (Kitajo et al, 2003) shows that random Gaussian noise introduced to only one eye during a periodic change in intensity of a patch area of illumination on a computer screen viewed by both eyes increased the observers' ability to detect the periodic change below the visual threshold compared with the eye without noise added. Although this indicates SR occurring in the cortex, it is not for improvement of edge detection which is quite a different neurological process which is not susceptible to Gaussian noise in our model, for stochastic resonance. Nevertheless it supports our approach of using signal interactions with $1/f$ noise at the visual striate cortex.

Other applications of the system may include resolving identification uncertainties between some types of calcium deposits and pulmonary nodules in chest X-rays, as suggested to us by a senior radiologist who had participated in our experimental observations.

Forthcoming opportunities for other new technology from digital electronics and spectral properties of photonics materials hold promise for visual detection aids, based on the principles presented in the thesis.

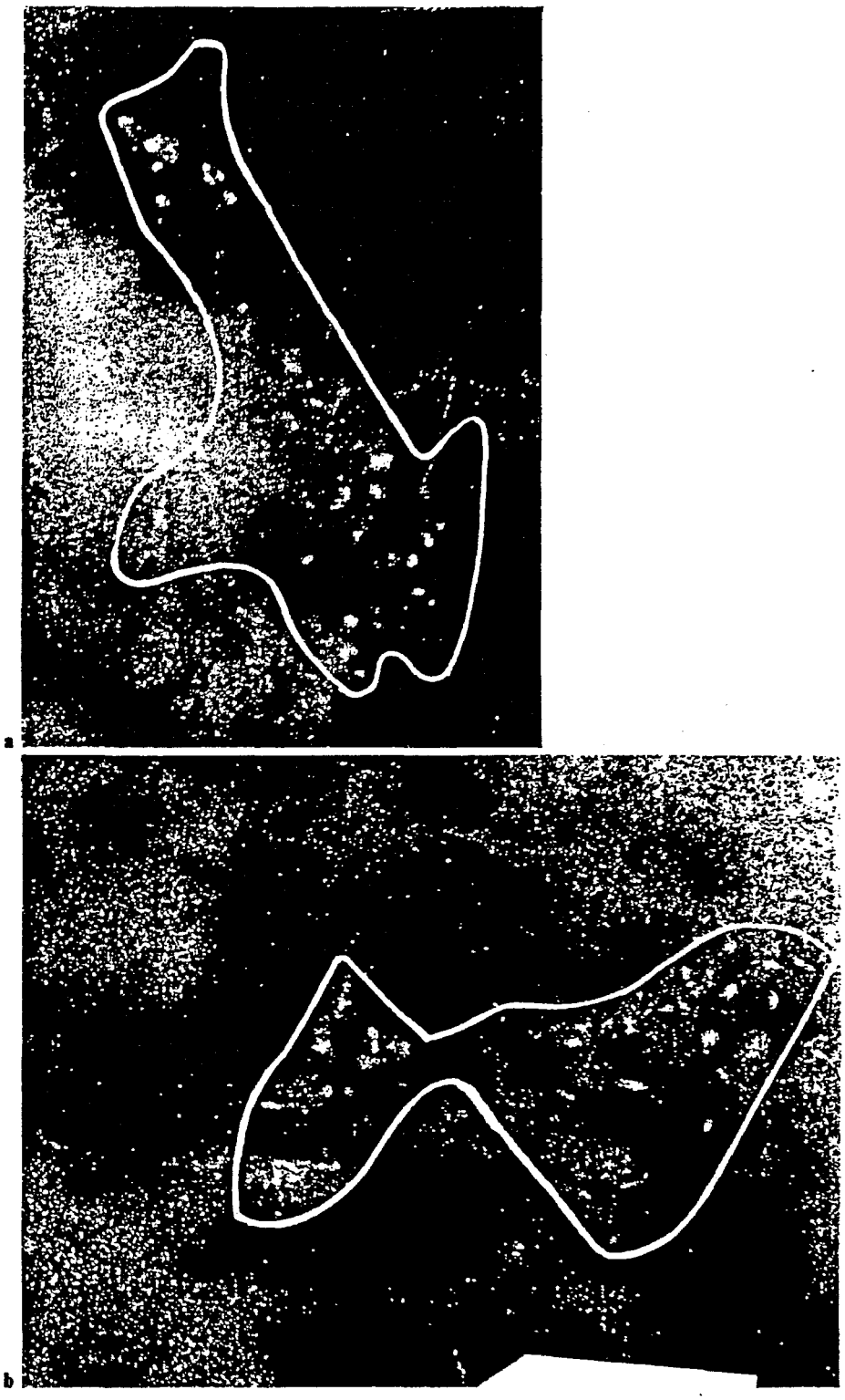

Fig 1 a,b. (Lanyi, 1988)
Details of mammograms (5 X).

a. Lateral view: faint cluster of polymorphous microcalcifications. The cluster shape is difficult to evaluate (bottle-shaped? Triangular?).

b. Craniocaudal view of the same area: the cluster is propeller – or butterfly-shaped

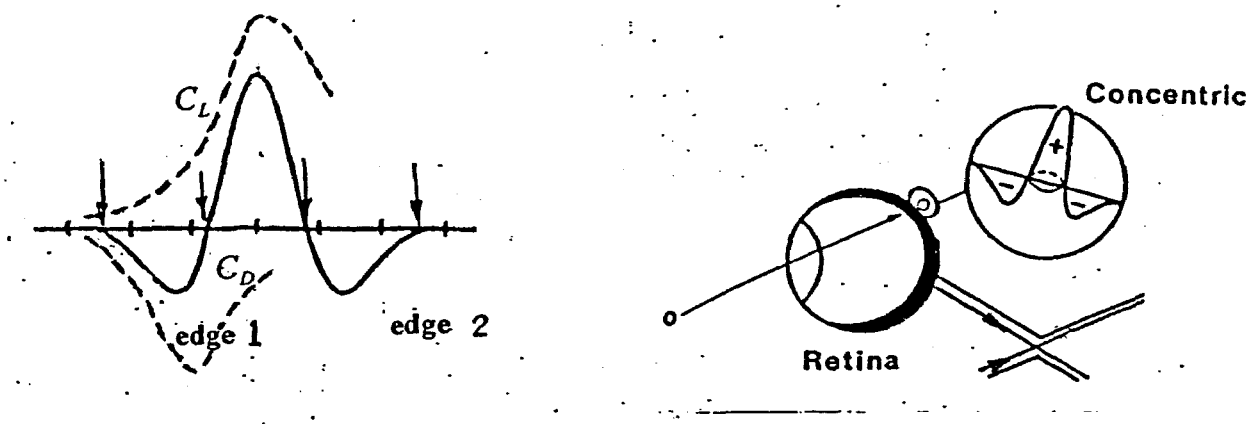

Fig 2

Observed intensity shape resulting from C_L and C_D responses of an object of finite width. Zero crossings marked with arrows.

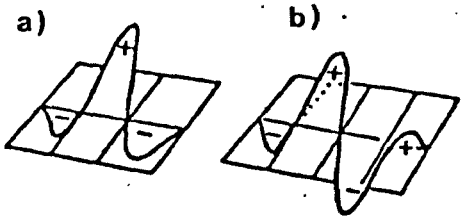

Schematic diagram of the receptive fields of simple cells in the visual cortex: (a) line detector, (b) edge detector

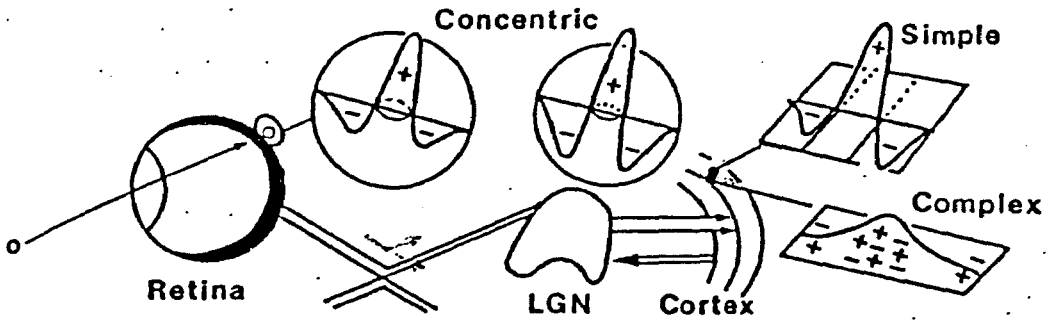

Fig 3a (Kulikowski, 1979)
Schematic diagram of the main visual pathways from retina to occipital cortex, showing the response profiles of receptive fields at various points along the pathway (positive to light spots, negative to dark spots). Also a separate diagram of the receptive fields of simple cells in the visual cortex: (a) line detector, (b) edge detector

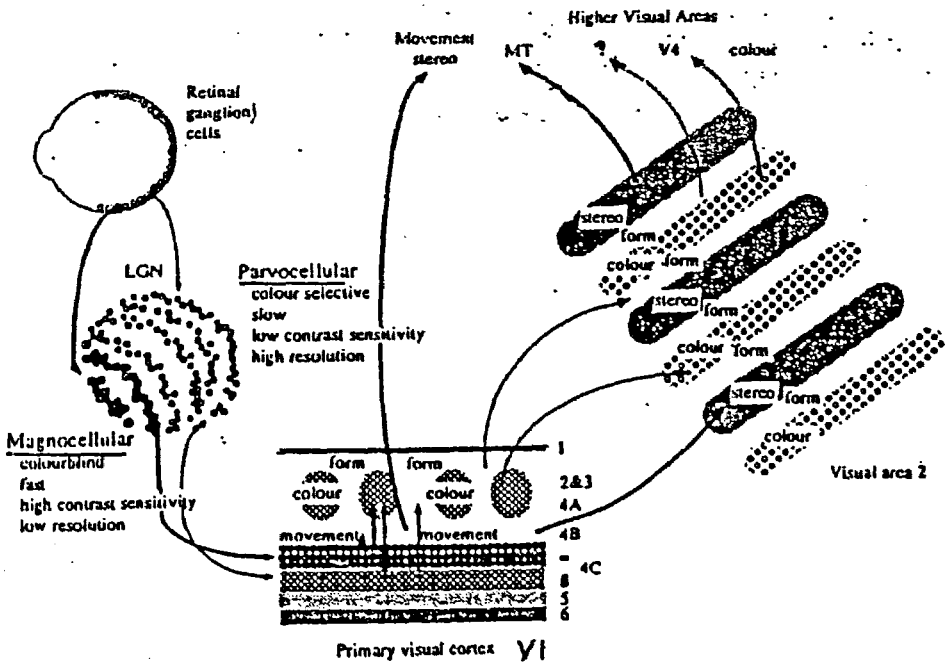

Fig 3b (Milner and Goodale, 1995)
Magno and Parvo Paths from LGN to V1 laminae

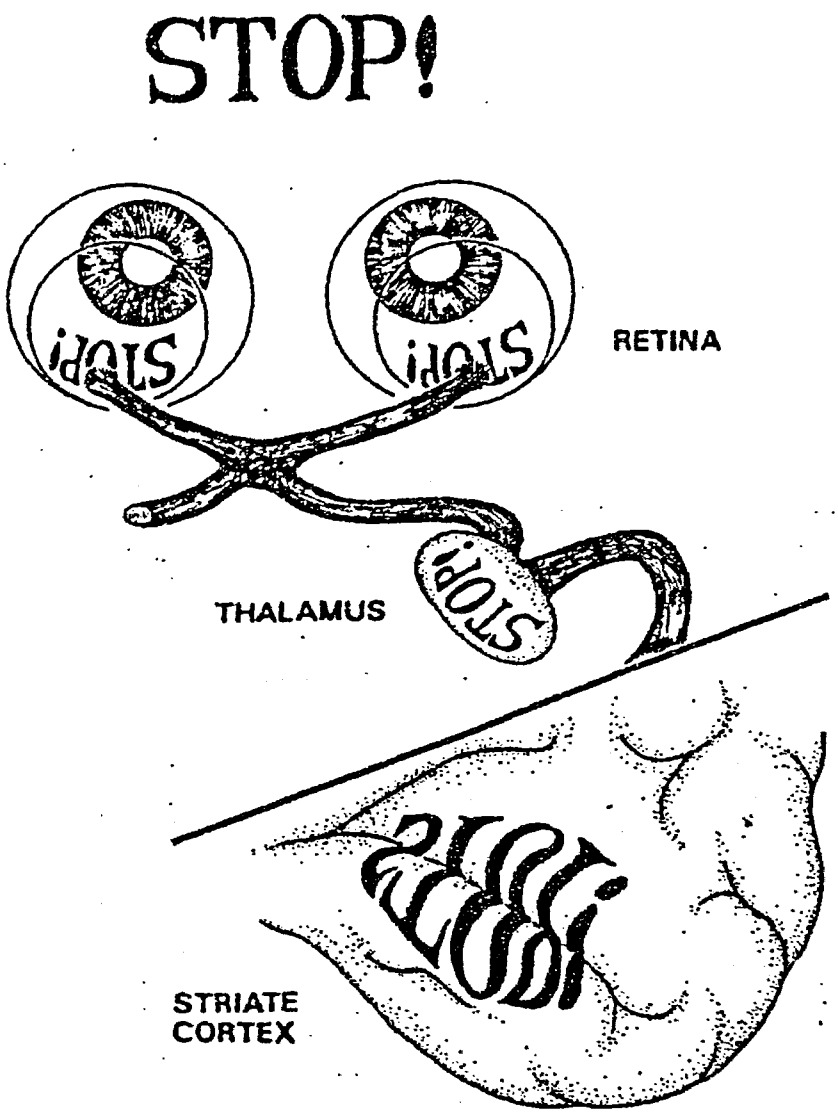

Fig 4 (Cook, 1986)
The Primary 'Retinotopic' Map
In the visual system, the retinal image in the eye maintains its basic configuration as the pattern of stimulation is transferred from the retina to the lateral geniculate body in the thalamus to striate cortex. In the human brain, the central one or two degrees of the visual field (5 – 10 mm wide at a reading distance of 45 cm) is represented bilaterally.

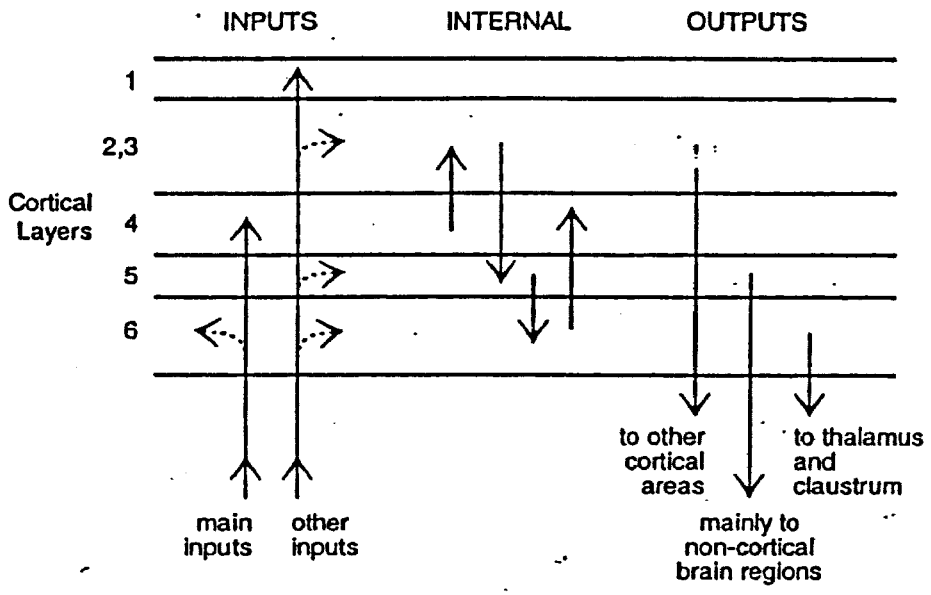

Fig 5 (Crick, 1994)
A grossly simplified diagram showing some of the major pathways within cortical area V1. There are many sideways connections that are not shown in this diagram.

Chapter 1

Diagnostic Signs in Viewing Mammograms

Breast cancer is a disease that afflicts approximately one in twelve women during their lifetime (Cancer Society Reports 2003) and significantly contributes to female morbidity and mortality. The term "breast cancer" implies carcinoma arising in the ductal and glandular structures of the breast (Fig 1.1, shows the breast structures). In such circumstances there is a transformation of breast ductal (90-95% cases) or lobular (5-10% cases) cells where they become atypical and invasive with the propensity and capacity to metastasise to other body organs via the lympho-vascular system.

Aetiology/Risk Factors

Cancer, in general, is a multifactorial disease and breast cancer is no exception. With specific relevance to breast cancer some aetiological factors are thought to be:

- **Genetic**
  (5% heredity factors, oncogenes, genetic mutations)
- **Environmental**
  (including exogenous and endogenous hormones especially excess oestrogen).
- **Viruses**
  (Mouse Mammary Tumour virus (MMTV)
- **Other**
  (lifestyle, carcinogens, unknown)

"Seeing" objects in everyday life is primarily dependent upon edge detection by our vision system. In applications with medical images it is of particular importance, such as when searching a mammogram for diagnostic details in breast screening. This is because a mammogram is a "soft" (low energy) X-ray of the breast where small or subtle features of importance need careful attention in a mixed background of X-ray attenuations giving "shadows on shadows".

Considerable benefit could result from better means of mammographic detection and perception of features for discrimination between benign and malignant breast lesions. This is because mammograms from screening are typically read at 60 to 80 per hour by expert radiologists with a false positive rate of around 15% and a false negative rate of less than 10% but not all screening centers achieve these. Any aid for detection of detail in real time would be desirable. Improved means of mammographic detection would not only decrease misdiagnosis, yet would also reduce patient anxiety problems and could also decrease the cost of screening programs. In addition, it would aid breast surgeons in determining the appropriate surgical margins with obvious benefit for patients.

It has been shown that only a very small percentage of total information from image features available in a mammogram is actually used (Zhou and Gordon, 1989). Image processing can be applied to digitised mammograms off-line to improve image detail but pixel size limits the amount of detail which can be revealed. Also in real-time readings of mammograms in screening, there may be information at or just below the visual threshold which may be important for the radiologist.

Microcalcifications

Microcalcifications are the earliest non -palpable signs of breast cancer and occur as byproducts of rapidly dividing cells (Fig 1.2). Calcifications, if present, may indicate either benign or malignant lesions but yet there are features that radiologists use to distinguish between the two. Calcifications associated with malignancy are typically clusters of tiny particles and sometimes characterised by linear, curvilinear or branching shapes originating from ducts. Examples are shown in a typical Reporting Sheet used by radiologists (Fig 1.3)

However, difficulties in interpretation can arise if calcifications are not typical. In these situations biopsy is often recommended. A careful off-line visual magnification may also help to differentiate in such circumstances.

The perception of features such as type, non uniformity of shape and size, the extent of the deposits plus the number per square centimetre in a cluster are critical factors. Of the microcalcifications characteristic of malignancy detected mammographically, approximately 25% are found to be a consequence of ductal carcinoma in situ (DCIS) (Lanyi, 1996). DCIS may progress to invasive carcinoma and the early detection of its subtle microcalcifications can lead to early intervention and a successful outcome. (DCIS refers to malignant cells that have not spread beyond the duct, yet may have a capacity to invade if not detected and acted upon early).

Breast Masses

"Masses" are the actual growths themselves and include cysts (harmless) and tumours, circumscribed or of stellate type including ones which have architectural distortion. They are often difficult to visually detect in the early stages. The biophysics and biochemistry relating to the formation of tumours is a complex phenomenon consequent to the breakdown of normal cellular interaction and control of replication.

For the visual evidence of the early signs, edge detection is of great importance in a mammogram for both initial detection and for detail. Early detection and diagnosis are crucial for successful treatment outcomes in breast cancer.

Screening for Breast Cancer

A mammographic study usually consists of two images of each breast. The images are obtained from two different angles of projection of the X-ray beam relative to the breast and a mammographic compression unit is shown in Fig 1.4. The images are reviewed by radiologists and reported on with the aid of a reporting sheet such as shown in Fig 1.3 where various types of microcalcifications and masses are also shown. Further details are given with many examples in Film Screen Mammography, An Atlas of Instructional Cases. (Bassett et al, 1991).

The names of the image views, the craniocaudal (cc) and the mediolateral oblique, $(m\ell)$, are derived from the angle of the X-ray beam as it is projected onto the breast and

received by the film/screen system. Compression of the breast is necessary to decrease breast thickness, allowing lower radiation doses. Compression also improves image sharpness by decreasing breast motion and radiation scatter which degrade resolution. Although other modalities such as ultrasound and Magnetic Resonance Imaging (MRI) are valuable adjuncts to mammography, mammography remains the accepted 'gold standard'. The criteria for screening for any type of disease have been established by the World Health Organisation and are listed in Fig 1.5. Details of these criteria are given for breast cancer in a paper published by the writer (Thornton E., 2001).

A detailed literature review of the background leading to mammography as the gold standard plus other information prior to beginning this thesis was initially presented by the writer (Thornton, 1998).

Frequently, careful mammographic analysis will yield distinguishing features which allow the radiologist to determine whether a process is benign or malignant. Thus, a choice can be made between a continuation of the routine bi-annual/annual mammogram, or short-term follow up for additional analysis. However, since there is a great overlap between the mammographic appearance of benign and malignant processes, biopsy is often necessary to exclude breast carcinoma. The present thesis aims at providing a method to assist in the detection of features. The method involves the addition of $1/f$ coloured noise in real-time viewing of mammograms. It is applicable for both microcalcifications and masses.

The method requires a study of the processes of the vision system for the perception of detail and edges so as to develop a model by which the proposed method for improvement can be tested.

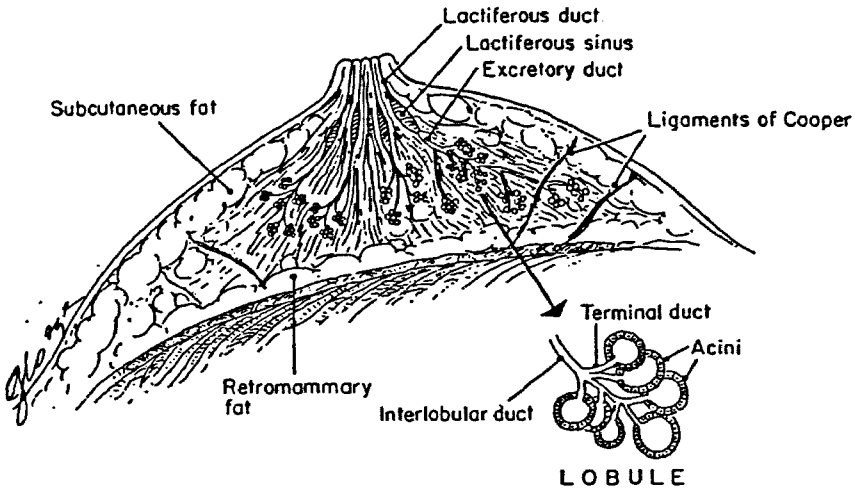

Fig 1.1 (Bassett et al, 1991)
Schematic diagram of mature breast in axial section

Calcifications Within the Lobular and Ductal System of the Breast

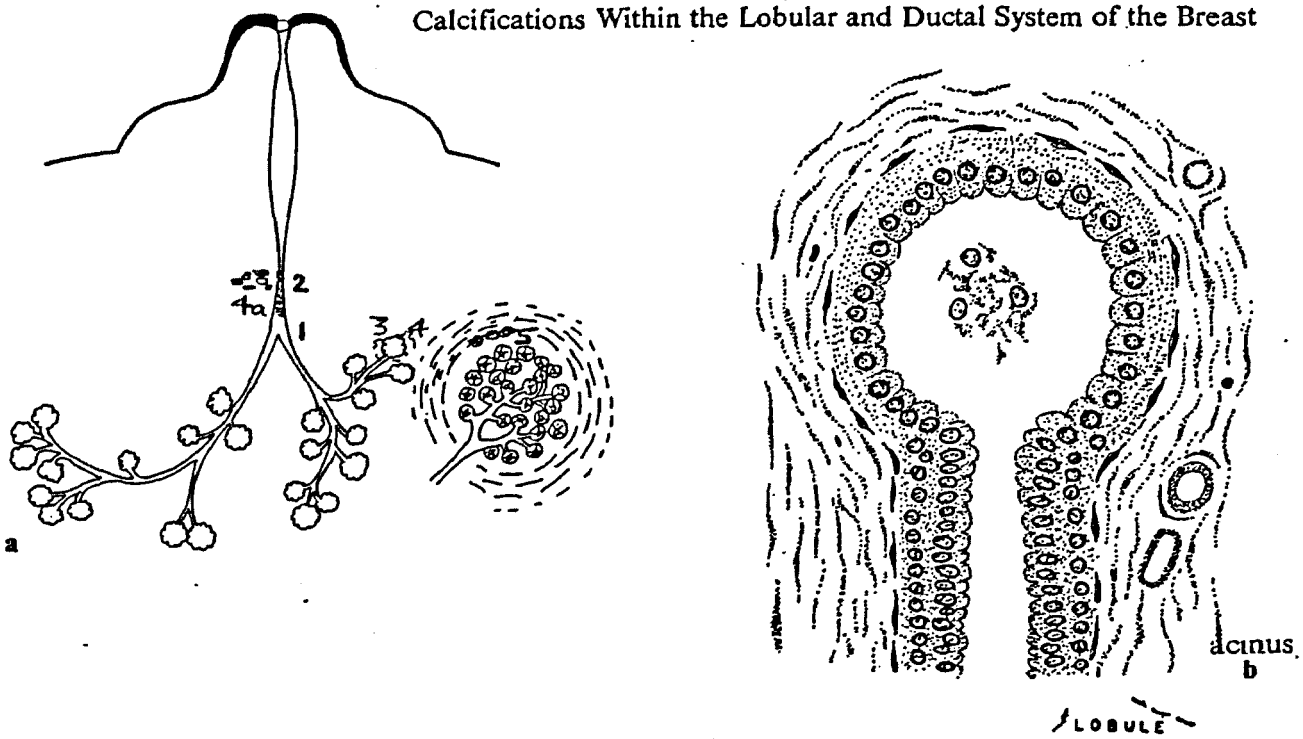

Fig 1.2
A Schematic diagram of the ductal system (adapted from Bassett et al, 1991)

Main Steps in Breast Cancer Microcalcification Formation

1. **Diseased tumoorous epithelial cells grow and multiply into the duct. Duct becomes spongy and the cells exude C^{a++} into all spaces. This can result in punctuate deposits which is one of the "signs" which can indicate malignancy (particularly if more than 15/cm²). Other types of deposits can be "in situ" along the duct and some (eg branching) shapes can be an indicator of ductal carcinoma.**

2. **The bad cells eventually block the duct (ie stasis) (Paget's disease' in the duct if near nipple).**

3. **As a result of duct blockage the internal pressure in the lobe(s) increases.**

4. **The node enlarges and can become cystic: fibroblasts and scar tissue can follow.**

4a. **Bad cells burtst through the wall of the duct and deposit Ca^{++} outside the tissue. Also some of these bad cells may be cancerous and are then "free" and can enter the lymph nodes and the blood stream. If so, distant metastases can occur.**

5. **Dead cells ac cumulate inside the wall and in the fluid in the lobe. Tissue macrophages are then attracted to these necrotic cells at the wall. Phagocytes may also be attracted by chemical signals, (although this is not certain). Any remaining debris from autolysis or necrotic cells may act as foci for calcium deposits in malignant of benign cases.**

Guide to Using the ACR Mammography Lexicon with MRS

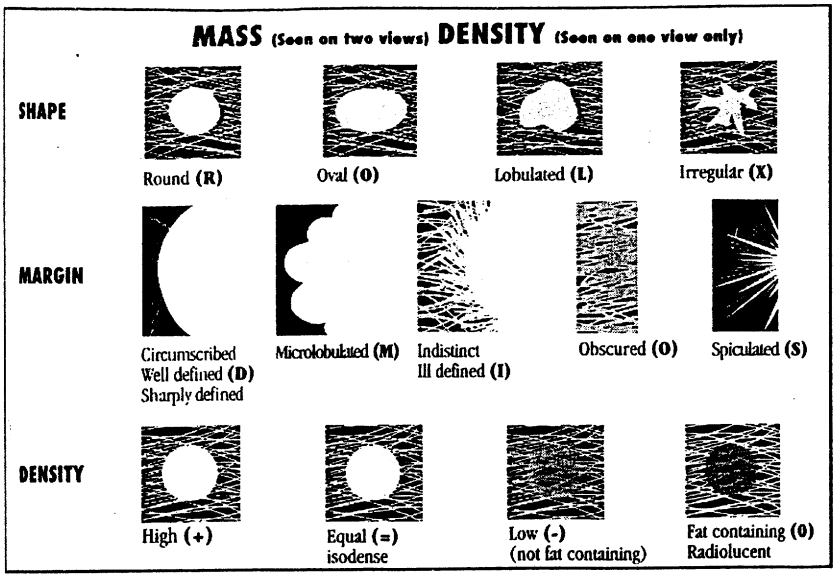

INSTRUCTIONS

Fill in the mammogram section of the MRS worksheet according to the instructions below. If dictatin; follow the order of the worksheet.

Record positive mammographic findings by choosing from the words in blue and/or the codes in ( ) Describe masses in terms of their size, shape, margin, relative density, and location.

Example: There is a 1 cm round spiculated mass of density equal to the surrounding parenchyn in the 9 o'clock middle position of the left breast.

Describe calcifications in terms of their appearance, distribution, and location, or by the histology th represent. Description of typically benign calcifications is entirely optional.

Example: There are **EC** *in a* **S** *distribution in the* **P** *12 o'clock position of the* **R** *breast.*

Use the key words in any order, with any other description or discussion you wish. Codes are optiona

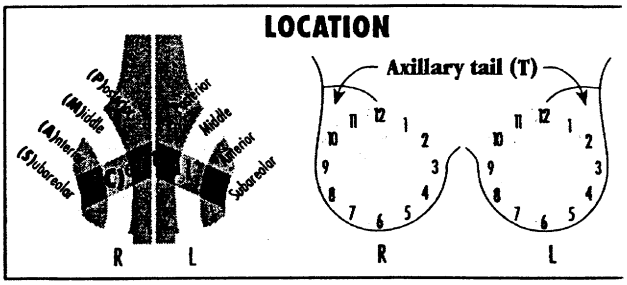

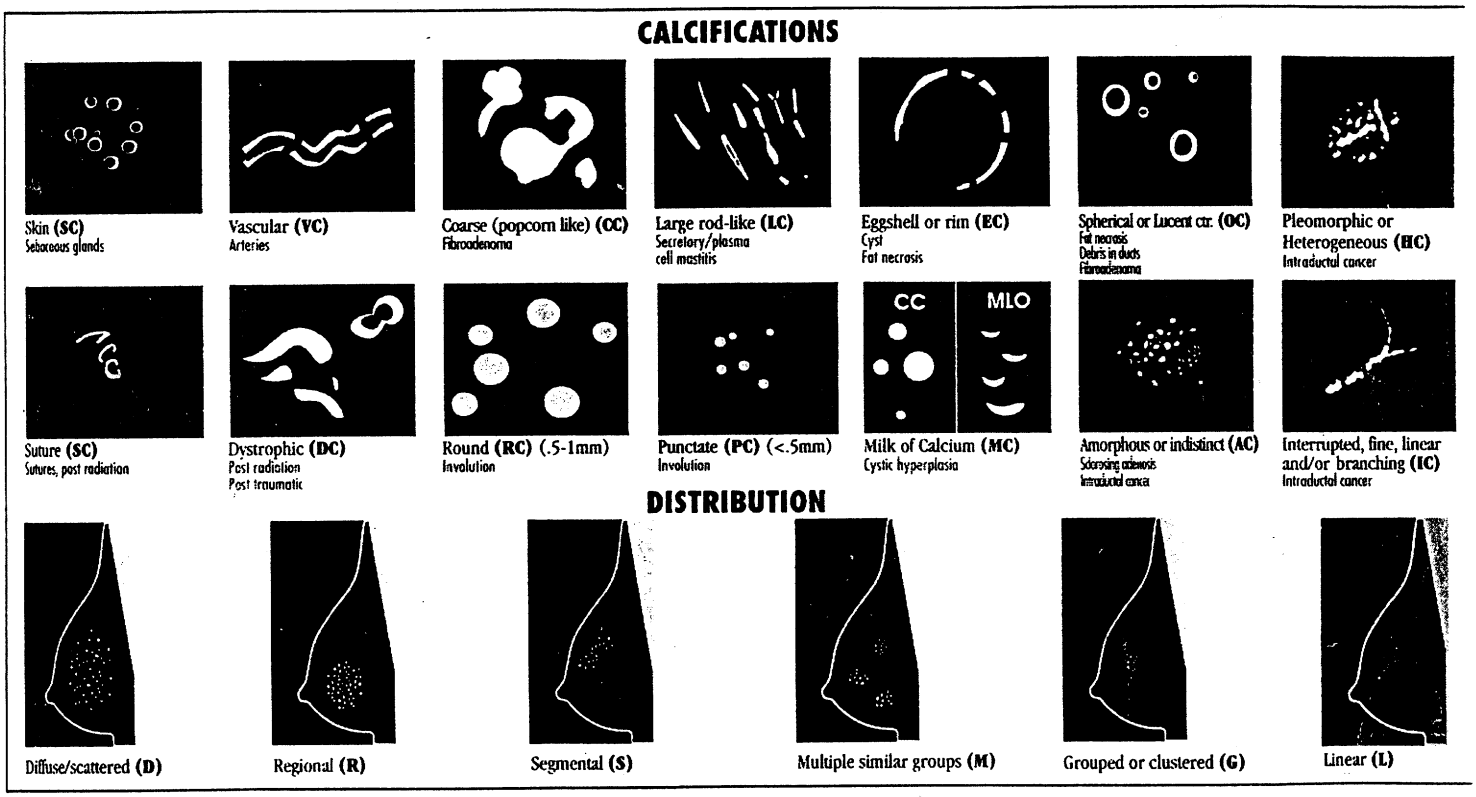

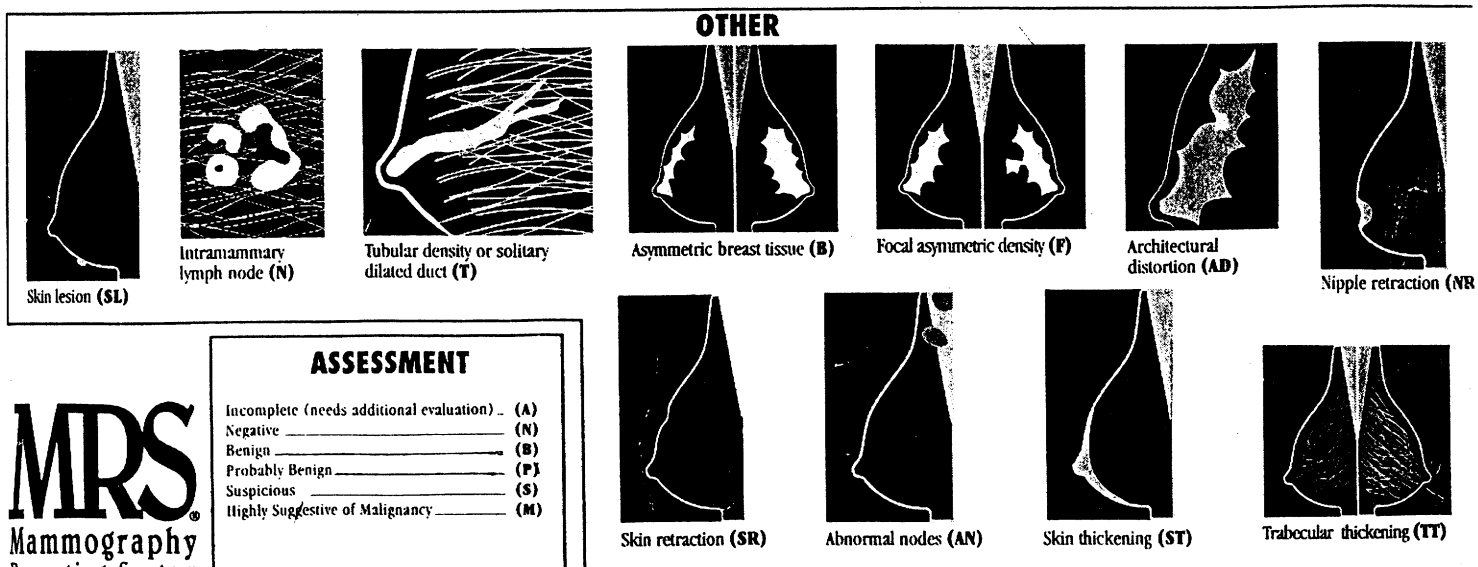

ASSESSMENT

Incomplete (needs additional evaluation)	(A)
Negative	(N)
Benign	(B)
Probably Benign	(P)
Suspicious	(S)
Highly Suggestive of Malignancy	(M)

MRS® Mammography Reporting System

Illustrations & Poster Design: Olivier Mel

Fig 1.3 (Breast Screening – Western Sydney)
Example of Radiologists' reporting sheet

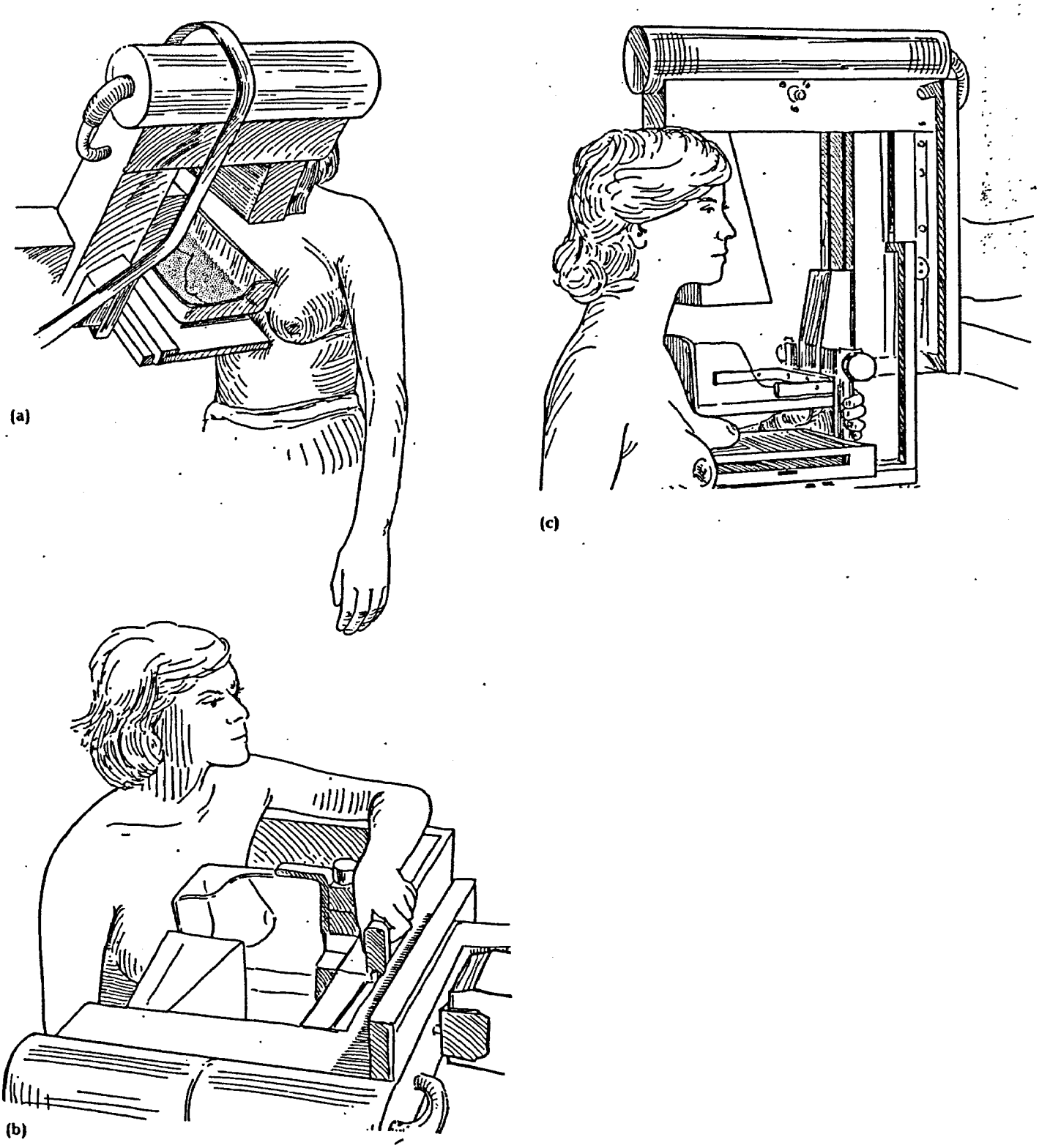

Fig 1.4 (Bassett et al, 1991)
Positioning for film-screen mammography

(a) Mediolateral oblique view. Breast is distracted from the pectoralis major muscle and compressed at an angle parallel to the plane of the muscle.

(b) Lateral vies. This view can be performed either mediolateral or lateromedial. The mediolateral view is shown here. The patient is rotated slightly inward, and the arm is supported by the C-arm of the dedicated unit.

(c) Cephalocaudal view.

- The condition should be an important health problem;
- the condition should have a recognisable latent or early symptomatic stage;
- the natural history of the condition from latent to declared disease should be adequately understood;
- there should be an accepted treatment for patients with recognised disease;
- there should be a suitable test/examination;
- tests should be acceptable to the population;
- there should be agreed policy of whom to treat patients;
- there needs to be facilities for diagnosis and treatment;
- the cost of case funding should be economically balanced in comparison to the entire cost of medical care as a whole; and
- testing should be a continual process.

Fig 1.5 (Thornton E., 2001)
The criteria for selection for screening have been established by the World Health Organisation as listed

Chapter 2

Basic Physiology of the Retina and its Edge Responses sent to the Lateral Geniculate Nucleus

In this mammography project we are interested in "seeking what to see" in mammograms. In fact "we can regard all seeing as a continuous search for the answers to questions posed by the brain" (Young, 1978). In general, the signals sent from the retina constitute "messages" conveying these answers to the brain to construct a hypothesis about what is present and any decisions to make as a result.

The retina is a vital component of the vision system which translates visual information to a series of pulses to the optic nerve channels. Fig 2.1a displays the layers of the retina. There are two kinds of receptor cells in the human retina, namely rods and cones. Rods are important for peripheral vision and are more sensitive to dim light. Cones, on the other hand, are especially important for visual acuity and for colour vision. As can be seen in Fig 2.1a there are a variety of neural cells present in the retina along with the receptor cells whereby impulse signals travel from the ganglions to the nerve fibre layer along the optic nerve. Fig 2.1b illustrates the information flow from a structured receptive field of the receptors via a network of retinal cell connections. The result converges on a ganglion cell which discharges the result to the optic nerve fibres. In darkness the retinal photoreceptors continuously release excitatory neurotransmitters. With the absorption of light there is hyperpolarisation of the photoreceptor membrane to inhibit neurotransmitter release. This is a unique property of the vision system (Keirnan, 1998).

The retina is not simply recording a picture but detects a series of information items which are reported to the brain. It is interesting to note (Granit, 1977) that if the eyes are prevented from moving (i.e no saccadic actions) the signals fade within one second and no picture is seen. The continuous small saccadic movements of the eyeballs are

necessary for good visual acuity (Forgus, 1966). A review of the retinal processes now follows in order to formulate our model for the retinal output.

The Cells of the Retinal Layers and On-Centre and Off-Centre Properties

Three independent types of retinal cell involved in producing responses are the layers of receptors, bipolars and ganglions in that order. The direction of light input is actually in the opposite order to that sequence even though the stimulus begins at the receptors and progresses to the ganglions (see Fig 2.1). There are two lateral operating layers of neurons which mediate the overall process. These are the horizontal cells at the base of the receptors and the amacrine cells at the level of the bipolars and ganglions. The mediating effect of these horizontal cells is not an actual direct input. As will be now described below there is an antagonistic excitation and an inhibition process from the complementary on-centre and off-centre structure of the retinal cells. The overall interplay of excitation and inhibition characterises the whole nervous system and occurs at the first physical site of the vision system.

As shown in Fig (2.2a, b) receptive fields of two of the main types of retinal cells have concentric arrangement: (1) Cells increasing their impulse activity when a light spot is incident on their receptive field centre and a dark spot is presented on the surround, whereas the light spot shone on the surround reduces the response. These cells are called 'on-centre'. (2) Cells being activated by a dark spot presented to the centre and by a light spot shone on the surround are inhibited when the dark spot (no light) is presented to the surround. These cells are called 'off-centre' cells. There is a further more complex type of cell with substantial inhibitory input from amacrine cells of the transient type. They are known as the on-off ganglion cells which usually give a brief on-response to the start of a light stimulus and a brief off-response to a reduction in light intensity. They are less understood regarding their excitatory input.

The two main types of 'on-ganglion and 'off-ganglion' cells just listed were called "simple" cells by Hubel and Wiesel in the 1960's. There are other neurons in the primary and secondary visual cortex which they called "complex" cells and are larger and have

on-responses and off-responses from every part of their receptive field, not just the concentric arrangement of "simple cells". They can receive inputs from "simple cells" and can be responsive to lines of specific orientation. In accord with most mainstream literature this thesis considers only the basic on-centre and off-centre type of ganglion cells.

Groups of on-centre and off-centre cells are best activated when a light-dark (or dark-light) change is presented on the border between the centre and its surround area and very little when a uniform light stimulus covers the whole receptive field. This property therefore can produce initial contrast sharpening from the two types of responses sent via the optic nerve to the lateral geniculate nucleus (LGN) of the thalamus as indicated in Fig 2.2b (Grusser and Grusser-Cornehls, 1987). We will follow the on-centre responses C_L and the off-centre responses C_D in the pathway from retina to LGN to V1 (Fig 2.3). The combination of signals and processing interactions within the visual cortex yield contrast intensity for the first stage of perception of an image by the brain to provide acuity (resolving ability) and acutance (edge sharpness) for the observer. We begin with a model for the retinal response for the output of the retinal ganglions.

The Retinal Cell Signalling Network

The process of seeing begins when light passes through the eye and is selectively absorbed by the sensitive photo receptor cells of the retina. Electrical potentials are generated, serving to stimulate nerve responses in various successive neural cells already mentioned: amacrines, bipolars, ganglions in the vicinity of excitation (Fig 2.1). Intracellular distances are so short that membrane depolarization and repolarisation influence neighbouring neurons directly ie electrotonically, without having to transform into an action potential for an axon. In the final output to the optic nerve, impulses emerge from the potential discharges of the ganglions' action potentials as studied previously.

Because of anatomically localized convergence and divergence, the visual receptive fields tend to be fairly small, about 1 or 2mm diameter circumscribed regions on the

retina (Fig 2.1b). Light stimuli impinging on the retina outside the RF region will not affect the cell in question. The particular RF structures and morphology have advantages for use in computational vision as shown by Sheridan (1987). In the central region of the on-centre receptive field, small spots of light produce on-response excitation while in the annular surrounding region, an off-response inhibition is produced. Complementary to the on-centre receptive fields are a roughly equal number of cells with off-centre (and on-surround) characteristics. This arrangement results in not only temporal changes in stimulation, by means of the transient nature of the responses, but also spatial contrasts (light-dark edges in the visual field). Thus with uniform illumination of the entire receptive field the 'on' and 'off' responses tend to cancel each other out and the cell is passive for edge detection. It is from the different responses at an edge which provide a contrast process. The human eye is slowly drifting and constantly executing small but imperceptible saccadic movements. The retina is geared to produce an active display of 'on' and 'off' neuron discharges resulting from light-dark-light variations in the image such as change across an edge. The essential factor is a change in the balance between excitation and inhibition and this prompts our concept of two signalling species.

The Concept of Two Signalling Species

We begin with the retinal processes based on a model somewhat related to the formulation of the Lotka-Volterra differential equations for two populations of competitive species. Beginning in the retina we have excitatory and inhibitory signals from these two cell species. These opposing processes in a signalling cell network of neurons yield the membrane potentials of the on-centre and off-centre ganglions. From these ganglion potentials the repetitive discharge spikes are launched by action potential into the optic tract to the lateral geniculate nucleus (LGN) of the thalamus in the respective left or right pathway. After subsequent processing the on and off signals are transmitted to the primary visual cortex (V1). At the cortex the signals from both eyes interact to produce the intensity response contrast of the edge as perceived by the observer. Since each eye contains more than a hundred times as many sensory cells as optic nerve fibres, it appears that considerable integrative action of signals in the pathways occurs within the retina itself and the rod and cone pathways carry information

about different properties of the image. The cone pathway P (small cell, parvo) is associated with small cell spatial information and most of the chromatic information. The rod pathway M (magno) with large cells, mainly involves contrast information. Our model for excitation and inhibition signaling is applicable for both systems but the fovea contains the highest density of cones $\left(\approx 10^5 / mm^2\right)$ for observing small details in the image and this information is carried by the parvo system. The direct and indirect excitatory and inhibitory pathways are shown in Fig 2.4.

Considerations for a Signalling Model for Edge Detection in the Retina

The model presented is prompted by a partial similarity, yet with more complexity, to the original formulation of the differential equations by Lotka in 1925 and by Volterra in 1931 (L-V). Their equations (Williamson, 2000) described the temporal changes in two populations of interacting species with extinctions possible in an environment of finite resources. Their work was based on the time rate of change in the actual numbers in the populations and each of the two species had a different initial number in their population.

In the retina the actual physical numbers of the two species on-centre and off-centre ganglions are closely equal along a narrow line strip region ℓ, yet the *number and strength of inputs* to them from the preceding cell network of excitatory and inhibitory processes across an edge region are different. The difference in the two types of antagonistic inputs is due to the bipolars as well as the indirect processes by the amacrines, which input to lateral interactions at the ganglions' two receptive field components across the limited environment of a dark/light boundary edge region.

Let $N_1(\ell)$ and $N_2(\ell)$ be the numbers of inhibitory and excitatory inputs of potentials from bipolars and amacrines to the respective off-centre and on-centre ganglions responding to the visual edge transition along the spatial coordinate ℓ towards the edge. We will let $N_1 = \sum_i n_i \sigma_i$ be the potential (strength) of n_i inputs of potential charge σ_i to the off-ganglions at a spatial location ℓ and N_2 for the on-ganglion case. The potential changes are from the electrotonic processes between retinal bipolar and amacrine cells

prior to the ganglions. Across the light and dark sides of an edge region the number of processes of additive and subtractive potentials differ in number and strength of inputs to the on-centre and off-centre ganglions and we will designate for the results as $C_L(\ell)$ and $C_D(\ell)$, (L for light, D for dark effect) at location ℓ.

The perception of an edge depends on the rate of change of light intensity seen by the observer across the image of the edge. This depends on the rate of spatial change of the membrane potentials of our two species of ganglion signals across the edge boundary region ℓ between light and dark. In the excitation and inhibition process of convergence and divergence of connections in the signalling pathway, the spatial rate of change at a given stage is proportional to the number of cells influencing it at that location.

The electric potentials are additive but the *number* of possible interacting signals of N_1 and N_2 is proportional to the product $N_1 N_2$ (similar to interaction of species in Lotka and Volterra models). The interaction of a single excitatory signal pulse e with an inhibitory one i at the same spatial location on the edge requires these two signals $i(\ell,t)$ and $e(\ell,t)$ to correspond closely in location ℓ and time t at the particular retinal cell. We can express this requirement in terms of a correlation between them over a small spatial length $s(t)$ of the duration of a single electrotonic signal "pulse". The correlation can be written as (Crandell, 1994 p200) $I = \int_{-\infty}^{\infty} e(\ell) i(\ell - s) d\ell$ where the even function signal i gives a selective value to the integral only over the small distance s, as required (an even function has the same value for positive and negative values of its variable). We see that the resultant interaction potential will be of a product form. The exact function is not known but we will see that our model's results (Fig 2.5a) show that a simple product form for interaction yields responses for an edge consistent with known ganglion potential measurements of changes in levels of intensity (Fig 2.5b) encountered at edges. The simple product form of the interaction term in Lotka and Volterra original equations has sometimes been criticised regarding the unknown actual predator-prey action for removal of a prey. However, the simple nonlinear product has generally

yielded good results for a range of data in practice. The form of our main results shows that the governing equations from our model for on and off responses are of the general L-V form. In a subsequent chapter we will also show that, in our model, this behaviour is consistent with the retinotopic general shape-preserving property of the early vision system for the retina, LGN and V1. This implies that the on-responses and off-responses which generate an image intensity distribution could be consistent with the same equation family of Lotka Volterra type.

The Model for On-Responses and Off-Responses at an Edge

Consider a given location ℓ across the image edge where there are $\alpha_1 N_1$ direct off-centre ganglion inputs and a proportional function $\beta_1(N_1, N_2)$ representing indirect component of inputs via amacrines. There will be an increment ΔN_1 in signal strength, from the lateral amacrine connections over an incremental length $\Delta\ell$ from ℓ towards the actual edge boundary. We will use excitation E_1 and inhibition J_1 as functions of the direct and indirect excitatory and inhibitory inputs to a group N_1 of ganglion membrane potentials from the associated amacrines, on-bipolars and off-bipolars. This is set out in the description below and indicated in Fig 2.4. Therefore, as the 'light' edge is approached over the incremental distance $\Delta\ell$, the increment ΔN_1 of the signal strength to the off-ganglions will be the difference between excitation and inhibition multiplied by $\Delta\ell$

$\Delta N_1 = (E_1 - J_1)\Delta\ell$ resulting, in the limit, as

$$\frac{dN_1}{d\ell} = (E_1 - J_1) \tag{2.1}$$

For the on-centre case we have

$$\frac{dN_2}{d\ell} = (E_2 - J_2) \tag{2.2}$$

The Excitation and Inhibition Processes E_1 and J_1

There are four main processes ((Grusser and Grusser-Cornehls, 1987)

(a) The off-centre ganglions receive direct excitatory inputs from the off-bipolars

and

(b) lateral excitation from amacrines which are excited by the on-bipolars and give indirect excitation input to the off-ganglion cells via their outer surround region

plus

(c) direct inhibitory inputs from the on bipolars (RF centre)

and

(d) lateral inhibitory contacts from the off-amacrines being indirect input via the outer section of off-ganglions.

Therefore for E_1 and J_1 in Eq(2.1) we have:

For the Excitation E_1

E_1 is the direct proportion α_1 of N_1 plus an indirect proportion β_1 of the result of interaction between N_1 and N_2 via amacrines. We can write this as the sum of two terms.

$$E_1 = \alpha_1 N_1 + \beta_1 f(N_1, N_2) \tag{2.3}$$

The proportional coefficients α_1 and β_1 are determined with respect to (a) and (b); α_1 by the convergence of a number of direct inputs of off-bipolars on to off-ganglions and β_1 by the lateral number of inputs via amacrines excited by on-bipolar signals to the surround sections of the off-ganglions' receptive field. Therefore the result is a function of N_1 and N_2 as indicated in Eq(2.3).

Note that the proportional coefficient β_1 is the product of two proportional factors β_i and β_j being, respectively, for the initial proportional signal and the subsequent secondary proportional signal of the combination of the two. For convenience we write the result as $\beta_1 f(N_1, N_2)$.

For the Inhibition J_1

In a similar manner to forming Eq(2.3) for E_1, the processes (a), (b), (c), and (d) give the inhibitory coefficient as

$$J_1 = \delta_1 N_1 + \gamma_1 (N_2, N_1) \tag{2.4}$$

where γ_1 is determined by the amacrine signals from the on-bipolars and which input laterally to the outer inhibitory region of the off-centre ganglions thereby yielding an inhibition input to the off-ganglions. (γ_1 is, in a similar manner to β_1, the product of two proportional factors).

From equations (2.1), (2.3) and (2.4) we can write for the spatial rate of development of off-centre inputs to form the rate of change of membrane potential across the edge region (defined as the change from the unexcited state), as

$$\frac{dN_1}{d\ell} = E_1 - J_1 = \left[\alpha_1 N_1 + \beta_1 (N_1, N_2)\right] - \left[\delta_1 N_1 + \gamma_1 (N_2, N_1)\right]$$

$$= (\alpha_1 - \delta_1) N_1 + \left[\beta_1 (N_1, N_2) - \gamma_1 (N_2, N_1)\right] \tag{2.5}$$

In a similar manner for Eq(2.2) we obtain for the on-centre case of change across the boundary edge

$$\frac{dN_2}{d\ell} = (\alpha_2 - \delta_2) N_2 + \left[\beta_2 (N_1, N_2) - \gamma_2 (N_2, N_1)\right] \tag{2.6}$$

These two variables N_1 and N_2 which represent the totals of the input strengths for each of the off-centre and on-centre ganglion potentials which we will label as $C_D(\ell)$ and $C_L(\ell)$, as stated previously. Across an edge there are different values and proportions of α, β, γ and δ for the variables giving changes of sign in the bracketed coefficients of Eq(2.5) and Eq(2.6).

As a result, equations (2.5) and (2.6) are of the L-V type and characterise the opposing potential responses (not the impulses/sec) for on-centre and off-centre ganglions.

The internal amacrine processes are not quantitatively known. However, in the off-centre case, we take the functions $\beta_1(N_1, N_2)$ and the $\gamma_1(N_2, N_1)$ as proportional products of N_1 and N_2 because it would be the simplest non-linear product form which could be assumed for two variables. We see a similarity to the Lotka-Volterra type of model.
The L-V responses are for the rise and subsequent fall of potential. They have good agreement with known experimental data when plotted with suitable parameters fitted for Eq(2.5) and Eq(2.6) for an exponential photon flux intensity I increase at an edge dark $\rightarrow$ light. This is shown in Fig 2.5a where both opposing potentials are plotted for relative magnitude values. We also note that for finite limited resources (light flux), the canonical form L-V differential equations are easily refined (eg see Williamson, 2000) and have the same basic properties and type of responses as in our model.

The stability of the solution of L-V differential equations is dependent upon the relative magnitude and relationship of the coefficients (Gotelli amd Murray, 1995). In the present case, the required conditions are satisfied based on the physiology and neurological parameters on which the coefficients depend.

Edges in Mammograms and other Films – Comparison of our Retinal Model with Measurements

The practical application of the model to mammographic observations appears appropriate in viewing edge boundaries of objects in the film (or digital version) being less than a clear sharp jump in image density. The acutance in an image representation in a film has been used in many applications as a measure of the image quality. The acutance of an image in a film is defined (Biberman, 1973) as

$$A = \overline{G}_x^2 / D^1$$

where $$\overline{G}_x^2 = \left[\sum_{i=1}^{n} (\Delta D_i / \Delta x_i)^2 \right] / n$$

and ΔD_i represents the density at n positions Δx_i leading to the edge. D^1 is the total range in density over which the measurements are made. Observers' subjective impressions of degree of sharpness have been well correlated with such measurements (Biberman, 1973, p23) on film images of various qualities. If we take the practical case of an actual film image with an exponential rise of luminance in the narrow boundary region of a dark to light transition, we can compare the known ganglion potential versus stimulus response with the L-V response spatially across an edge region. A typical result for an on-centre case which closely matches published experimental measurements (Baylor and Fuortes, 1970) is shown in Fig 2.5b. An on-centre and off-centre plots of relative magnitude are shown together in Fig 2.5a. Individual plots are shown in Fig 2.5d. The basic ganglion shape obtained from the L-V model when the simplest non-linear product term $C_L C_D$ is used, is of similar form to the measured response from a single ganglion (Fig 2.5b). Both the spatial scale ℓ and light stimulus intensity as log I are shown on corresponding scales across an edge in Fig 2.5a for comparison We have shown the associated light intensity change for the "edge" in an actual mammogram image at the top of Fig 2.5a as a rapidly rising (3 decades) exponential.

In a spatially extended situation with other cells, lateral spatial inhibition is also present (see Fig 2.5c) and the effect is then indicated in Fig 2.5a by a dashed line.

Comment on the LV Repeated Responses in the Retinal Model

The repeated cyclic property of the L-V differential equations response corresponds to the "recharge" of the respective ganglion potential after its pulse discharge group. The axon hillock of the ganglion acts as a trigger. When the algebraically summed inputs to the cell body exceed the threshold of the axon hillock the ganglion fires. The process is governed by the time constant of the cell body (Kent 1981). The frequency is determined by the slope of the depolarisation which begins immediately after the point of maximum repolarisation of the ganglion's action potential. The process is repeated corresponding (in time) to the repeat cycles of the L-V differential equation solution. This yields a sequence of the on-response and off-response responses over the same spatial distance and provides the spatio-temporal temporal pulsed spike discharges carrying information to the LGN.

It is appropriate at the present stage, following the ganglion's output, to summarise the nature of signal transmission via the optic nerve for input to the LGN neurons. The basics of neuron operation are given in Appendix B. Also, some analogies of neuron processes for differentiation and integration computer operations are mentioned for reference to our model in a later chapter.

In our retinal system model the ganglion spike discharges are directly related to C_L and C_D, the relative excitatory level of the respective ganglion's membrane potential in each case for its discharge. We recall that in cells in the retina only the ganglions have action potentials and generate pulses to the optic nerve. Grusser and Grusser-Cornehls, (1987) give an equation to represent $\overline{R}$, the spike impulse frequency relation as $\overline{R} = R_0/(1 + k_i I) + k_g I/(1 + k_i I)$, the second term being proportional to the receptor potential $kI/(1 + k_i I)$ governing the ganglion excitation. The k values are for the

receptor adaptation states in the retina which change with light and dark via switching by the horizontal cells and size of the receptive field (RF) of the neurons and depend mainly on wavelength of illumination. R_0 is the low level spontaneous background discharge frequency and I is the light stimulus intensity. The expression is stated as valid over a working range of three decades of I values as was used in Fig 2.5a.

The Action Potentials from the Retinal Ganglions for Signalling to the LGN

Action potentials are of essentially fixed amplitude, usually reaching a value of 5 to 10 mV positive. Information cannot be carried in the amplitude of an action potential. Post synaptic potentials (PSPs) are of variable size (see Appendix B) and spread passively across the cell membrane, suffering a decrement in amplitude in the process, whereas action potentials propagate nondecrementally. That is, they retain their initial amplitude all the way down the axon. Action potential propagation (a few metres/sec) is actually a wave phenomenon and nothing physical moves down the axon. An action potential occurring at a given point on an axon provides suprathreshold de-polarisation of the axon tissue immediately in front of it. This generates a new action potential at that point and so the propagation continues. This corresponds to the repetitive cycles of the ganglion L-V responses for C_L and C_D in the retinal model.

The LGN input neuron encodes information about stimulus magnitude contained in the action potentials. The information is carried in the frequencies of pulses i.e. pulse frequency modulation (PFM). (This does not rule out more sophisticated encodings at given times or places in the nervous system. However all such encodings are based on the PFM principle of variation in the temporal distribution of pulses). In our case, this is spatial stimulus values for an edge. Convergence of inputs from a line of retinal ganglions use this analog spatial information in integration processes over spatial frequency channels at the LGN, as will be discussed in later Chapters for our model. The result is converted back to digital form for further transmission to the striate cortex V1. Such processes are part of the extreme properties of neurons not all of which are always required.

A brief comment on the processing abilities of neurons using their interconnections which are relevant to our application in later chapters is worth noting.

When we consider that some of the inputs to a neuron, eg at the LGN and at V1, may represent feedback from the neuron's own axon, and that an average neuron may have very many inputs, one can appreciate the powerful possibilities. With its connections it is often stated that it can "*integrate*" and "*differentiate*" and do other functions by virtue of feedback and analogue operation, similar to electronic devices. However, Crick has pointed out that the terms "integrate" and "differentiate" should not be taken at face value as a property of a single neuron itself as is sometimes implied in texts.

Because the information need not be synchronous for neurons (Kent, 1981, Geisler and Banks, 1995) other information may be coded in the temporal relation of the pulses. Examination of the electrical behaviour of a neuron reveals that the greater the positive input drive to the cell body, the more quickly the analogue voltage will reach threshold, and the more quickly a new pulse will be placed on the axon after the reset following the preceding pulse. This means that it is very easy to use frequency coding to indicate the magnitude of the summed input activity. Because of the "pulse stretchers" at the inputs to the neuron, and the time constant of the cell body, sequential pulses on the incoming axon can sum with one another to produce a greater analogue voltage. This voltage is proportional to the frequency of the incoming pulses and thus transforms frequency-coded input back to the analogue mode.

Interaction of inputs from different axons is termed "spatial summation", and interaction of sequential pulses on the same axon is termed "temporal summation". The basic "byte" has both a spatial and a temporal dimension. Two independent sets of information can be encoded in these two dimensions, and they can then interact in the receiving structure (ie: the postsynaptic neuron) in a way determined by physical and chemical properties of the cell's membrane. The spatial aspect of the byte is essentially digital information, and that the temporal aspect of the byte is essentially analogue information, although it is encoded in the frequency of digital pulses as illustrated in Fig 2.6.

Another desirable property of the neuron as a computer element is that speed of transmission of pulses down the axon can vary over a wide range, although it is always the same in any given axon. This means that high-speed axons can move data quickly, but low-speed axons may be employed effectively as delay lines (Kent, 1981). Because axons can have branches coming off at any point, we can have the equivalent of tapped delay lines for use in processing. There are some surprising examples of the utility of this feature in the central nervous system (CNS). It is apparent that the basic neuron is an enormously powerful tool. In practice, few situations call for all of the complexity of neurons and their connections – but the visual system neurology is complex. Fortunately the relevance to Information Theory prompts us to consider the concept of "information content" in our model. In essence, the information content of a process is the number of symbols and expressions inter-relating them which are required to formulate the process to a particular level of accuracy. This permits us to simplify the formulation of processes at the separate levels in the development of the information carried by the spatial gradients of C_L and C_D within the primary visual pathway.

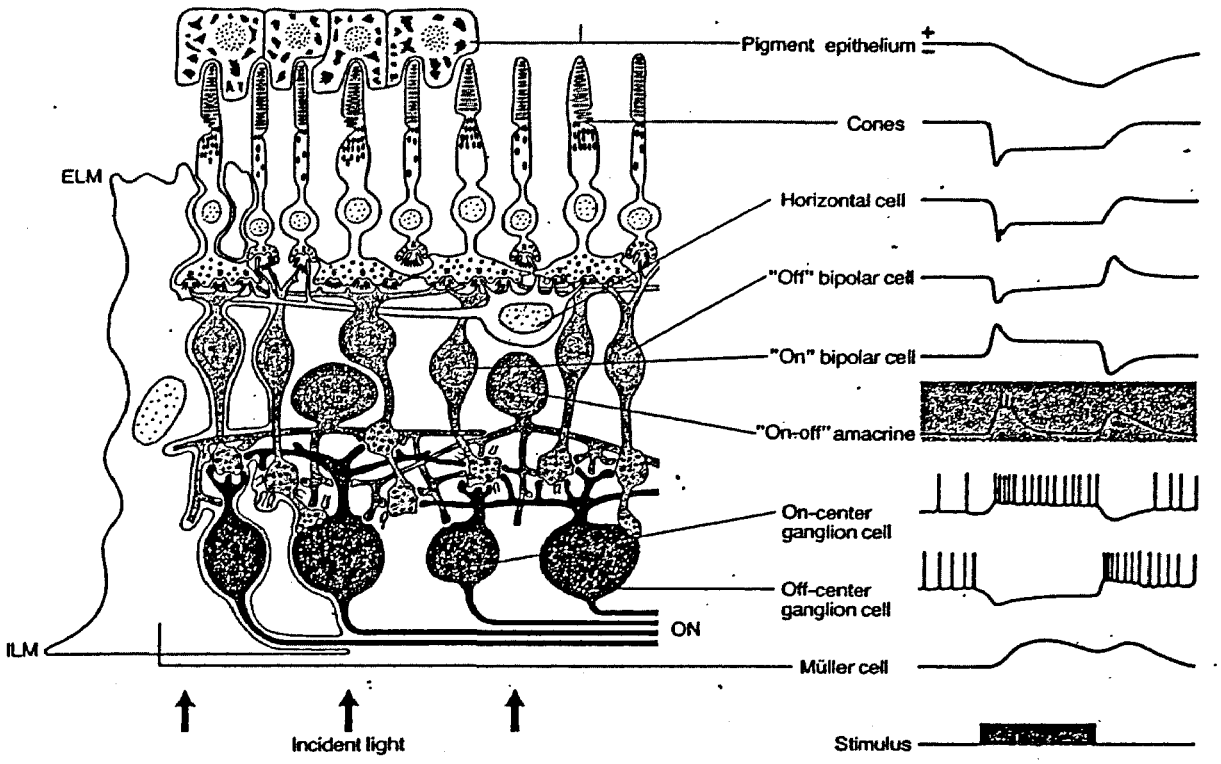

Fig 2.1(a) (Grusser-Cornehls, 1987)

Structure of the primate retina [redrawn schematically from an illustration by Boycott and Dowling, Proc.Roy.Soc. (Lond.) 166m80 (1966)] and diagram of the responses of single neurons in the retina to a light stimulus [Grusser, Fortschr. Opthalmol.80,502 (1983)]. ELM: external limiting membrane; ILM: internal limiting membrane; ON: axons of the optic nerve. Horizontal cells make additional contacts with bipolars that are not shown.

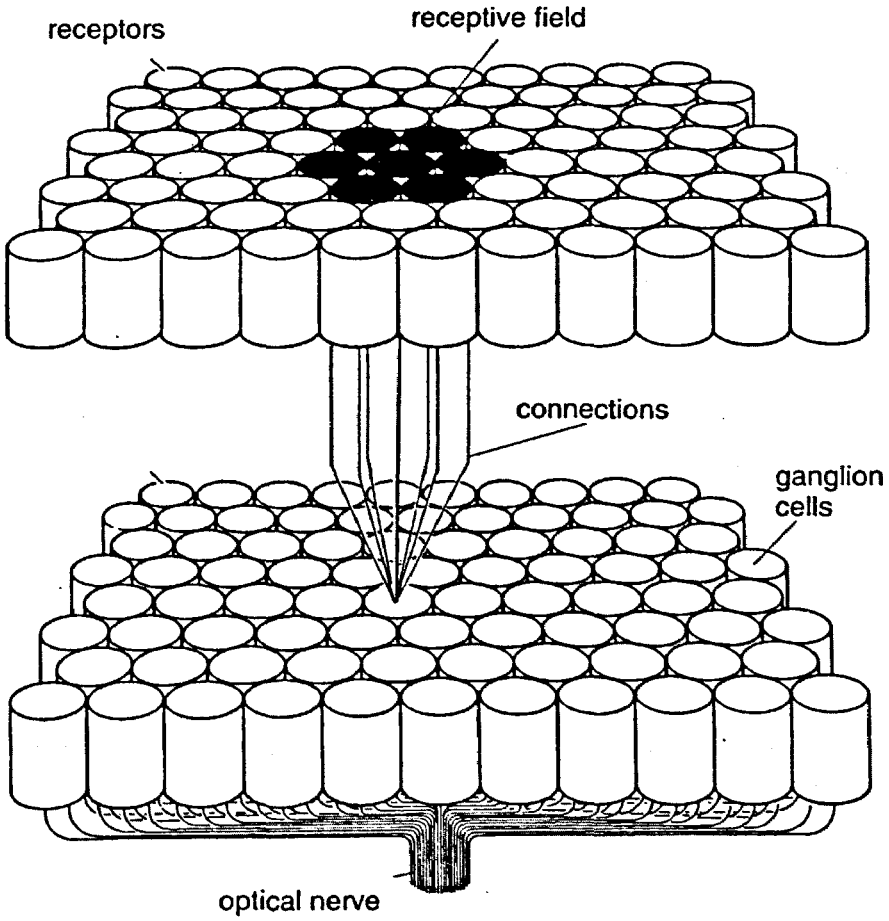

Fig 2.1(b) (Gross M. 1994)
Illustration of a receptive field that belong to <u>one</u> ganglion cell

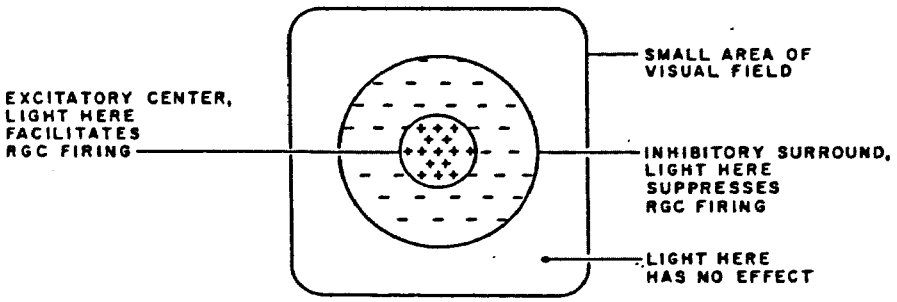

Fig 2.2(a) (Kent, 1981)

A small area of the visual field, showing the portions which can influence the output of a single, retinal ganglion cell (RGC) when illuminated. Some visual areas have an excitatory action (+) and others have an inhibitory action (-) on the RGC's firing rate

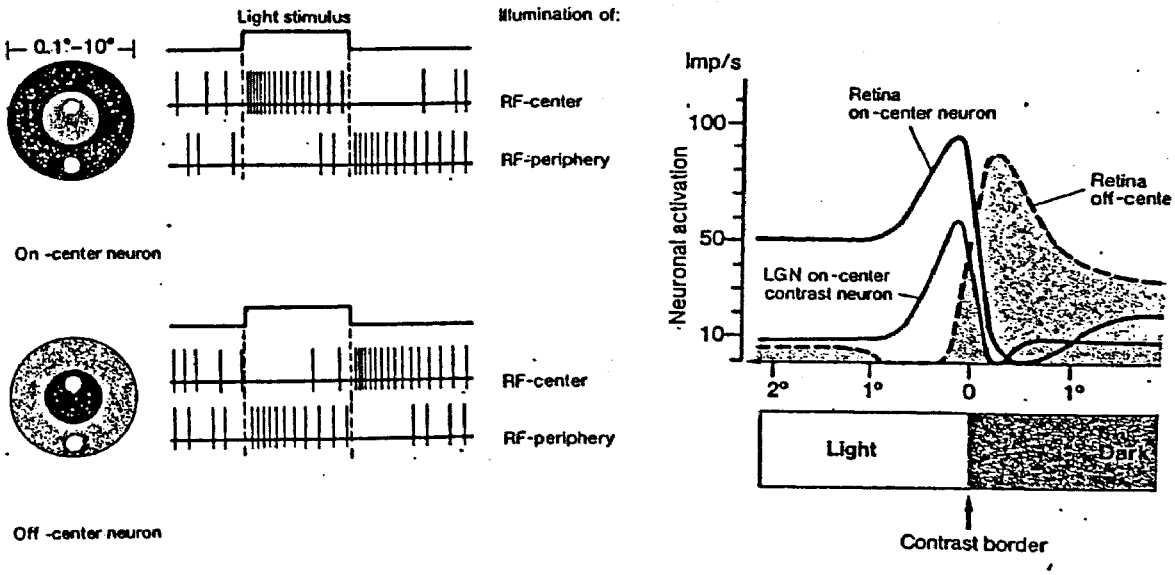

Fig 2.2(b) (Grusser and Grusser-Cornehls, 1987)

On-centre and off-centre neuron spike responses for activation light spots shown (left) and the activation level in impulses per second of retinal neurons at light/dark edge (right) also shown is the response from a subsequent LGN on-centre contrast neuron.

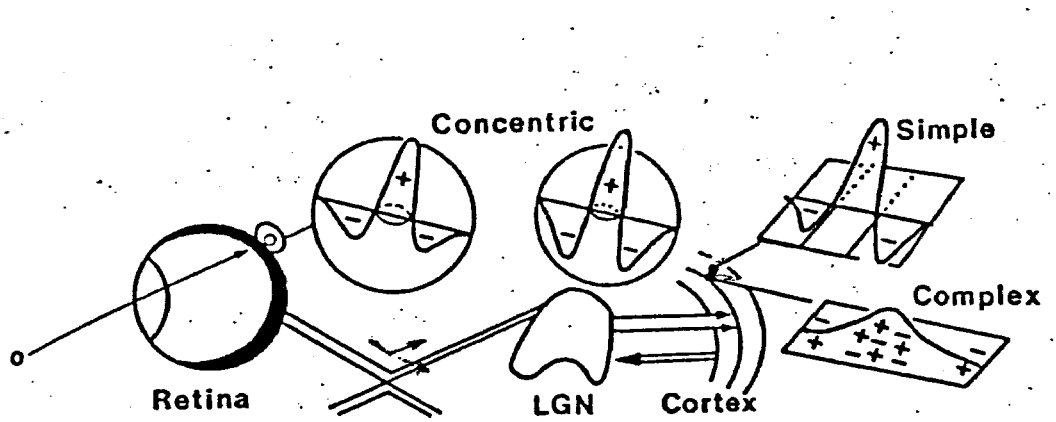

Fig 2.3 (Kulikowski, 1979)
Schematic diagram of the main visual pathways from retina to occipital cortex, showing the response profiles of receptive fields at various points along the pathway (positive to light spots, negativeto dark spots).

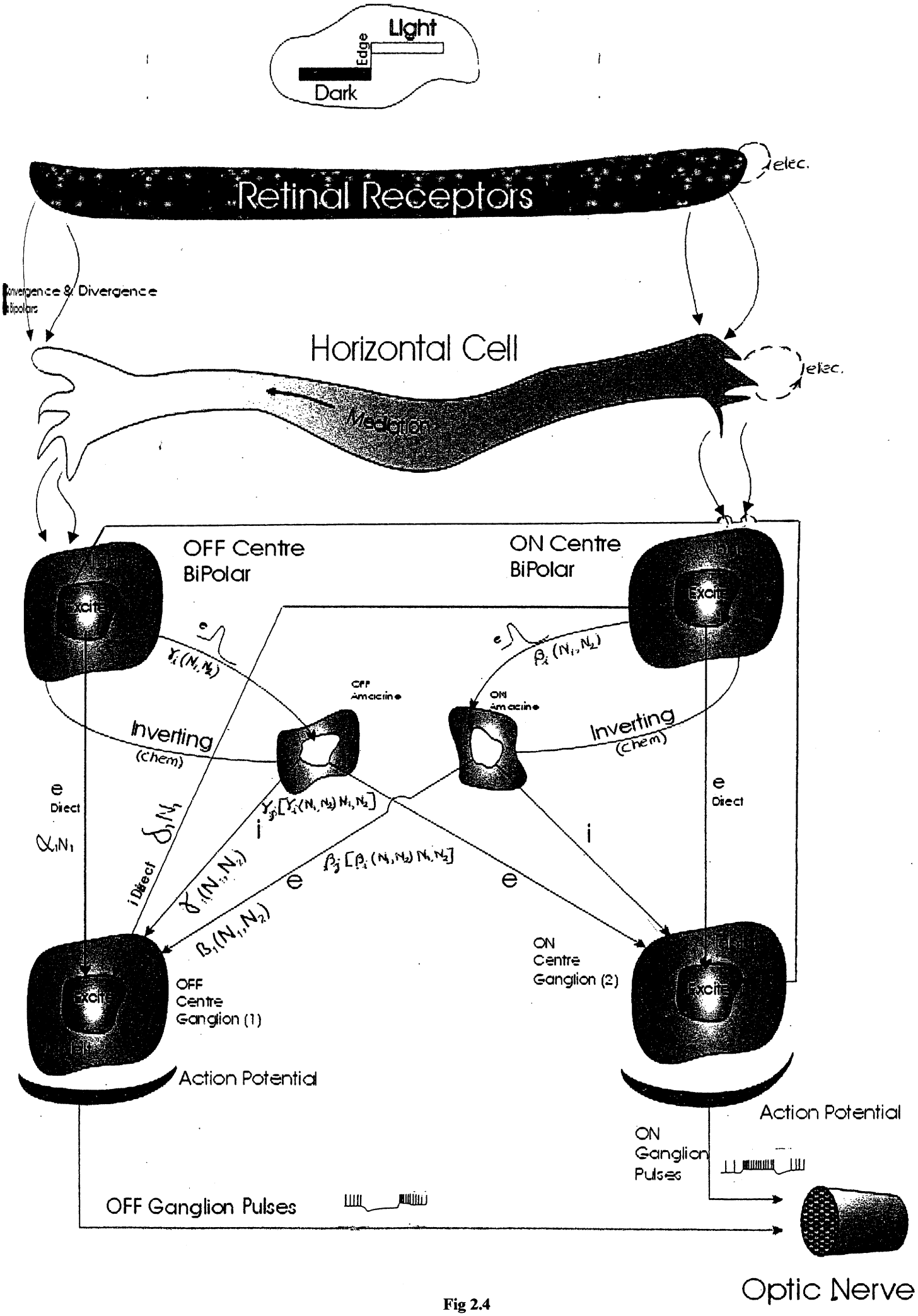

Fig 2.4
Signalling pathways of retina from receptors to ganglions and optic nerve

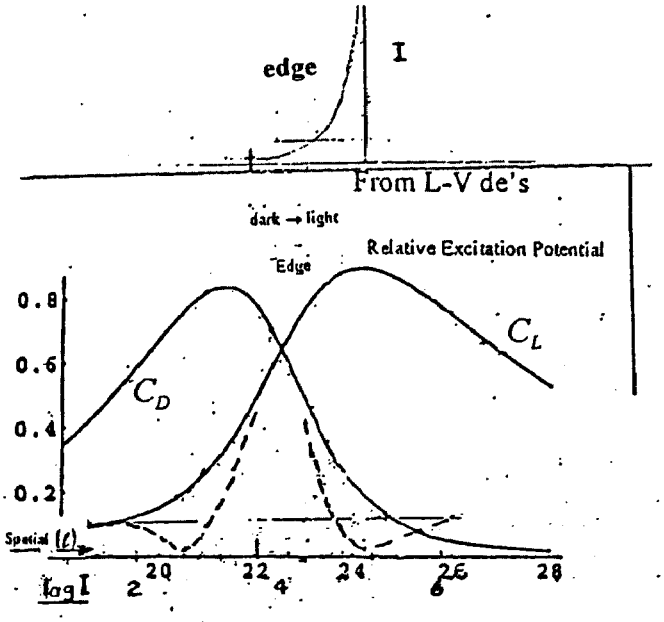

Fig 2.5a

Computer plots of C_L and C_D for L-V differential equations for an edge with scale for comparison with Fig 2.5b

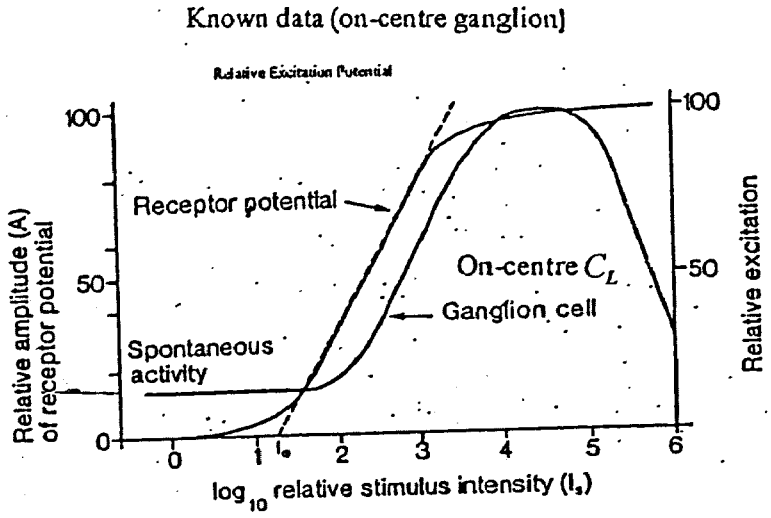

Fig 2.5b

Actual experimental data for C_L (Baylor and Fuortes, 1970)

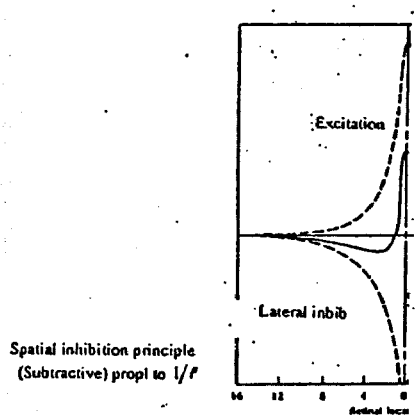

Each receptor excites a single cell body, which in turn sends impulses up the optic nerve and also along collaterals that spread over the retina. Wherever a collateral comes near to a cell body, an inhibitory synapse is formed.

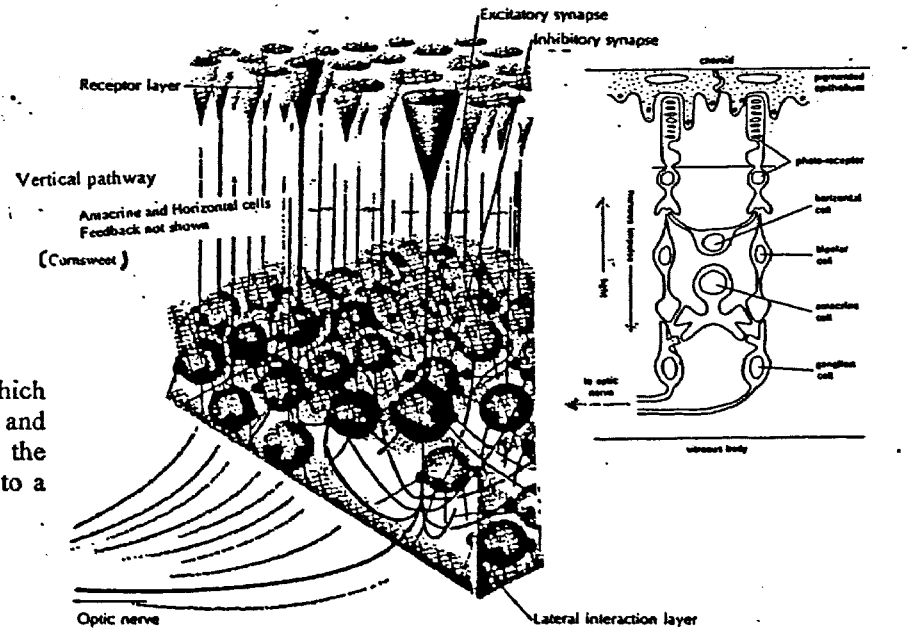

Fig 2.5c

Illustration of retinal physiology plus responses showing vertical pathway to ganglions and lateral inhibition layers

```
In[1]:= <<Graphics`PlotField`

In[11]:= sol = NDSolve[{x'[t]==0.5 x[t] - 1.5 x[t] y[t],
         y'[t]==-0.2 y[t] + 1.0 x[t] y[t],
         x[0]==0.2,y[0]==0.9},{x[t],y[t]},{t,18,28}]
         Plot[Evaluate[x[t] /. sol], {t,18,28},PlotRange -> All]
         Plot[Evaluate[y[t] /. sol], {t,18,28},PlotRange -> All]

Out[11]= {{x[t] → InterpolatingFunction[{{18., 28.}}, <>][t],
           y[t] → InterpolatingFunction[{{18., 28.}}, <>][t]}}
```

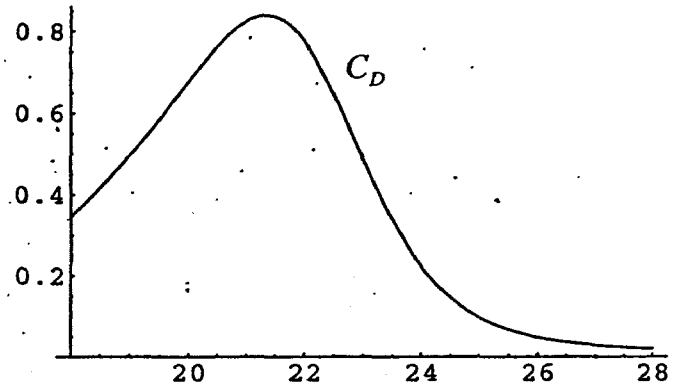


```
Out[12]= -Graphics-
```

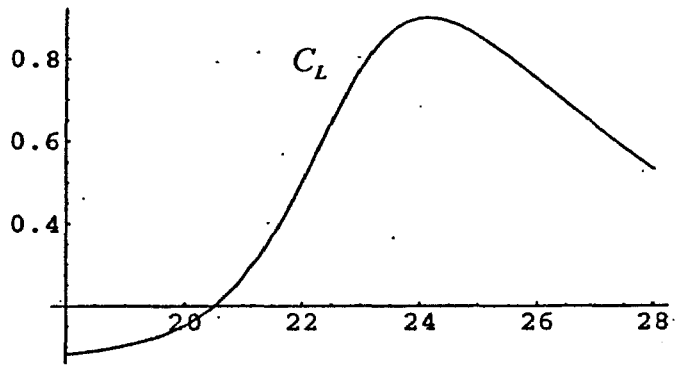


```
Out[13]= -Graphics-
```

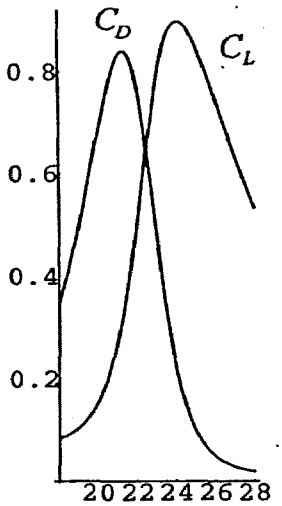

Fig 2.5d

Computer plots (from L-V de's) of C_L and C_D on the same scale as Fig 5a and also plotted together on a spatial scale of 10 units (18 to 28) equal to 0.5mm for a physical edge example.

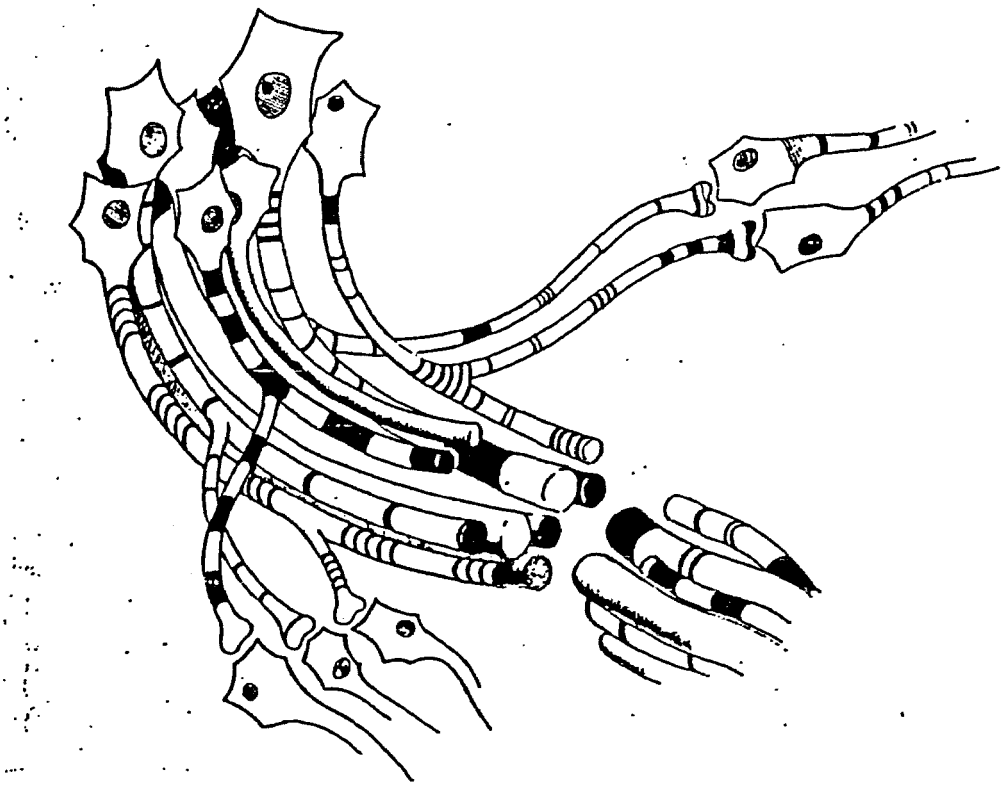

Fig 2.6 (Kent, 1981)

This figure illustrates the "two-dimensional byte" of the neural bus structure. A bundle of axons constituting a "bus" is shown coming from a group of neurons in the upper left. Neural pulses traveling down the axons are shown as dark areas. In a cross section through the "bus", we see that some axons are active and others inactive. These "spatial byte" permutations may be decoded by selecting fibres from the bundle to terminate on particular receiving elements. This is frequently accomplished, as shown here, by taking off collaterals from the desired elements of the bus. In addition, the active axons carry intensity information, which is seen in this figure as the pulse frequencies indicated by the spacing of the dark areas. The origin of the selected axon determines the kind of information it carries and its relative activity carries information about the intensity associated with that kind of data.

Chapter 3

Spatial Frequency and Colour Information sent to the Lateral Geniculate Nucleus

We briefly outline below the physiology in more detail. This leads us to considerations needed for information based modelling and the design of our experiment for adding noise in chapters to follow. It includes spatial and colour sensitivity of rods and cones and the distribution of information via the lateral geniculate nucleus in the visual pathways to the visual cortex.

As discussed in Chapter 2, the vertebrate visual system begins with the receptor cells in the retina. Light reaching these receptors has already been gathered and focused by the pupil and lens system of the eyeball. The structure of the human retina was shown in Fig 2.1 of Chapter 2 and more details for properties and distribution of rod and cone cells are shown in Figs 3.1 a,b,c,d of this chapter.

The rods and cones are physically located at the back of the retina and make synapse-like connections with bipolar cells. Because the spatial, spectral and temporal information gathered by the retina depends, in the first instance on the rod and cone receptors, we pause to give further details relevant to our application before proceeding to discuss the bipolars and other cells. The two major types of photoreceptors, rods and cones, play very different functional roles in vision as previously mentioned. Rods are important for peripheral vision and sensitive to dim light whereas cones are important for colour vision and visual acuity in brighter light. There are three types of cones, each with a different spectral sensitivity (which is the result of having different photopigments in the outer segment). The "long" (L), "middle" (M), and "short" (S) wavelength cones have peak spectral sensitivities at wavelengths of approximately 570, 540, and 440 nm, respectively. Information about the spectral wavelength distribution of the light falling on the retina is encoded by the relative activities of the L, M, and S cones. All rods have the same spectral sensitivity (and the same photopigment), peaking at about 500 nm.

The quality of spatial, temporal, and wavelength information encoded by the photoreceptors depends upon: (1) the spatial distribution of the photoreceptors across the retina, (2) the efficiency with which individual photoreceptors absorb light at different wavelengths (the absorbance spectrum), (3) the area over which the individual photoreceptors collect light (the receptor aperture), and (4) the length of time over which the individual photoreceptors integrate light.

The spatial distribution of cones and rods is highly nonuniform. Figure 3.1a shows the typical density distribution of rod and cone photoreceptors across the retina. Cone density decreases very rapidly with eccentricity; rods are absent in the fovea and reach a peak density at about 20 degrees. Moving across the retina away from the fovea to the periphery the cone density falls rapidly and is soon far exceeded by the rod density. An image is normally focused on the fovea and within the fovea the diameter of a cone reaches its minimum value. The cones are tightly packed with a spacing, centre to centre, of 0·12 – 0·15 mrad. The fovea is capable of the best resolution of an image: in fact the cone spacing can be shown to be well-matched to the highest resolvable spatial frequency for high mean luminaries (Chesters, 1982).

The neuron spatial response which produces contrast in defining an edge or other image at the visual cortex V1 and higher levels by a change from dark to light, or vice versa, consists of a number of separate Fourier frequency components of the retinal image variation in illumination such as across an edge region. The response shape across the region for any particular frequency component will cross from dark response to light response along the spatial axis. The spatial location of the crossings along the axis are called "zero crossings" and their location can differ from one spatial frequency component to another. For a "true edge" of an object the crossings are close together but for a false edge this condition is not maintained and the image is likely to be an artifact (Marr and Hildreth, 1980). We shall see how this condition for responses in the early vision system is incorporated in our model in a later chapter and is important in mammographic detection of edges in breast cancer lesions.

Typically, many receptor cells project to a given bipolar cell (i.e convergence) and a given receptor projects to many bipolar cells (divergence), although cones in the fovea at the centre of the retina appear to have their own bipolar-cell-lines. Convergence and divergence are very general principles of neural organisation and in the retina represent an early opportunity for some processing of the visual input. Bipolar cells do not support action potentials for pulse transmission but communicate via depolarising or hyperpolarising graded electric potential signals with the ganglion cells.

As outlined in Chapter 2, the on-centre and off-centre structure of the two basic types of ganglion cells provide an antagonistic process which, along with the convergent and divergent processes of neural connections, aids in the detection of boundaries. Further opportunities for retinal information processing are provided by the horizontal and amacrine cells, which laterally interconnect retinal elements at the receptor-bipolar and bipolar-ganglion interfaces respectively. The ganglion cell axons (which do carry action potentials) are gathered together into a "cable" as the optic nerve. The long axon (nerve fibre) of the on-centre and off-centre ganglion cells actually conducts the on-centre and off-centre ganglion information signals, C_L^g and C_D^g respectively, to the lateral geniculate nucleus of the thalamus. Some interactions, processing and reorganising of the message take place at the LGN for distribution to the primary visual area V1 of the brain located in the occipital cortex. Stimulus intensity is thus converted first to receptor potential magnitude which is in turn expressed in neural signals, as a frequency of action potentials. Action potential frequency is an approximately logarithmic function of stimulus intensity, a relation which is useful for encoding large ranges of intensity while maintaining high sensitivity to intensity differences at low levels of stimulation. In most cases the logarithmic transformation occurs in the generation of receptor potentials, followed by an approximately linear conversion of receptor potential to neural signal to the optic nerve. That signal is a spatio-temporal frequency modulated signal from which the spatial information, represented by gaps in the signal, can be extracted as analogue data by subsequent neuron processes. Details are in Appendix B.

We now note some relevant aspects of the cells of the LGN to which the retina transmits its signals. The axons of the retinal ganglion cells (RGC) make synaptic contact with the cells of the LGN just as the retinal elements made contact with the RGCs. Electrical activity experiments have found that the cells of the geniculate nuclei have response patterns rather similar to those of the RGCs, ie central spots and antagonistic surrounding rings. Essentially the same pattern is maintained from the ganglions to the LGN cells. This is illustrated for a typical on-centre, off-surround LGN thalamic cell in Figures 3.2a,b where the RGC receptive fields overlaps on to a thalamic cell and an integration with respect to spatial frequency occurs. This is an important hierarchical step in the evolution of information content.

Spectral colour responses occur in cells at the LGN and V1 and our experiment will be seen to utilise this property. As mentioned in Chapter 2, in addition to an on-centre response to one colour (eg red) and an off-surround response to a spectrally opponent wavelength (green), there are also "Type II" fields which give opposite responses to opponent colours but over the entire field (no centre-surround distinction). It is sufficient to say that a great deal of preliminary processing of colour information is done at the lateral geniculate level.

At the LGN level there is also processing which includes not only signals returning from the cortical areas to which the thalamic cells project, but also data from other brain regions that contribute to the analysis of visual information as indicated in Chapter 2. In addition, a form of information selection including attentional mechanisms and some spatial information from the cortex takes place from the brainstem's reticulate formation [see Appendix D] and is a further component of information contribution. The above will be described at a later stage for their role in the process.

At the next stage of the pathway, the visual cortex, with which the LGN has interactions, Hubel and Wiesel (1965) discovered a hierarchy of increasingly complex receptive fields. Many cortical cells examined responded to stimuli from either eye and had receptive fields with closely corresponding positions in the two retinas. This feature arises from

left and right eye inputs via the respective LGN's (Fig 3.3) and is the basis of many important properties of human vision. This includes the actual observer "perception" of image features as a result of interactions of inputs to the laminae of the primary visual cortex V1 and other visual areas.

Before proceeding, it is interesting to note the important relationship of the retina to the cortex. Despite the great ability of the human retina, a classic paper in 1959 by Lethin, Maturana, McCulloch and Pitts entitled "What the frog's eye tells the frog's brain", showed that the receptive fields of the frog are actually much more complex than those of the cat, monkey or human. The frog has a much more complex and highly organised retina. For example, it has a specialised class of ganglion cells responsive to small, dark convex moving edges ("bug detection"). However, the superior visual properties of the human come from the difference in deferring much of the complex processing and cognition of information to more powerful and flexible higher centres of the brain.

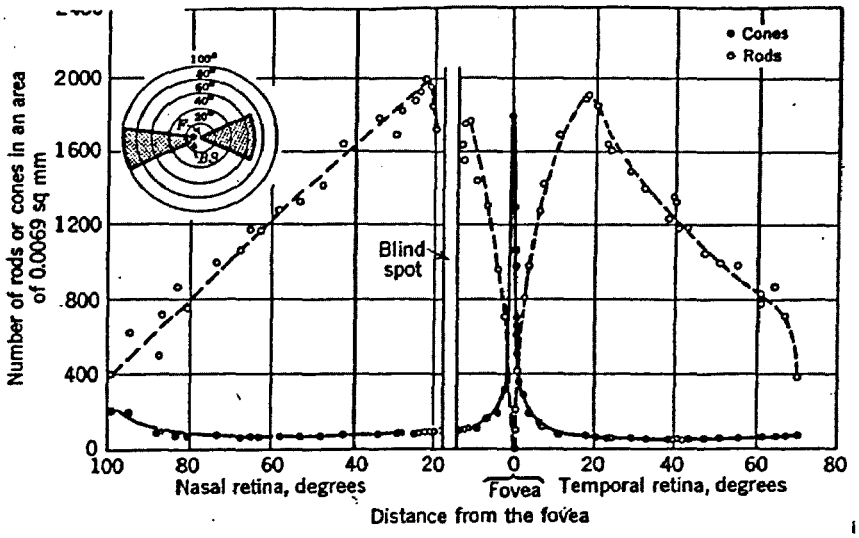

Fig 3.1(a) (Forgus, 1966)
Distribution of rods and cones throughout the retina. The number of end organs per unit-area from the fovea to the extreme periphery has been plotted. Cones are represented by solid, rods by open, circles. The inset shows the regions in obtaining the counts.

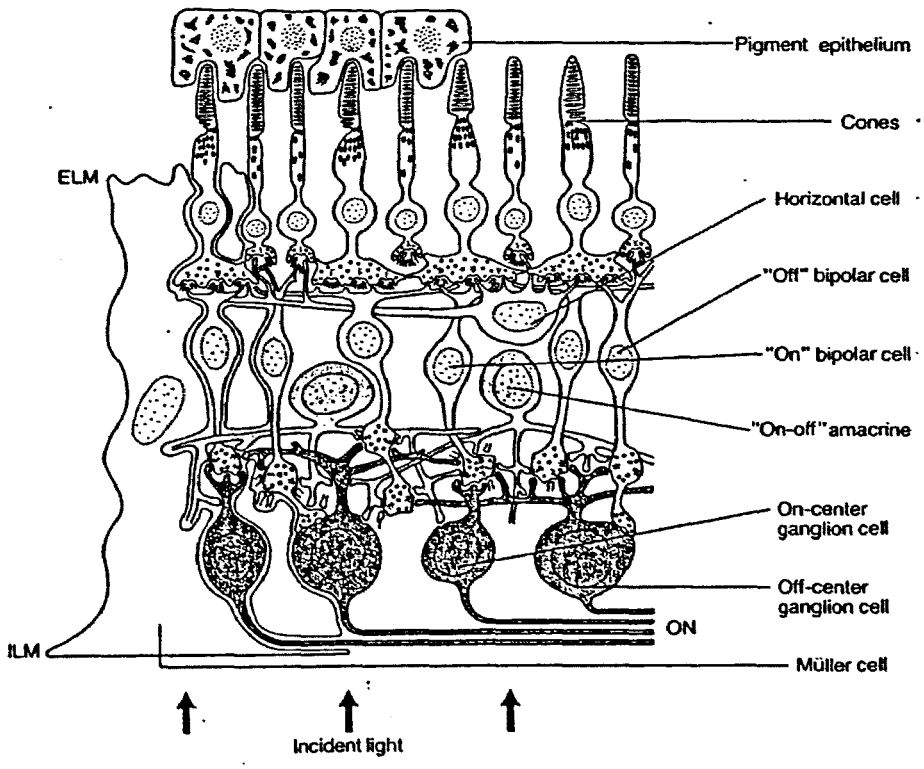

Fig 3.1(b) (Grusser and Grusser-Cornehls, 1987)
Structure of the primate retina

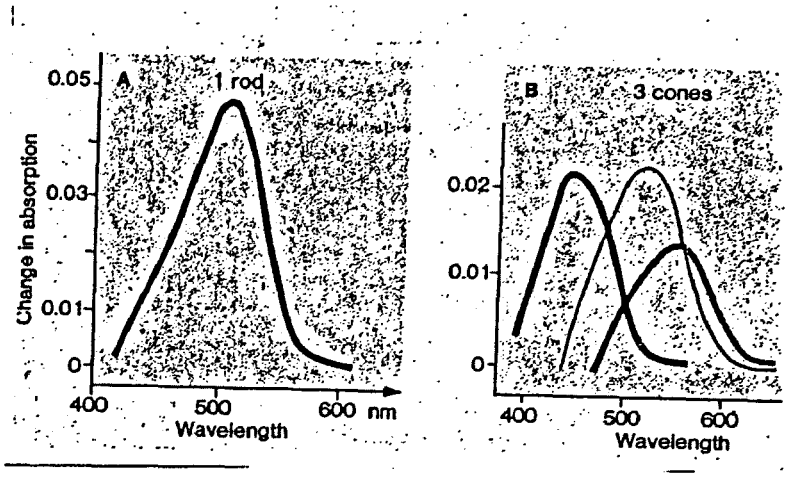

Fig 3.1(c) (adapted from Grusser and Grusser-Cornehls,1987)
Results of microspectrophotometric measurements of the spectral absorption of single receptors in the human retina (specimens from operations). The curves represent difference spectra (ie the difference in spectral absorption before and after bleaching). Three types of cone can be distinguished.

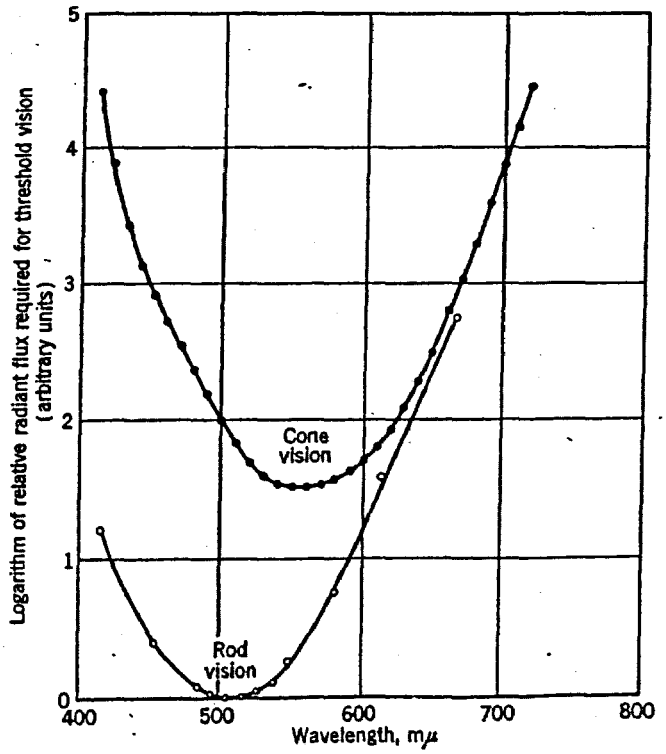

Fig 3.1(d) (Forgus, 1966)
Photopic (cone) and scotopic (rod) visibility curves compared. The relative amounts of energy needed to reach absolute threshold as a function of wavelength

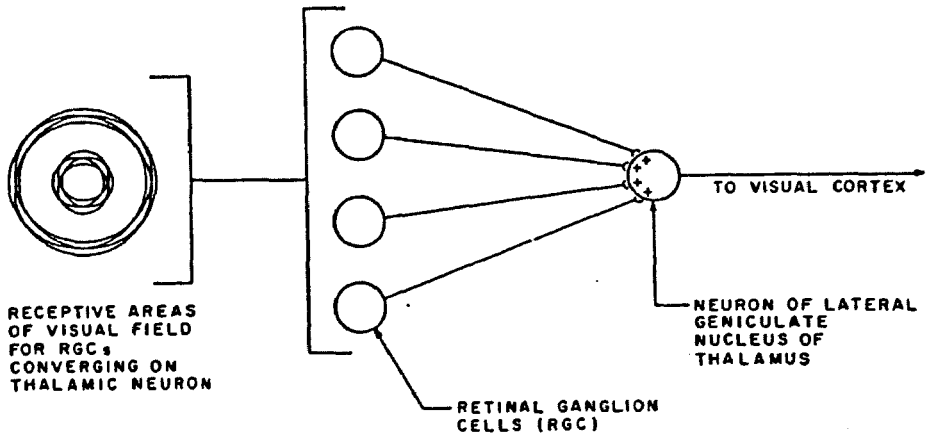

Fig 3.2(a) (Kent, 1981)

The convergence pattern of retinal ganglion cell (RGC) units on a thalamic cell, showing the spatial relations of the receptive fields of the RGCs which project to the same thalamic cell.

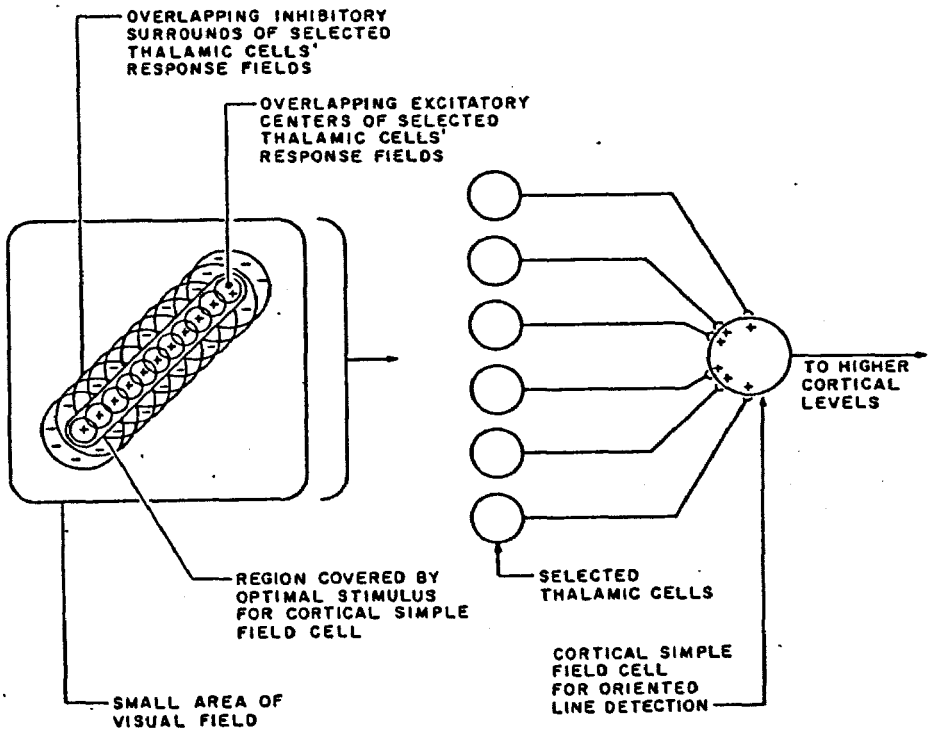

Fig 3.2b (Kent, 1981)

The pattern of convergence of thalamic cells onto a cortical oriented detector (simple field cell). The spatial relations of the receptive fields of the thalamic cells which project to this cell in an excitatory manner is so chosen that their own excitation regions lie in a straight line.

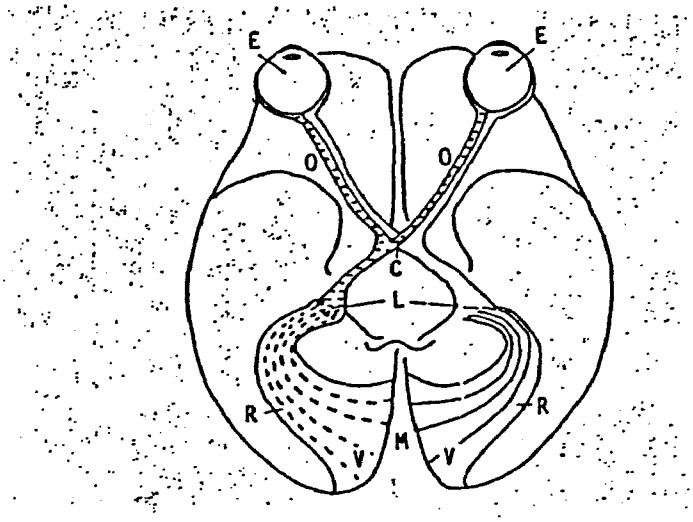

Fig 3.3 (Chesters, 1982)
Schematic view from underneath the brain of the primate visual system. E, eyes; O, optic nerve fibres; C, optic chaisma; L, lateral geniculate bodies; R, visual radiation (or geniculo-calcarine tract); V, visual cortex; M, mid-line between the two halves of the brain.

The optic nerve fibres from the inner half of each retina cross at the optic chiasma and are connected to the opposite side of the cortex: those from the outer half are connected to the same side. Thus, the left hemisphere receives input from the left half of the retina of each eye and similarly for the right hemisphere. Therefore it is possible for the brain to compare the messages received from both eyes.

Chapter 4

Processes at LGN, V1 and Signalling Interchanges

This chapter examines functions of the LGN and those at V1 in order to progress to a spatial model for edge detection in subsequent Chapters.

The majority of the information encoded by the retina is transmitted to the LGN of the thalamus. The LGN, although only a small part (approximately 1.5 million cells) of the thalamus is "a baffling combination of apparent simplicity but important complexity" (Crick 1994).

We will now consider further functions of the LGN. Supporting background material is given in Appendix C. The LGN is divided into six layers. Each layer of the LGN receives input from one eye only, three layers from the left eye and three from the right eye (Fig 4.1). The upper four LGN layers (the parvocellular laminae) receive synaptic input from the P ganglion cells, the lower two layers (the magnocellular laminae) receive input from the M ganglion cells. Simple features extraction from the input information is the result of thalamic LGN $\leftrightarrow$ cortical interchanges plus some control effects from the reticulate formation as will be discussed later.

The LGN transforms the signals by subdividing its on-centre and off-centre signals and selecting or enhancing components used by the selective neurons of the cortex for sizes, orientations, direction of motion, colour and binocular disparition. The two M and P streams from the relevant retinal ganglion types are input to the LGN as designated in Fig 4.1. It is generally believed that the magno stream subserves crucial aspects of motion and depth perception and that the parvo stream subserves crucial aspects of spatial detail, form and perception of colour. Various cortical areas act as sub-processors performing detail work for the LGN as it routes information to and from the cortical regions.

The response of the human vision system in viewing an edge involves both the processes of neurology and psychophysical perception. The principle of spatial change of slope of the on-centre and off-centre ganglion response applies to acutance. Edge gradient is related to *subjective "sharpness"* by an observer. US Air Force studies (reference by Biberman (1973) have shown that when detail appears "sharp", target objects are more rapidly found in an image presented to an observer such as in mammographic screening. They can distract a less experienced observer from other subtle, less sharp but important features. The actual psychophysical process involves input from the reticulate formation (see Appendix D), an elongated structure in the upper brain stem for awareness and attention. In vision this involves the psychophysical Weber-based fraction $\Delta\varphi/\varphi$ of the stimulus change $\Delta\varphi$ relative to an initial stimulus level φ. We will be discussing psychophysical aspects of mammographic inspection in a later chapter but a brief comment on the reticular formation is relevant to searching a mammogram. The modulating inputs from the reticular formation are diffusely connected through the forebrain and serve to bias the cells there towards or away from the "firing" level. This not only has implications for the rate of activity in these cells, but also influences the nature of the processing and interactions they perform. Not only the level of activity and speed of processing, but also the *nature* of processing, is affected in ways appropriate to the degree of attention required by a particular situation such as in searching a mammogram .

There is clearly a great amount of processing done between the LGN and V1. The basic processes are noted below with regard to spatial information content. As a guide to the following descriptions listed below, Fig 4.2 is a representation of the functions performed in the visual pathway from retina to V1 via the LGN. It will be used again in Chapter 5 with equation formation shown for processes at V1.

(i) **Signal Transmission and Information Extraction**

Spatial information is contained in the spatio-frequency modulation of the pulses where the spatial analogue part is in the code of the retinal ganglion signals. It can be extracted and this is an important biophysical property of neurons (see Appendix

B). As pointed out previously, no information can be carried by the fixed amplitude of an action potential. It is the combination of spatial and frequency modulation of the pulses which carries the information.

(ii) **LGN Processes**

LGN neurons have concentrically organised receptive fields (RF) similar to those in the retina. In some LGN neurons the mechanisms of simultaneous contrast are distinctly enhanced ("contrast neurons"). Others transmit predominantly the local light/dark value in the visual pattern ("light-dark neurons"). Others are characterised by RF's which are "colour-specific". An important fact for our model is that the LGN cells receive positive inputs from retinal ganglion cells whose positive centres are close together as shown in Chapter 3 Fig 3.2a. So, essentially, the same spatial information including pattern shape is maintained with regard to relative positions of the image.

(iii) **Spatial Frequency Channels**

Separate spatial frequency information is sent from the LGN to the visual cortex V1. There are also exchanges of information between V1 and LGN. This process is often considered as the equivalent of several filters in parallel, centred at different frequencies in order to cover the spatial information content of the signals (Chesters, 1982). With reference to Fig 4.3a, the contribution to the spatial analogue value $\frac{dC_L}{d\ell}$ at the LGN in liaison with exchanges with V1 can be expressed as $\int \frac{dC_L}{d\ell} df$. This covers the spatial frequency content of the ganglion cells involved from the overlap mentioned in (ii). Similarly for $\frac{dC_D}{d\ell}$. Both C_L and C_D are functions of ℓ and f. However, the extraction for use of the separate frequency bands f_i is done at V1 not at the LGN (Kent p118).

The actual process of a spatial frequency integration in the brief time required by V1 can be modelled by discrete entity principles for approximation. It would require only a (matrix) multiplication of the spatial gradient frequency components in sequence to form the (matrix) summation products with the vector of frequency components. The ability of groups of neurons for integration and differentiation processes are outlined in Appendix B, as mentioned previously.

At V1 the result of LGN/V1 exchanges affecting spatial gradients is that the single lines of the selected LGN results from spatial frequency integration are integrated but now spatially, over lines ℓ of line detector neurons. This takes place at V1 in conjunction with V2 in particular. As indicated in Fig 4.2, integration is provided spatially with respect to ℓ, of the result given for the spatial frequency integration (using selected cells) at the LGN in (iii).

The Fourier spatial frequency components from the LGN and utilised at V1 provide the subsequent "spatial coincidence" components for a true or false edge. A true edge requires that the zero crossings along the spatial axis should be consistent, ie "reasonably close", as stated by Marr and Hildreth (1980), for the groups of spatial frequencies.

(iv) **Other LGN Processes**

As mentioned previously, the LGN neurons receive numerous synapses from optic axon terminals having cells in the brainstem for spatially directed attention, associated eye movements and wakefulness originating from the reticulate formation. It is believed that these may also influence the spatial visual signal in the LGN (Grusser, 1987 and Kent, 1981) regarding wanted, or not wanted, parts for the observer's processing action. In other words, there is a selective spatial frequency suppression effect as discussed in more recent research papers (Nestares and Heeger, 1997 and Carandini et al, 2002).

The processing in the LGN is still not well understood (Crick 1994). For example, there are many back projections from layer 6 of V1. Their effect is not known but may be subdued because of their destination locations at the distant dendrites of the LGN. The LGN contrast neurons' output have a reduced spontaneous firing rate response compared with those of the retinal ganglions. This can be seen in Fig 4.3 from Grusser, (1987) but the ratio of peak to trough in the LGN contrast neurons' output is somewhat improved by some process such as that in (ii) above.

(v) **Magno and Parvo Signals**

The outputs from the two LGN sublayers of layer 4C project, in turn, to three other layers of V1 (Fig 4.1). Sublayer $4C\alpha$ projects to layer 4B and sublayer $4C\beta$ to layers 2 and 3. These are the main inputs. The magno, (M) and parvo, (P) channels with their particular information contents, stay separate as they progress to the primary visual cortex and have separate inputs but can then interact for various cooperative requirements (Zeki, 1993, p301 and 187).

In other words, although the M and P pathway have different input locations to V1, there are interactions between the P and M systems at V1. The specialised visual areas of the cortex provide back (re-entrant) projections to both area V1 and area V2. These could serve to unite signals derived from the M and P pathways (Zeki, and Shipps, 1988). Zeki points out that anatomically there is no total isolation of the two systems in the cortex. The organisation seems to be such that the specialised areas of the visual cortex will draw on signals from any source, be it in the P or the M, to undertake their specialised functions. In this regard it is noted that there is a complementary property if the processing capacity of the M and P channel for temporal and spatial frequency (Fig 4.4) is required (Zeki, 1993). Therefore, the general properties of C_L and C_D components for M and P signals may not need to be visually distinct at V1. The foregoing also suggests that the properties of the governing differential equations for M and P components can belong to the same class of equations, which we will see in following chapters.

(vi) **Laminae Messaging Abilities for Integration of LGN Inputs and C_L, C_D Interactions**

At the cortical area the known rapid messaging required indicates that there is only a limited amount of iterative computation done before sending messages to other areas (Crick 1994). There is no evidence of a set of inhibitory synapses which would be required before the axon exits from that part of the cortical sheet for many computations to be done. It probably implies that connections between various cortical areas can be as important as those within each single cortical area when the brain needs to establish a working coalition of activities very rapidly. Also we note new experimental and theoretical evidence for local recurrent cortical micro circuits (Fig 4.5) (Martin, 2002).

There are known line integrations at V1 with respect to ℓ of the spatial frequency integration from the LGN in (iii) ie $\iint \frac{dC_L}{d\ell} df\, d\ell$. Similarly for the off-centre case, plus other results at V1 from interactions between V1 laminae of components of C_L and C_D. Both processes could actually be achieved simply and rapidly within the V1 laminae as follows:

(a) **Integration in V1 Laminae of the LGN Output over the Spatial Strip ℓ**

As mentioned previously in the interpretation from the LGN, simple successive displacements of a sequence components of the integrand can be used in the laminae to produce a sequence representing the integration. The actual interactions to be integrated are presented below.

(b) **The Interactions of C_L and C_D**

The simplest nonlinear interactions would be of a bilinear product form. However, more sophisticated processes involving such product forms will

also be present as indicated by Crick (1994) in Fig 4.6. The requirements of various V1 outputs are different such as for spatial, form and colour which would require different combinations of product interactions.

What is required for our spatial model is a simple method which can represent the multiplicity of separate, non-sequential interactions of the combinations of the sequences of components of the C_L and C_D inputs to V1. This is a more involved operation than simple "integration" because it involves both previous and current interaction of components. The information inputs are both *along* parts of the V1 structure and also to individual layers in *depth* as indicated in Fig 4.6 (Crick 1994), ie the interactions of components from the several sources are between various layers of V1 and at locations along V1.

(vii) **A Possible Laminae Interaction Algorithm**

A simple mathematical convolution process is suggested for consideration and is similar to the simple process for the rapid line integration of the C_L and of the C_D spatial frequencies. The method is shown for example in Cuenot and Durling, (1969). It seems neurologically possible and is shown in Fig 4.7, in principle, for the case of C_L, C_D interactions where the S(G) sequences (left hand column) are simply displaced one at a time, for successive processes of addition, as shown in the last line convolution result. It can be adapted to the neuro-physics and could provide the requirement for this type of processing in the laminae of the visual cortex for simple and fast messaging to other cortical areas and exchanges with the LGN. The process is outlined as follows for the interaction of C_L, C_D components.

Let us represent the spatial ℓ and spatial frequency f components for C_L and C_D as a temporal sequence of units of (ℓ, f) information in the neuron signals as $S(A) = a_0, a_1, a_2, \ldots\ldots$ for $C_L(\ell, f)$ (to avoid awkward symbol superscript and

subscript notation). Likewise for $C_D(\ell, f)$ signal information components we have the sequence $S(G) = g_0, g_1, g_2, \ldots\ldots$ (Some a_i and g_i may be zero). The result of interactions of the two sequences in the V1 laminae will be taken as the convolution of sequence A and sequence G components, ie the sum of products of the components in the algorithm of Fig 4.7. "Convolution" allows for non-sequential combinations of the interactions. It also shows how a simple time difference of two sequences of components (such as indicated in Fig 4.7) can produce a new sequence result written as $S[B] = S[A] * S[G]$ which contains the low order interactions (eg $a_1 g_0$) followed by $a_0 g_1 + a_1 g_0$ with progressively higher order interactions for use in a working coalition at V1.

In summary, the output sequence terms begin with the low order combinations in the initial terms eg (a_0, a_1) of C_L with those of the initial C_D components (eg g_0, g_1) giving $(a_1 g_0 + a_0 g_1)$ and follows with separate sequence terms involving the sum of progressive higher order combinations as shown in Fig 4.7. Operations for addition, subtraction, differentiation and integration using impulse sequences are given in texts, (eg Cuenad and Durling, 1969). In the foregoing manner any combinations are separately available from V1 for the functional specific regions of the prestriate cortex including the spatially sensitive V2 (Fig 4.8).

(viii) **The Form of the Interaction Result**

As can be seen in the last component of the sequence in Fig 4.7 the resulting final interaction term for spatial components between a lamina i and a lamina j would be $F = \sum_{i=0}^{k} a_i g_j$, $j = n - i$ and n is the number of laminae involved for the spatial information required. In our V1 C_L and C_D notation it corresponds to $F = \sum(b_{ij} C_{Li} . C_{Dj})$ where b_{ij} is a weighting factor dependent upon the strength of

the neuron-to-neuron synapse. Some $b(i,j)$ will be zero where there is no interaction between an i and a j lamina. This spatial F component is also the basis of the observer's selective spatial frequency suppression effect for unwanted detail surrounding the image acting on F, as will be included in our model. The V1 product summation result of interactions is in addition to the integration at V1 with respect to ℓ of the spatial frequency information from the LGN. This can also take place in the laminae processes by a simple sequence process as indicated previously

(ix) **Conversion of Temporal to Spatial Pattern in the Cortex**

Such a time-channel pattern of neuronal signals can be shown to be converted uniquely into a *spatial* pattern in the cortex under conditions which are not too restrictive. This was first demonstrated with quantitative support in a computer graphical model by Farley and Clark (in 1961), (see Appendix E). There has also been related temporal→spatial transfers noted in a neural net simulation of patches of cortical neurons which are dynamic in time but have a simplified spatial response (Cook, 1986). The processes of temporal→spatial have also been supported by recent work included in a review article by Syme et al (2002). As a result of the foregoing temporal→spatial relationship we will use spatial derivatives in our model.

(x) **Limitation of Models of V1 Processes**

Needless to say the V1 and other associated cortical regions are much more complex than our (or any other) model can fully represent. They defy modelling even if they were better known. However, the point we wish to make is that the processes required and the specific interaction result, F, for C_L and C_D signals to achieve the requirements in speed, could arise in the manner suggested in our interaction model illustrated in Fig 4.7. It is also consistent with the fact that visual areas are not connected strictly serially with each other. This is known medically from specific visual defects (Grusser and Grusser-Cornehls, 1989).

We now proceed in Chapter 5 to organise the foregoing processes operating on C_L and C_D as the basis of information content enabling a formulation for a functional model for the spatial gradients for edge responses.

The use of information content from Information Theory is also desirable in respect to the foregoing interaction processes at V1 in the present chapter. The primary visual cortex V1 is dominated by complex cells which is, at first, surprising because complex cells are insensitive to spatial phase which is generally believed necessary for perceptual recognition of images. However, Shames and von der Malsburg (2002) have shown that whereas *individual* complex cell responses are phase insensitive, population group responses contain sufficient information for provision of image perception. This supports our modelling and use of information content for C_L and C_D group responses.

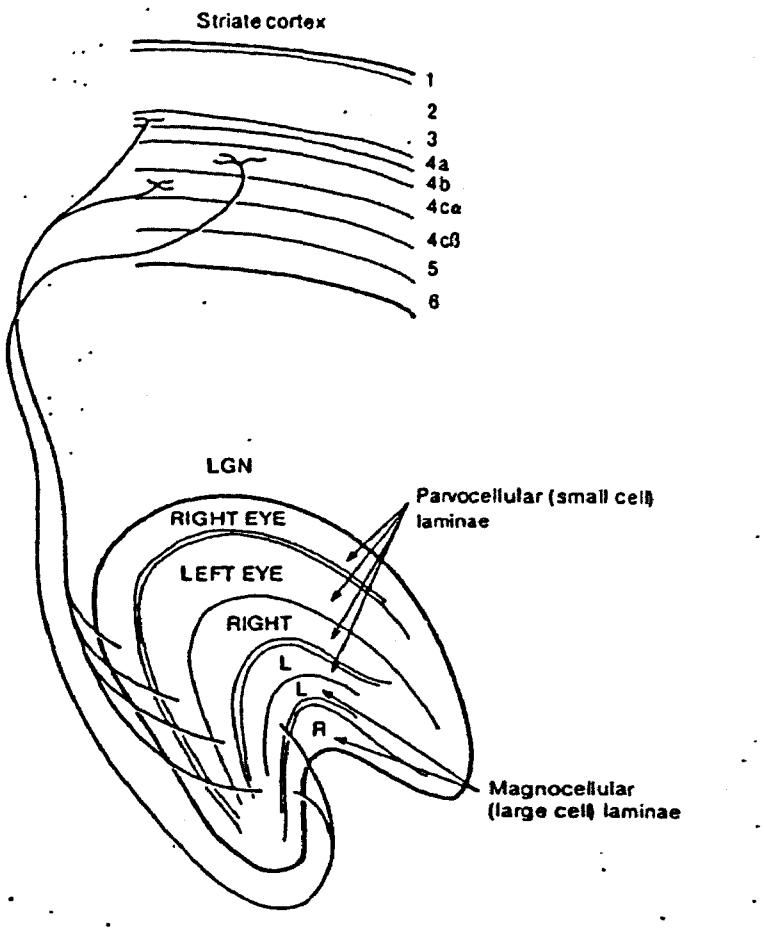

Fig 4.1 (Geissler and Banks, 1995)
Schematic diagram of a vertical section through the lateral geniculate nucleus and through striate cortex (V1) of the primate visual system.

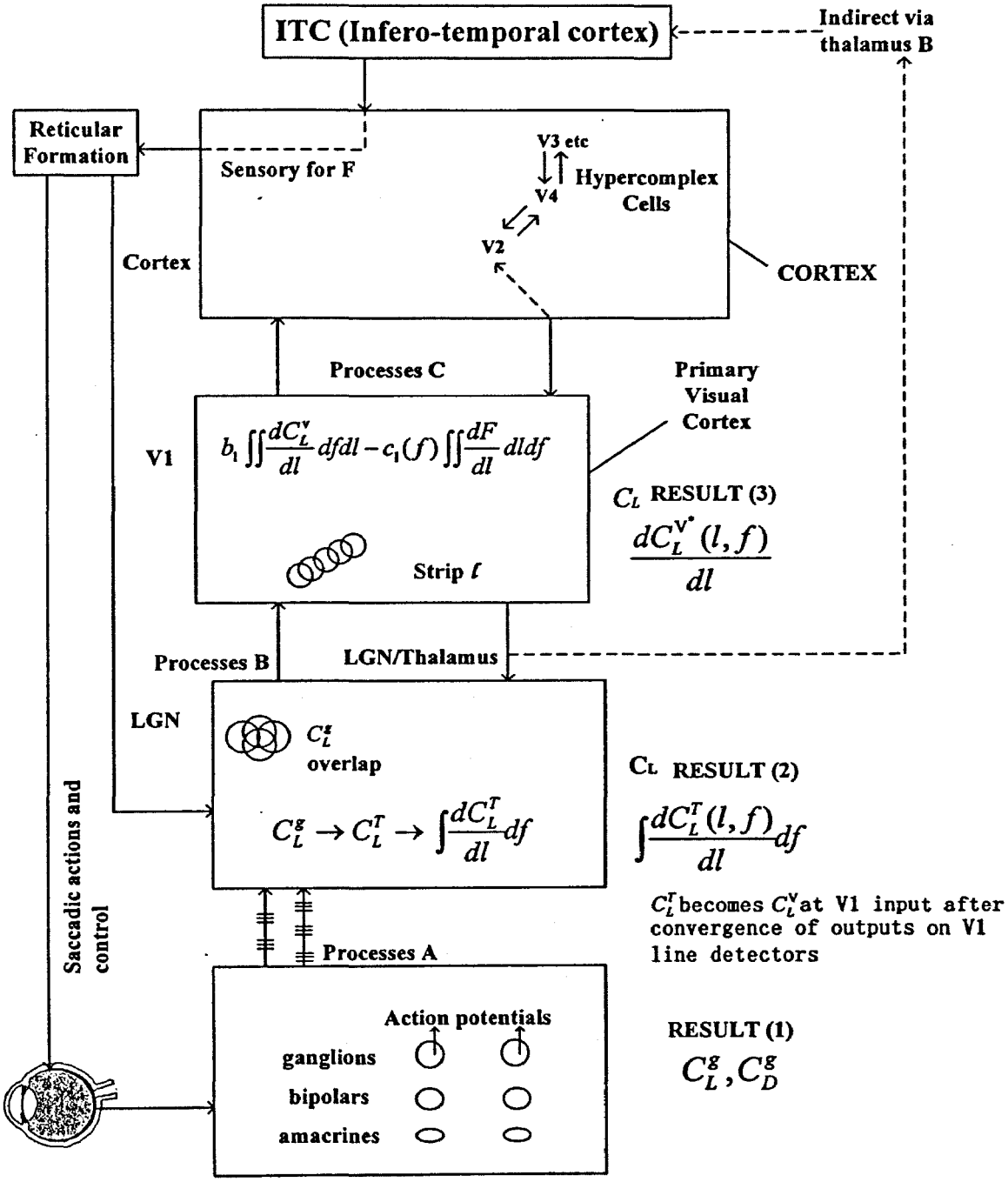

Fig 4.2
Illustration of the physiological component processes listed in the text.

one edge

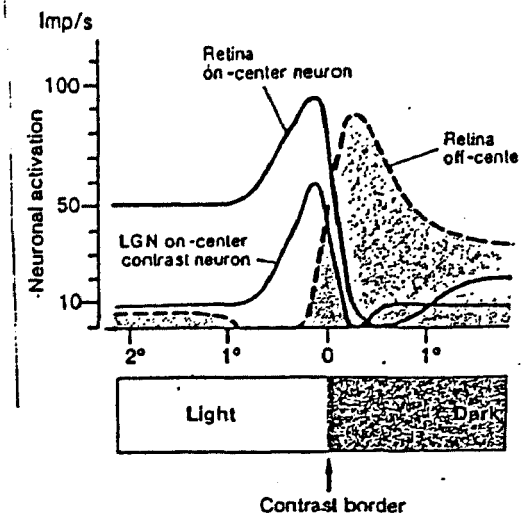

Fig 4.3 (Grusser and Grusser-Cornehls, 1987)
Retinal on-centre and off-centre neuron activation (impulses per second) at an edge of light to dark illumination. Response for an LGN on-centre contrast neuron also shown.

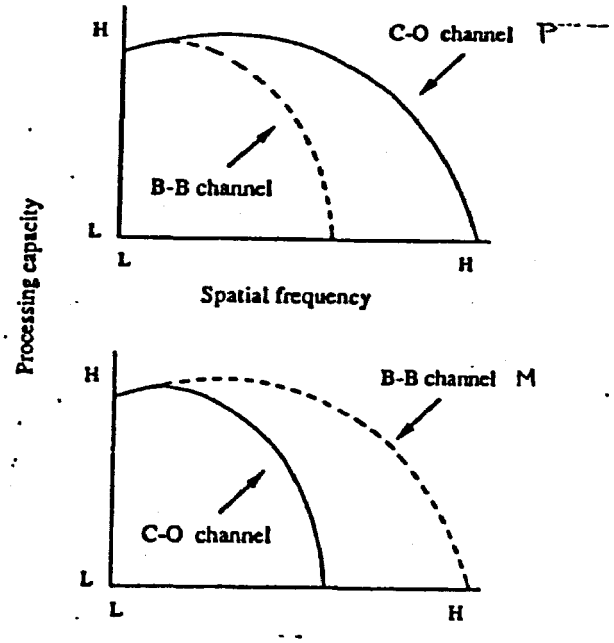

Fig 4.4 (Milner and Goodale, 1995, adapted)
Illustration of the different processing capacities low L to high H, of magno (M) and parvo (P) channels for spatially modulated (upper diagram) and temporally modulated stimuli (lower diagram).

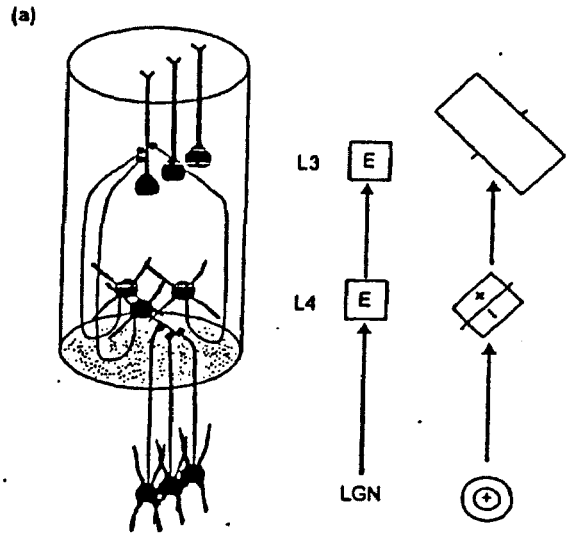

Fig 4.5a (Martin, 2002)
Basis of visual cortex hierarchical model of Hubel and Wiesel.

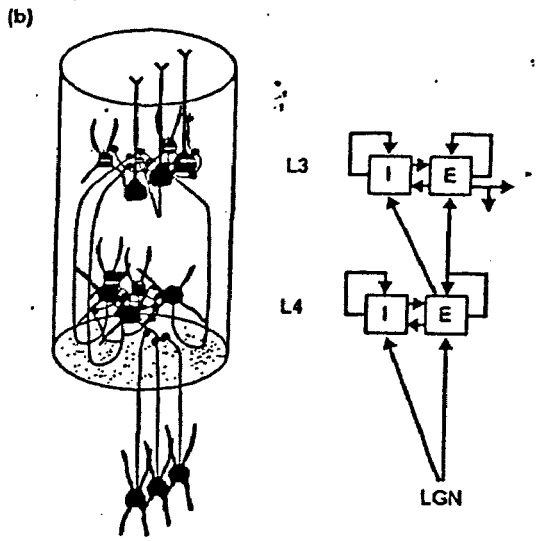

Fig 4.5b (Martin, 2002)
More recent alternative hierarchy with recurrent connections indicated

"Current Opinion in Neurobiology", 2002

Schematics of the vertical columns of visual cortex. (a) The hierarchical model of Hubel and Wiesel. It has two stages: neurons of the LGN with their concentric centre-surround receptive fields converge on layer 4 (L4) neurons to form 'simple' receptive fields. The layer 4 neurons then converge on layer 3 (L3) neurons to form 'complex' receptive fields. Both simple and complex cells lie within the same orientation column, indicated by cylinder. The cardinal characteristic of the complex cells is their position invariance – an optimal oriented stimulus placed anywhere in the receptive field gives the same response. Responses of simple cells are highly position-dependent and sign-dependent. Only feedforward excitatory connections are considered in their model. Lefthand column indicates schematic of circuitry, righthand columns the receptive field structure of neurons at the three stages of the hierarchy. (b) An alternative hierarchy. Layers 3 and 4 contain ex citatory (E) and inhibitory (I) neurons that are recurrently connected in every possible combination. Most recurrent connections to any neuron are from neighbours. It is out of this collective computation that the functional maps are formed.

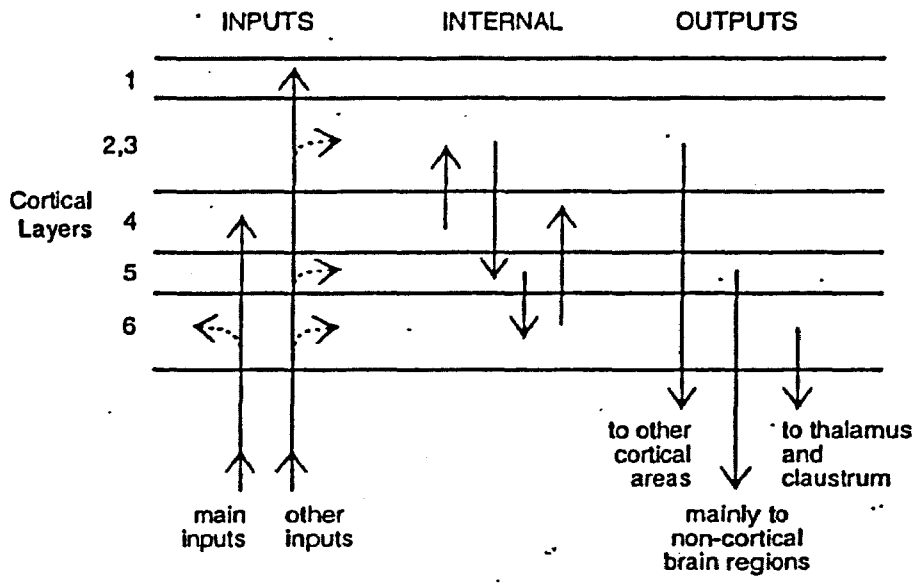

Fig 4.6 (Crick, 1994)
A grossly simplified diagram showing some of the major pathways within cortical area V1. There are many sideways connections that are not shown in this diagram.

The main, but not the only, entrance to a cortical area is into layer 4 or, when this is small or absent, to the lower part of layer 3. Layer 4 connects mainly to the upper layers, 2 and 3, and they in their turn have a large local connection to layer 5. Layer 5 sends longish "horizontal" local connections to layer 6 beneath it, which in turn sends some short "vertical" connections back to layer 4. There are also important inputs (from other cortical areas) into layer 1. These can contact the pical dendrites of tall pyramidal cells from most of the lower layers.

This simple summary conceals the intricate nature of many of the axonal connections within a small piece of cortex, in particular the many connections of one layer to itself, some of them surprisingly long. There is clearly some logic behind all these regularities, (Crick, 1994).

$$S(B) = S(A) * S(G)$$

$$= \left[a_0 g_0,\ a_1 g_0 + a_0 g_1,\ \cdots,\ \left(\sum_{k=0}^{n} a_k g_{n-k}\right) \cdots\right]$$

The sequence convolution may be tabulated by the following algorithm

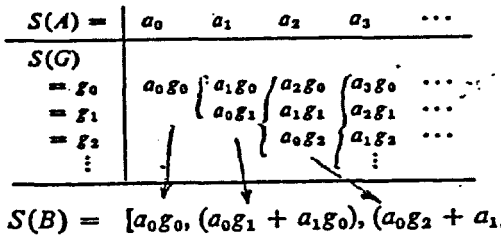

$$S(A) * S(G) = S(B) = [a_0 g_0,\ (a_0 g_1 + a_1 g_0),\ (a_0 g_2 + a_1 g_1 + a_2 g_0) \cdots]$$

Fig 4.7 (Cuenad and Durling, 1969)

An algorithm representation for the convolution principle two sequences S(A) and S(G) to provide interaction of C_L and C_D components in V1 laminae. By displacing the components $a_0, a_1, a_2, \ldots$ of C_L laterally one step at each c ell cycle, non-sequential interactions with C_D components $g_0, g_1, g_2, \ldots$ are available by simple column summations as indicated by arrows.

Required sequence combinations are available th this method for specific $C_L C_D$ interaction outputs from select ed laminae combinations.

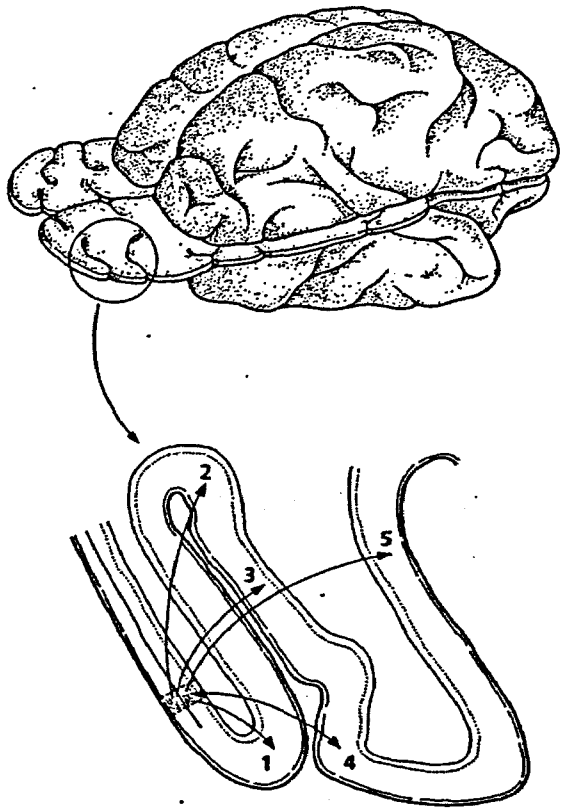

Fig 4.8 (Redrawn from Zeki, 1975)
The parallel anatomical outputs from a given small region of the primary visual cortex (area V1), which receives an input from a corresponding part of the retina and thus has all the visual information registered by that part of the retina and thus has all the visual information registered by that part of the retina represented in it. (Redrawn from Zeki, S. (1975). Cold Spring Harb. Symp. Quant. Biol. 40, 591-600).

Chapter 5

A Functional Model for Edge Responses V1

We have described the several hierarchical levels of the early vision system. We wish to utilize this functional information to obtain the responses at V1 locations from the information content of C_L and C_D. The nervous system, including vision, is organised with excitatory and inhibitory controls and, as pointed out by Granit (1977), "The consequences of an enormous redundancy – not reproduced by any computer – are incalculable. For such reasons mathematical circuit analysis, which is limited to model-making with simplified wiring diagrams, is useful only insofar as the approximations approach some fraction of reality"... "in general, circuits only rarely can be lifted out of their context for isolated treatment guided by circuiting rules". We therefore seek an alternative approach for our edge detection requirement and will base it on the functional responses for the two entities C_L and C_D which represent the "single unit activity of large groups of single cells" in primary vision processes as has been observed (Siegel, 1990). Other references related to information encoded across synchronised ensembles of many neurons in neural pathways are noted in studies by MacLeod et al (1998).

We also note that efficiency also results from the fact that for a encoding and decoding of signals from information content at nanoscale and quantum level only become efficient when performed collectively in large groups (Bennett and Shor, 2004) as it does with the great number of neurons involved in the vision system. It is known that large blocks of inputs and outputs occur collectively in the exchanges of signals between the LGN, V1 and the higher cortical regions; also from the reticular formation to the LGN via the infero-temporal cortex (ITC).

Use of Information Content in Model Formulation

An early and innovative paper in Information Theory applied in microbiology by Rescigno and Maccacaro (1961) gives a particular advantage for our functional approach. They pointed out that "information content" H, although applied with different names

such as "capacity" and "entropy" for different application areas, none of those uses were particularly suited to their *functional* classification problem for micro-organisms. They stated that the original expression for information content H relates more to the potential *ability* of a system to produce a measure of information, rather than to the actual functions performed by the system. They therefore redefined the terms used in Information Theory to apply to functional properties. This was done in a formal manner and with rules listed in their paper consistent with Information Theory.

Our use of C_L and C_D and the results from differential and integral operations designated in Fig 5.1 complies with these rules and will be used to formulate our model. We will be able to develop a functional expression for the spatial rate of change $\frac{dC_L}{d\ell}$ and $\frac{dC_D}{d\ell}$ at V1 based on information content and then equate the second derivatives to zero, corresponding to zero crossings. Zero crossings correspond to the inflexions of C_L and C_D at V1 and zero crossings provide all of the information required in the light→dark transition process (Logan, 1977). As will be seen this provides the governing differential equations for C_L and C_D for the conditions required at an edge. We are then able to examine aspects of their behaviour, including properties which arise when noise is added at the level of the primary visual cortex.

Background to Previous Modelling

Crick (1994) has commented that modelling of the vision system has proven to be difficult since "neurons have not evolved for the convenience of mathematicians".

There appears to be two types of vision research groups: *computation neurologists*, and *experimental neurologists*, accompanied by considerable strong criticism of each other. Marr's famous treatise 'Vision" (1982), "the Bible of visual computational neurobiology which everyone admires yet few understand" (Zeki, 1993), has been cited as an example of "ignoring the facts of the nervous system". Zeki points out that Marr's theoretical

work does introduce a new way of defining the tasks of the visual cortex in particular systems but does not help in understanding the *functions* (p119).

Nevertheless, Marr and Hildreth (1980) did provide some conditions when they developed their 1980 formula to represent an edge intensity distribution. These are also of use to us in developing a functional model which aims at combining neurology and system functioning. We will show that our model for the LGN/V1 neuron processes incorporates relevant Marr and Hildreth conditions, such as the spatial coincidences of zero crossings for a true edge. For our model which uses the development of information content in the early vision pathway we proceed as follows.

As outlined previously, from the established principles of information theory, we can identify the functions involved for our particular application with a minimum number of variables and parameters in a formalised manner. At each physiological level (Fig 5.1 and 5.2) we will express functions of C_L and C_D consistent with the known processes presented in Chapter 4. These functions are continuously dependent on the data even though there can be digital↔analogue conversions of signals by neurons as outlined in earlier Chapters. We recognise that our modelling is, like all models of the vision system, a simplistic representation of the extremely complex processes most of which are known only in general form, especially in regard to the striate cortex V1.

Units of Functional Groups of Single Cells

We note that Siegel (1990), examined the encoded inter-spike interval data for the dynamics of single unit activity of groups of single neurons in the primary visual cortex of the cat. He suggested that the dynamics could be "not highly complex" and possibly modelled by a "small set" of coupled non-linear equations. This could represent at least 10^4 interconnected cells even in one local V1 column. The implication was that "temporal activity of a single neuron embedded in a matrix of 10^4 neurons is relatively simple". The advantages of modeling large scale neuron activity which exhibit coherent macroscopic organization are discussed by Sirovich et al (1996). No model was presented but organising principles for analysing and viewing data were present.

We can consider our method related to the foregoing comments in relation to "coherence" and "single unit activity of a group of single cells" in our C_L and C_D variables. In effect we use those groups of cells to simplify a highly complex system into a set of differential equations which subsume the micro circuitry, in accord with the benefits expressed by Siegel.

Notation

In the ganglion→LGN↔V1 pathway we use the notation C_L and C_D for on-centre and off-centre neuron responses at each physiological level. The spatial information which they represent in the transmission and exchanges is represented in the frequency modulated spike pulses. It includes the analog spatial information of C_L and C_D responses as a function of ℓ and the spatial frequency variables f. The C_L and C_D variables can be extracted from the spatio-temporal signals as shown in an earlier chapter. Orientation, θ and wavelength λ are also encoded. At the LGN of the thalamus (T) the notation C_L^T and C_D^T will be used and, C_L^V and C_D^V for their inputs after convergence at V1 and $C_L^{V\bullet}$,$C_D^{V\bullet}$ for outputs available at V1. However, sometimes we may omit a superscript in a process for simplicity if there is no ambiguity.

Use of Information Content Relationships for Spatial Gradients at V1 from LGN Inputs

We will be able to write an expression for the difference between $\int \frac{dC_L^V}{d\ell} df$ *at* V1 from the LGN, after the signals for $\int \frac{dC_L^T}{d\ell} df$ converge on selected line detector cells at V1 to become $\int \frac{dC_L^V}{d\ell} df$ to be integrated along them, and the resulting signal $\frac{dC_L^{V\bullet}}{d\ell}$ *after* the processes at V1, including the interactions F. This corresponds to the Fig 5.1 legend.

The processes include the selective inhibition for the observer's focused perception of detail arising from links in V1, 2, 3, 4 and 5 to the infero temporal cortex (ITC) and the reticular formation (Kent, 1981). This inhibition has the ability to provide increased attention by the observer by suppressing unnecessary stimuli detail (such as may surround tumour edges or microcalcifications) represented by associated spatial frequencies. In our formulation we will use a frequency selective coefficient $s(f)$ for the inhibition effect on the interaction term F. Suppression is generally interpreted as evidence for intra-cortical inhibition where a V1 neuron receives inhibition from other V1 neurons including those selective for spatial frequencies of unwanted detail. The inhibition term will become $s_i F$ for a spatial frequency channel i. Two possible methods by which complex field cells could provide "tuning" to specific spatial frequencies are shown in Fig 5.3a,b,c, where Fig 5.3a gives the experimental support. This also includes unwanted stimuli at different orientations (Neri and Heeger, 2002 and the cited references).

This form of spatial frequency inhibition has been described by (Kent, 1981) where he also notes that "applying this kind of control to the inputs of a feature extractor could be used to alter the shape and location of its receptive field, if there were a large body of inputs from which to select" as can be present in a mammogram. "It is even possible that the "selectivity" of selective convergence is actually established more by selective inhibition of *unwanted* inputs than by anatomical selection of desired inputs." The foregoing is important in appreciating how the observer is involved in our model and in the observations in our tests with mammograms. Supporting detail is given from evidence summarised in Appendix F.

With reference to Fig 5.1 our expression for the processes labeled C within V1, is the difference between the spatial gradient output (3) at V1 and its spatial frequency channel i component input (coefficient a_1) at V1 after convergences of output (2) from the LGN. The expression applies for each spatial channel i and is given by Eq(5.1) below for the on-centre case where the coefficient $c = 1 + s(f)$ in order to combine the interaction

effects and frequency selectivity effect. The orientation θ for our edge and wavelength λ taken as fixed values for the basic spatial response. A similar equation applies for the off-centre case with the coefficient $c = c_2$.

$$\left[\frac{dC_L^{V*}}{d\ell} - a_1\int_i \frac{dC_L^V}{d\ell}df\right] = b_1\int_i\int\frac{dC_L^V}{d\ell}d\ell\,df - c_1(f_i)\int_i\int\frac{dF}{d\ell}d\ell\,df \qquad (5.1)$$

The right hand side represents the processes in V1.

For the corresponding off-centre equation the dark response gradient $\frac{dC_D^{V*}}{d\ell}$ is negative when the light response gradient $\frac{dC_L^{V*}}{d\ell}$ is positive at a zero crossing near the boundary edge, so the right hand side of Eq(5.1) will then be of opposite sign.

So, for the off-centre case

$$\frac{dC_D^{V*}}{d\ell} - a_2\int_i \frac{dC_D^V}{d\ell}df = -\left[b_2\int_i\int\frac{dC_D^V}{d\ell}d\ell df - c_2(f_i)\int_i\int\frac{dF}{d\ell}d\ell df\right] \qquad (5.2)$$

Eq(5.1) and Eq(5.2) represent the case for complex cells where the f_i spatial frequency channels $(i = 1, 2....n)$ apply. The output of some LGN cells proceed via the thalamus to the ITC but most go directly to V1 where V1 laminae can extract the spatial information. The integrations with respect to spatial frequency in each case of equations (5.1) and (5.2) correspond separately to each of the channels i. There are a number of processes (Kent, 1981) by which the integrations are possible at the neuron level at the LGN and at V1 shown in Fig 5.3a, b, c using the extensive abilities of neurons as previously indicated. At the LGN neural inputs (Bear et al, 1995) there are enough inhibitory as well their excitatory inputs to the Parvo signal stream in particular (Fig 5.4), to perform the required spatial processes at the LGN. Support for our formation of the foregoing equations, in which we utilize the integrations of signals at both the LGN and at V1, is seen from Zeki (1993, page 306), pointing out that it is necessary for the vision system to allow signals to be accessible to integration at every stage and is therefore a multi stage process.

Differentiation of Eq(5.1) with respect to ℓ, can be made under the integral sign, since the integration limits for our spatial frequency channels $(i = 1,....n)$ are independent of ℓ. We assume that the channels are simple step functions across successive spatial frequencies as in Fig 5.5. This yields, at each f_i channel

$$\frac{d^2C_L^{V*}(f_i)}{d\ell^2} = a_1\int_i \frac{d^2C_L^V}{d\ell^2}df + b_1\int_i \frac{dC_L^V}{d\ell}df - c_1(f_i)\int_i \frac{d}{dl}Fdf \qquad (5.3)$$

$i = 1,2,....n$, for n spatial frequency channels.

ie

$$a_1\frac{d^2C_L^{V*}}{d\ell^2} = \int_i\left[a_1\frac{d^2C_L^V}{d\ell^2} + b_1\frac{dC_L^V}{d\ell} - c_1(f_i)\frac{dF}{d\ell}\right]df \qquad (5.4)$$

A similar set of differential equations can be obtained for C_D^V

$$a_2\frac{d^2C_D^{V*}}{d\ell^2} = \int_i\left[a_2\frac{d^2C_D^V}{d\ell^2} - b_2\frac{dC_L^V}{d\ell} + c_2(f_i)\frac{dF}{d\ell}\right]df \qquad (5.5)$$

The second differential $\frac{d^2C_L^{V*}}{d\ell^2}$ and similarly $\frac{d^2C_D^{V*}}{d\ell^2}$, are zero at these inflexions of the variables at the output which, together, form the basis of the intensity contrast formed by hypercomplex cells in the secondary cortex. The second differential inflexion condition is that the right hand side of both Eq(5.4) and Eq(5.5) is to be zero. The associated information corresponds to Logan's theorem at zero crossings.

We know that the integrand of the right hand side of Eqs(5.4) and (5.5) is not an arbitrary function which might be equated to zero to meet that condition. It must conform to a shape of the same form of response as projected from the LGN to V1 so our expression in square brackets is a correct candidate when equated to zero for a response at each of the spatial frequency

channels. This provides a differential equation as a function of ℓ at each of those channel frequencies for the on-centre and off-centre cases.

The result of all of the foregoing is that an image boundary edge requires the following conditions for C_L and C_D from the V1 processes. (We omit the superscript for simplicity).

$$a_1 \frac{d^2 C_L}{d\ell^2} + b_1 \frac{dC_L}{d\ell} - c_1(f_i)\frac{d}{d\ell}F = 0 \qquad (5.6)$$

Likewise $$a_2 \frac{d^2 C_d}{d\ell^2} - b_2 \frac{dC_D}{d\ell} + c_2(f_i)\frac{d}{d\ell}F = 0 \qquad (5.7)$$

The coefficients a, b and c govern the spatial properties of the solution of these two equations. The conditions for a true edge would be satisfied provided that the coefficients a,b,c in each channel do not differ greatly for the zero crossings for the separate frequency channels. Depending on the image quality of an edge region the associated coefficients c_1 and c_2 may be slightly different for each channel and result in small changes in the responses which then lead to displacements of the zero crossing points. As stated previously, true edges should not have significant displacements.

The coefficients b_1 and likewise b_2 can be of smaller values than a_1 and a_2 respectively because of a reduced effect from interactions at V1 may be reduced when back projected and exchanged with LGN neurons (Crick, 1994).

Integration of Eq(5.6) and Eq(5.7) with respect to ℓ yields the two differential equations of Lotka-Volterra form for each of C_L^V and C_D^V for each channel. The laminae interaction function F has weighting factors b_{ij} in the summation of component products of C_L and C_D as previously shown in Chapter 4. Whereas in the product form $\sum b_{ij} C_{Li} C_{Dj}$ for the interactions F, the weighting factors b_{ij} depend on the neuron-to-neuron synapse strengths arising from the particular intra laminae processes at V1.

The Retinotopic Property

As a result of the same L-V type of differential equations arising in both our ganglion outputs model and our V1 model, the general shapes of the C_L and C_D responses will retain the same general form from the ganglions to V1 (Wilson et al, 1990). That is to say, our previously developed retinal model for retinal ganglion output and the result now obtained from the conditions needed for the V1/LGN are consistent with the retintotopic property of the early vision system since both yield L-V type differential equations. It can be shown (Williamson, 2000) that some types of complexity in interaction terms in L-V differential equations can lead to instability but we assume from every day experience that this is absent in normal vision.

It appears worth noting in this regard, that although L-V type of equations govern responses occurring in our model at both the retinal ganglions and the primary visual cortex, the latter has a selective suppressive input component term $c(f)$ associated with spatial frequencies in the region of the edge. This arises from cerebral functions involving the observer and is particularly useful for suppressing unwanted detail, as previously mentioned, and perhaps aiding stability for some observers and not assisting observation for less experienced observers. The effect depends on their cortical functions associated with $s(f)$ at the ITC and reticular formation.

The coupled equations for the components of C_L and C_D in our model form a set of coupled non-linear L-V type differential equations. A set of equations is needed because of the separate spatial frequencies and provision for any orientations and different wavelengths involved. It is interesting to again note that the foregoing is closely related to a suggestion by Siegel (1990) who examined the interspike interval data for the temporal dynamics of neurons in the primary visual cortex of the cat and *suggested* that the dynamics could be "relatively simple and may be modeled using a (relatively) small set of coupled non-linear equations". He cites references which also suggest that such modelling may be able to independent of the detailed underlying circuitry.

Hierarchical Representation

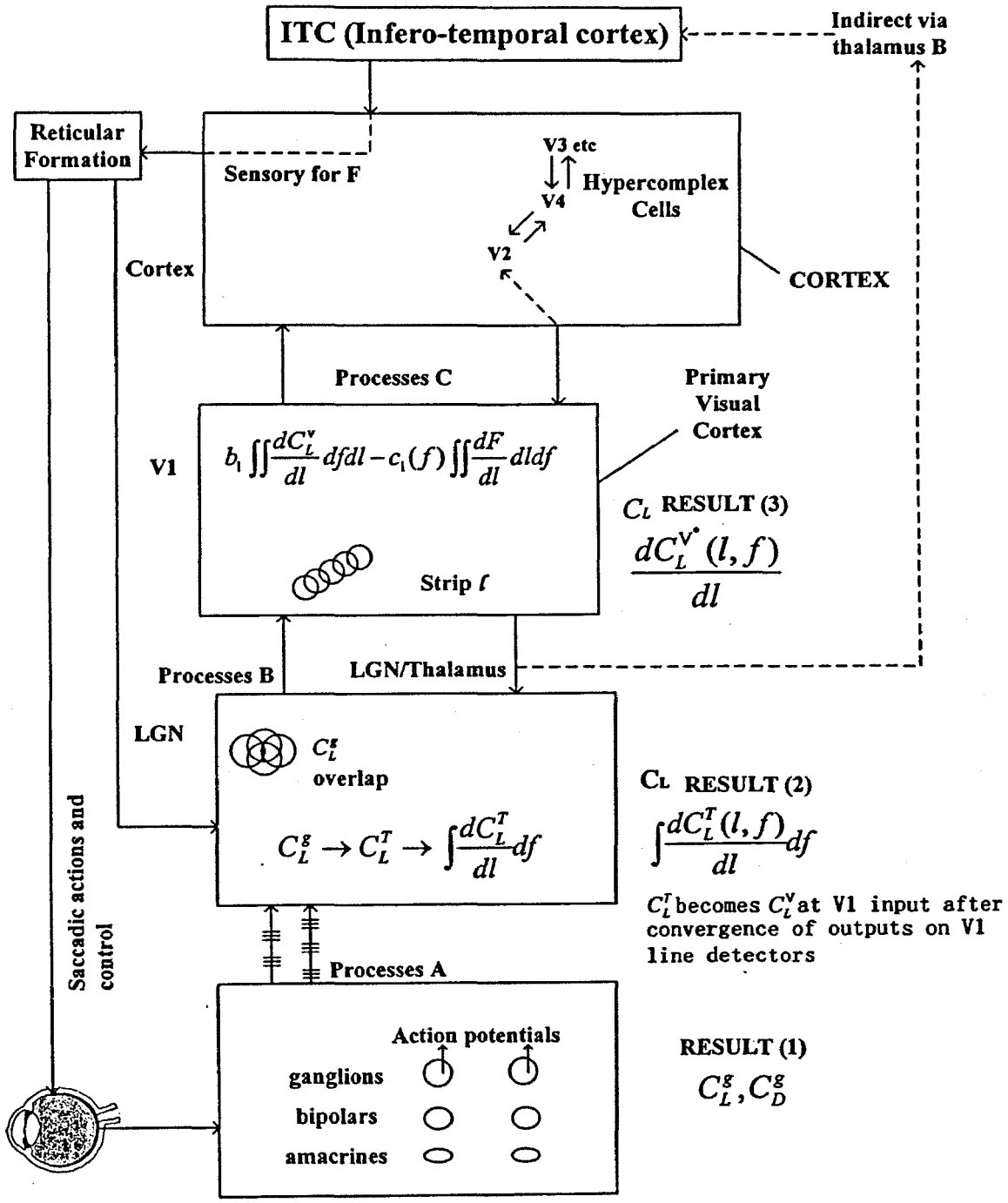

Result (3) – Result (2) after convergences on V1 cells = Result of processes C in V1. This gives Eq 5.1 and Eq 5.2 in text leading to L-V type differential equations

Fig 5.1

Representation of primary vision processes described in the text as both parallel and hierarchical and the result of the processes on C_L shown at retina, LGN and V1.

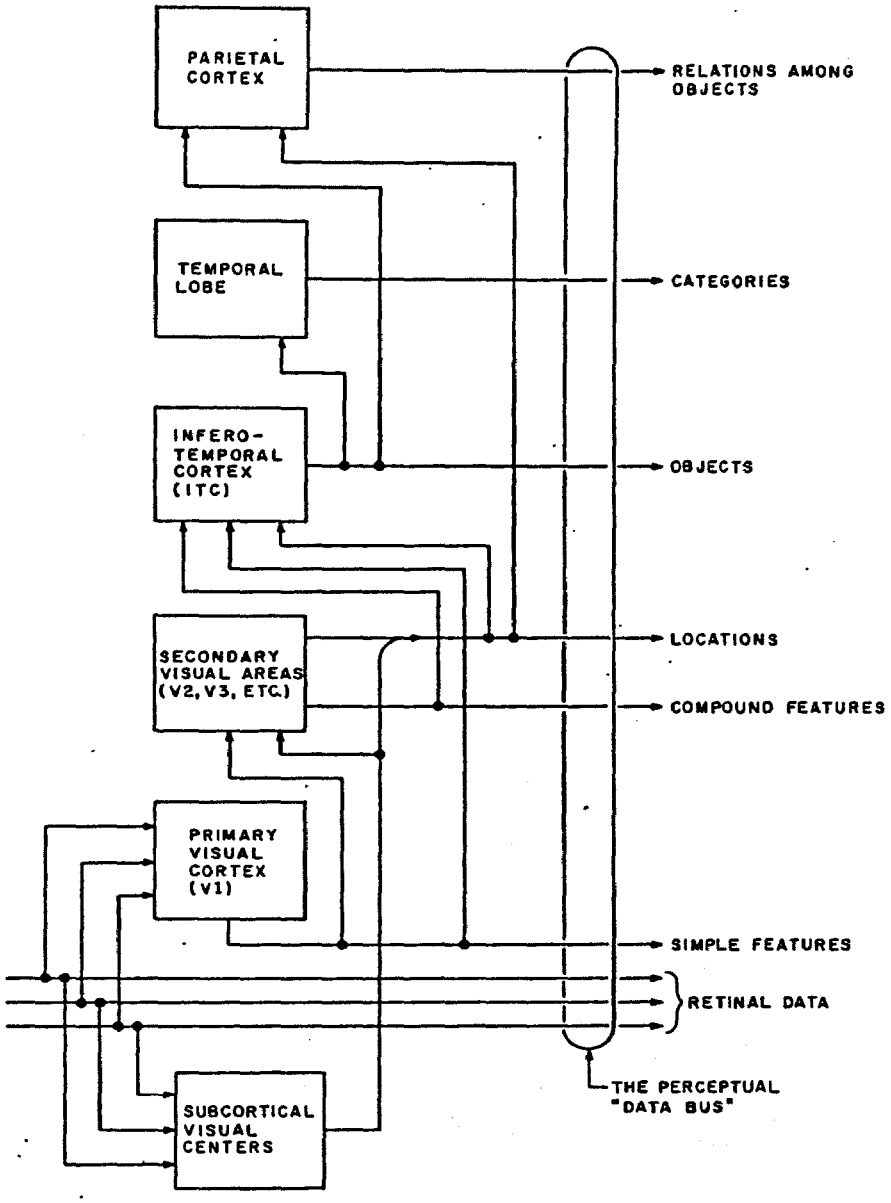

Fig 5.2 (Kent, 1981)

The hypothetical "perceptual bus" illustrating the fact that data processing proceeds in the perceptual function (and in the brain generally) by the addition of new lines to the existing data lines rather than by a series of transformations of the data on the input lines.

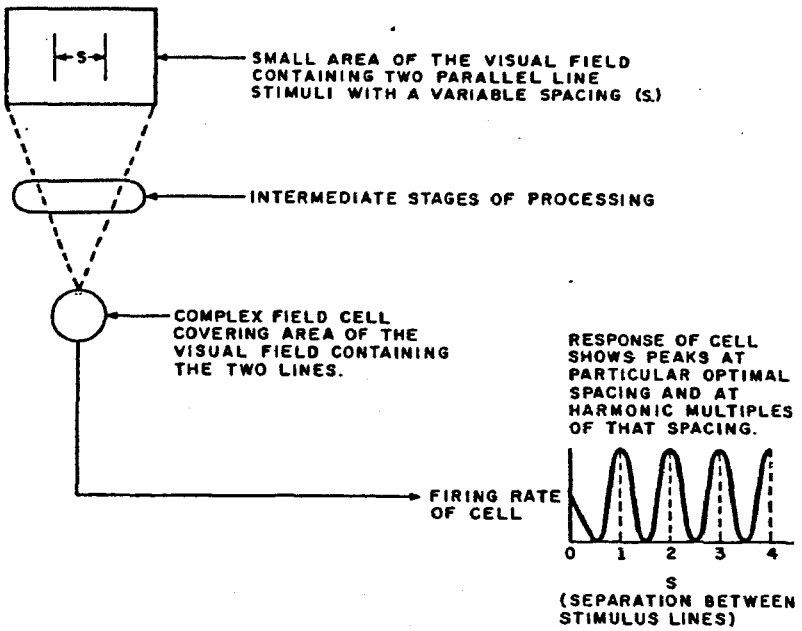

Fig 5.3a (Kent, 1981)

An experiment which supports the hypothesis that complex field cells fo have spatial frequency selectivity of "tuning". When two stimuli with a variable spacing are used, the cells' responses is a periodic function of the separation. When only one stimulus is used, the cell only shows the normal selectivity for orientation.

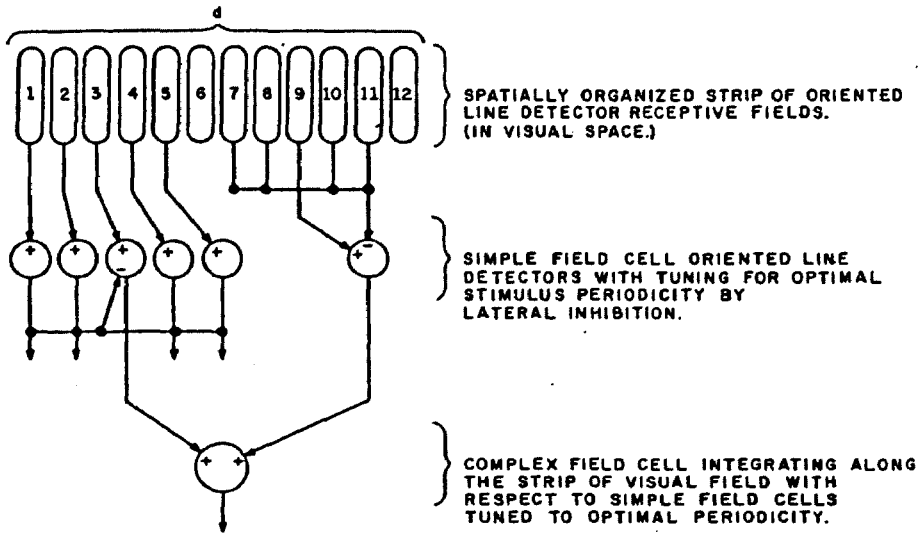

Fig 5.3b (Kent, 1981

A possible method of "tuning" complex field cells to specific frequencies. This model relies on tuning of the simple field cells by lateral inhibition.

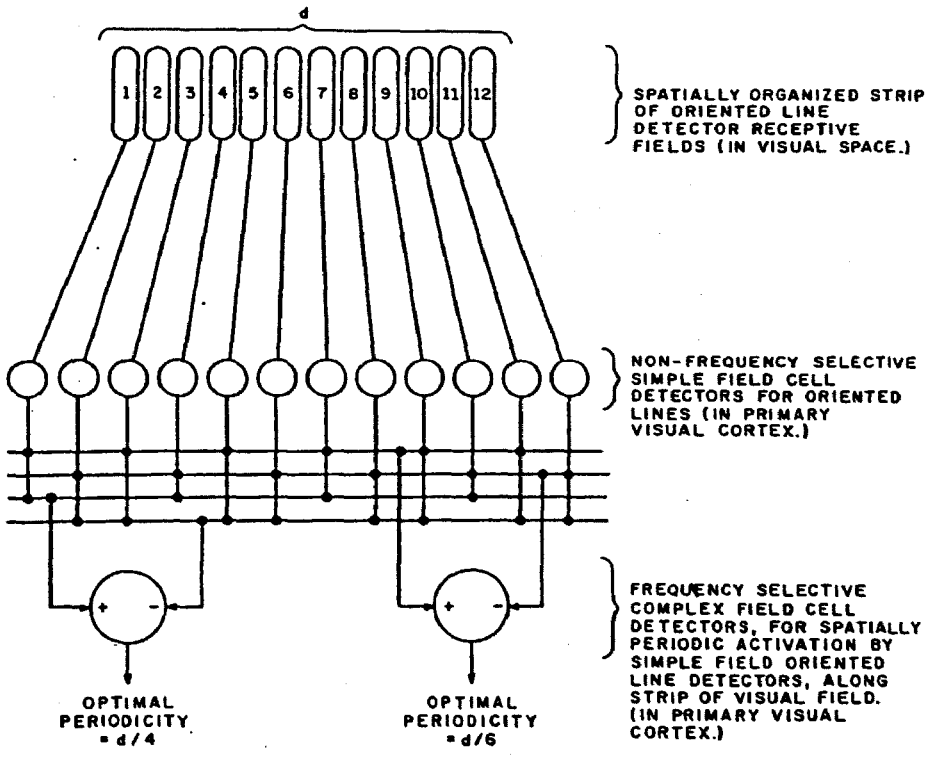

Fig 5.3c (Kent, 1981)

Another possible method of "tuning" complex field cells to specific spatial frequencies. This model relies on selective convergence and inhibition at the level of complex field cells.

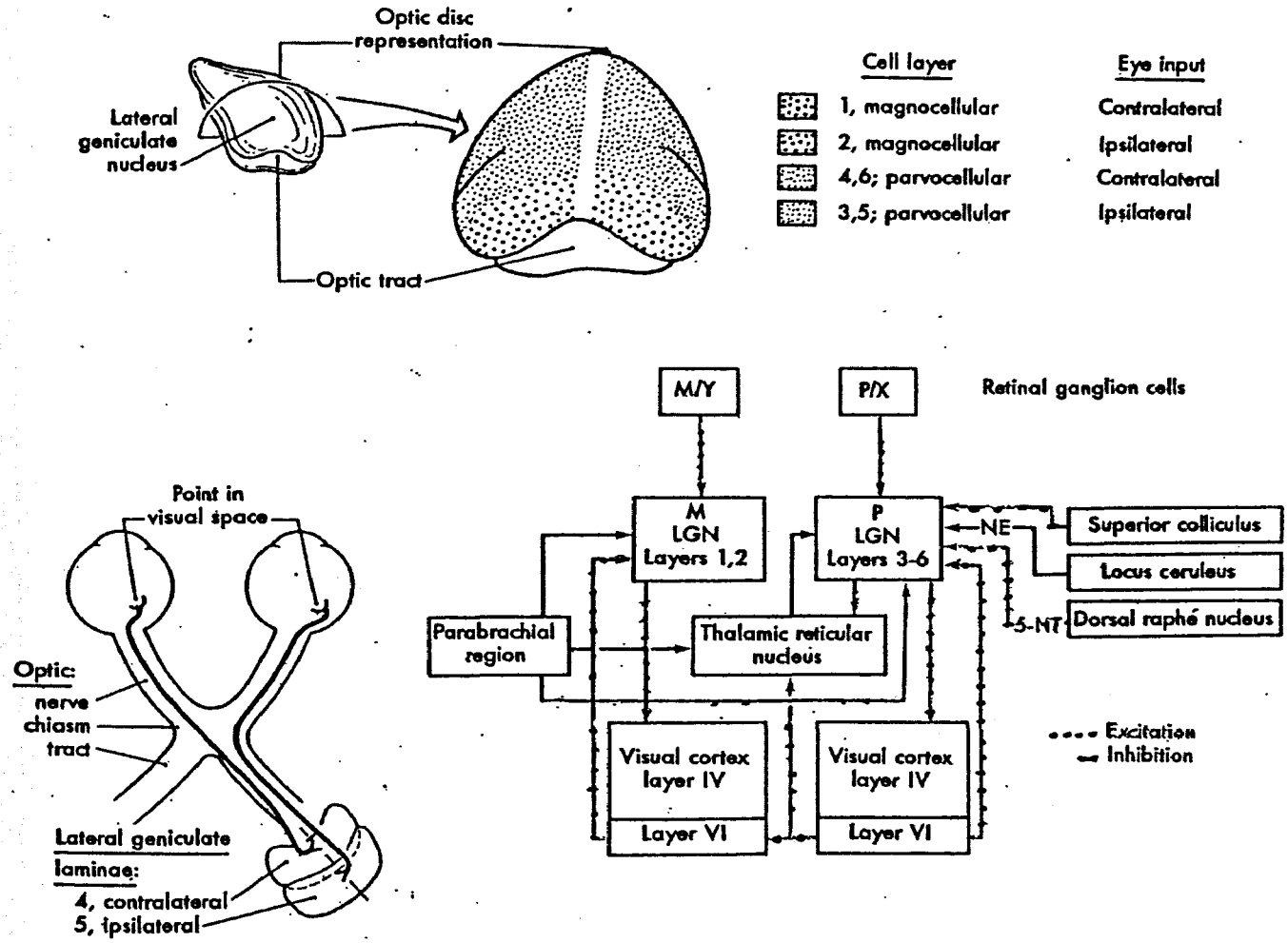

Fig 5.4 (Bear et al, 1990)
Details of the lateral geniculate nucleus showing the magnocellular (M) and parvocellular (P) pathways and associated excitatory and inhibitory exchanges.

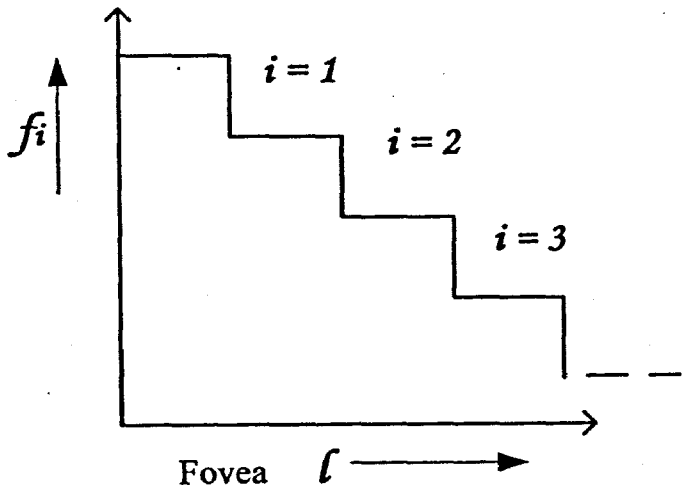

Fig 5.5
Assured steps of spatial frequency channels as dependent across fovea

Chapter 6

Possible Stochastic Resonance for C_L^V and C_D^V when Interaction Includes Coloured $1/f$ Noise

Coloured $1/f$ noise could assist in producing resonance effects in our L-V solutions for C_L^V, C_D^V combinations below the visual threshold. Most sensory cells which have been tested in experiments have shown clear evidence of stochastic resonance (SR) (Wiesenfeld and Moss, 1995). Conventional mammography demonstrates microcalcifications in about 30% of breast cancers, but many cancers have been shown to have calcifications by subsequent histological examination. Clearly, many breast cancers can contain microcalcifications that are smaller than the limits of resolution of most conventional mammography systems. If present, they are also important to recognize for the surgical margin. Also, for tumours, boundaries which can be indistinct do have Fourier components and for some of the frequencies a resonance may be possible with added noise and aid in perception. The writer's suggestion of using coloured $1/f$ noise for a possible stochastic resonance effect on L-V differential equations was because $1/f$ noise has the particular property of self correlations in its power spectrum over a wide range of its frequency components, which decline with frequency as spectral frequency f increases (see Note at end of this Chapter).

In a following chapter, we will show how coloured $1/f$ type noise is generated and introduced to parameters in our Eq(5.5) and Eq(5.6) of Chapter 5 for C_L^V and C_D^V for V1 outputs. The result is that a coloured noise component is introduced in the coefficients and of the respective interaction terms F_1 and F_2 of those equations at V1.

We recall that C_L^V and C_D^V are functions of wavelength λ as well as of ℓ and spatial frequency f_s. In Chapter 8 we will show that our experimental arrangement with a computer driven dynamic polaroid and polaroid eyepieces with colour filters, ensures that different and separate temporal inputs, with added noise, are provided to each eye and interact at V1. Subsequent responses from information at V1 in conjunction with V2 for

spatial interaction and from V4 for colour, produce contrast intensity distributions which are perceived in the cortex.

Stochastic Resonance (SR) Principles

We now briefly outline stochastic resonance principles before proceeding.

1. **Stochastic Resonance (SR)**

   Stochastic resonance is often described as a somewhat counter-intuitive phenomenon since, by appropriately adding noise to an already noisy system, it is possible to improve the signal-to-noise ratio (SNR). It has attracted increasing attention over the last two decades. In SR, noise shows a surprising ability to optimise the response of a non linear system to a subthreshold signal.

2. **The Signal-to-Noise Ratio (SNR) for the Stochastic Resonance Effect**

   There are several types of stochastic resonance but all the main types result in the same general form of expression given below, apart from some constant factors of the order unity. The signal-to-noise ratio (SNR) expression is (Wiesenfeld and Moss, 1995)

   $$SNR \propto (\varepsilon \Delta U / D)^2 \exp(-\Delta U / D) \qquad (6.1)$$

   where, in our application, ε is the signal strength of stealthy image features, D is the input noise intensity applied and ΔU is a constant related to the threshold level of visual perception. From Equation (6.1), the behaviour of the SNR is given below and shown in Fig 6.1.

   (i) As $D \to 0$ (no noise added) there is no effect because the expression $\to$ zero in the limit.

   (ii) The expression (1) rises sharply to a maximum at some optimal noise intensity as shown in the insert (a) in Fig 6.1.

   (iii) The SNR decreases gradually for larger added noise intensity D because its randomizing effect then, progressively, overrides the SR effect.

3. SR Principles and Relevance to our Application

A basic principle of SR, using Gaussian random noise for simplicity, is shown in Fig 6.1a,b,c,d. The noise can combine with peaks of a periodic signal which is below the threshold level for recognition and lift some of the original peaks of the low level signal above the threshold level. When these individual occurrences are plotted as a time series over an extended time, the power spectrum of the occurrences reveals a peak of the basic frequency of the original signal which was below the threshold. A harmonic or sub- harmonic may also occur for some signals.

There have been many studies of stochastic resonance in biology applications. Recently, stochastic resonance in the cortex for response of sensory motor neurons was demonstrated in an experimental system with 19 observers (Kitajo et al, 2003). It should be noted that it was for their recognition of the presence of progressively reduced sinusoidal *screen intensity* changes (not "edges") of a small square of initially uniform illumination. The observer's threshold level was registered by a button-press motor-sensory response system. The addition of white Gaussian noise was introduced separately into the vision of the left eye while a progressive reduction of a change of the sinusoidal screen illumination was separately presented to the right eye which was physically screened from the left eye. This ensured that the processing of the combined inputs was not done until they converged at the primary visual cortex. Even though the signals interact at V1 the processes are quite different from our problem of *edge detection* which is governed by different functional processes of on-centre and off-centre neurons.

In addition, in our experiment coloured $1/f$ noise is introduced into the parameters of our governing L-V differential equations for edge detection. We also note that previous studies (Arnold et al, 1979) have shown that Gaussian noise by itself can not produce resonances in L-V differential equations.

In the previous chapters we have seen that within the retina the optical image which excites the receptors in the input layer, is converted to multiple spike pulse patterns of excitation in the output signals of ganglion cells of different types. (Grusser and Grusser-Cornehls, 1987). These types relate to the magno(M) and parvo(P) properties. Their signals proceed in the separate M and P paths to V1 where the on-centre and off-centre signals interact at V1 advantageously for contrast at a boundary edge. It is at the V1 level where we have been able to make our externally generated noise take effect, as will be seen in subsequent chapters.

In our edge detection problem we are interested in revealing any hard-to-see features of microcalcification regions where there is a group of spatial frequencies, not just a single frequency as demonstrated in Fig 6.1. The spatial frequencies are for different sizes and/or shapes. Some microcalcifications can be outside the apparent region of interest border and some can be below the threshold level of vision.

Representation of Noise introduced into the L-V Equations

In our model, temporal spectral $1/f$ noise is introduced at the retina. On-centre and off-centre ganglions include colour sensitive types which are functions of wavelength of light as well as spatially. We also note that the horizontal cells include colour-opponent types. We will show that our method results effectively in adding coloured $1/f$ noise to the interaction coefficients in the Eqs (5.5) and (5.6) in Chapter 5. Our system with a dynamic polaroid and spectral polaroid filters system, to be subsequently described in our Experimental chapter, provides a spectral component of the noise to one eye (L) and a separate component to the other (R).

This yields C_L and C_D responses transmitted from the colour-specific receptive fields of the colour sensitive and high spatial resolution LGN cells, together with an added noise factor component. Inputs for left and right eye differ according to the time t of the

dynamic spectral filtering process which we use for input to each eye as the polaroid swings. The signals transmitted from the LGN and received at V1 become $\left[1+N_i\left(\lambda(t)\right)\right]C_L^V$ and $\left[1+N_i\left(\lambda(t)\right)\right]C_D^V$ which we will write as $A_\alpha(t)C_L^V$ and $A_\beta(t)C_D^V$ (α or β for left or right eye). For simple notation for either eye we will write $1+N\left[\lambda(t)\right]$ as $A(t)$.

After substituting the common factor $A(t)$ in each C_L and C_D term in Eq(5.5) and (5.6) of Chapter 5 the result leaves $A(t)$ only in the product term C_LC_D after cancelling throughout. Therefore, the equations acquire just a single noise coefficient $A(t)$ for the C_LC_D products and become, for either eye,

$$\frac{dC_L(\ell,\lambda)}{d\ell}=a_1\,C_L(\ell,\lambda)-c_1A(t)C_LC_D \qquad (6.2)$$

(omitting superscripts)

$$\frac{dC_D(\ell,\lambda)}{d\ell}=-a_2C_D(\ell,\lambda)+c_2A(t)C_LC_D \qquad (6.3)$$

In effect, this has introduced a time dependent coloured noise internally to the system via the now noisy $cA(t)$ parameters of the original L-V differential equations. In other words the noise acts on the non-linear interactive terms C_LC_D. We recall that a single bilinear term C_LC_D originated in our formulation (Chapter 2) for the ganglion action potentials and was consistent in comparing responses with published experimental measurements (Baylor and Fuortes, 1970).

Conversion of Temporal Noise Effect to Spatial Effect

The numerical value of the coefficients with time dependent noise, will produce an effect on the spatial solutions of the L-V equations for responses at V1. This arises from a temporal to spatial conversion as follows: We had noted from Farley and Clark (1961), that experiments with a network of neuron-like computer elements, showed in a sequence of dynamic outputs, that a network of transformed time channel patterns is converted into

unique spatial patterns of active elements. There was a one-to-one correspondence between input of time-channel configurations and spatial configurations, provided that the class of inputs was not too large. Further information is given in Appendix E. Recent reviews (eg Sharon and Grinvald, 2002) indicate support for Farley and Clark's earlier spatio-temporal work. It has come from experiments with tracer substances injected into layers of the primate visual cortex. How the brain accomplishes perception by reconstructing a stimulus from information in the spike train "remains largely unknown" for many reasons (Macleod et al 1998). Nevertheless it is known that information encoded in time across ensembles of synchronous neurons converges to single neurons downstream in the visual pathway, as we have already seen for the spatial components of C_L and C_D. We therefore assume that the original temporal noise interacts with the spatial information in the cortex for possible stochastic resonance.

Computer Simulations of C_L and C_D Orbits with Added Noise

We wish to observe if C_L^V and C_D^V, as a result of our added noise components, exhibit any maxima above the normal threshold level of responses if they occur close together in the cyclical orbits of the L-V equations. Any such repeated occurrences would imply an underlying stochastic resonance effect as pointed out by Stucki (1979). This would result in improvement in a subsequent contrast intensity response from the spatial component interactions in the V1 laminae.

To plot the L-V orbits we use Eq(6.2) and Eq(6.3), in the usual text book manner, to form $\frac{dC_L}{dC_D}$, giving

$$dC_L\left[\frac{-a_2}{C_L}+c_2A\right]=dC_D\left[\frac{a_1}{C_D}-c_1A\right]$$

which, after integration with respect to ℓ, gives

$-a_2\ell nC_L + c_2C_L = a_1\ell nC_D - c_1C_D$ (+ a constant of integration).

This expression is the basic form used for the usual two dimensional computer plot of C_L and C_D orbital trajectories. In our case we also have the temporal noise factor $A[\lambda(t)]$. In searching for edges of "low observables" in our image we are interested in small values of C_L^V and C_D^V signals which are of similar magnitude, in order to give contrast intensity for an edge. The 2D orbital paths are plotted with an additional third axis for recording the density of occurrences of C_L^V and C_D^V in progressive orbits, as in Fig 2a. Where a value of A of $[1+0\cdot1\lambda(t)]$ was used with noise $\lambda(t)$ from stochastic selections over yellow to blue wavelengths in the human spectral sensitivity response curve. We see groups of reasonably close low values of C_L^V and C_D^V (approximately 0.01 to 0.05) which have a high probability of occurrence from underlying stochastic resonance (Stucki 1979). This was also found in Stucki's orbital plots (Fig 6.2b) where he used $1/f$ noise affecting just one variable in one of the L-V differential equations (a_2 in our equation). Also the slope of the occurrence plots in our case indicates very sharp changes. Another group of approximately equal C_L^V and C_D^V values occurs for higher values (0.6 to 0.65) but the density of occurrences is much lower than for the low values. Our practical interest is in the latter situation.

According to Arnold, et al (1979), resonance can occur in L-V differential equations responses with a parameter subjected to a $1/f$ noise perturbation. It requires that the power spectrum avoids a particular eigenvalue condition resulting in a spectral profile illustrated in their paper. Our experimental arrangements comply with the conditions which would allow resonance.

Practical Implications

If approximately equal values of C_L^V and C_D^V could occur in orbit cycle times within an observer's time for persistence of visual information, (approximately 0.2/sec), we would expect an increase in response at *non-stationary locations* as a result of the underlying resonance effect. This may provide an aid for edge detection. Stucki's original plots

showed stationary occurrences which were shown (Arnold, Stuki et al, 1979) to be in doubt in favour of non-stationary behaviour as in our results.

From all of the foregoing we see that to gain the benefit of the selective processes of stochastic resonances which could be applied for detection of edges of "stealthy low observables" in a region of interest we require:

(a) Polaroid timing segments in the experimental system to be consistent with short-term retention time of visual image information, (decay to 65% in $\sim 0.2\,\text{sec}$), in observing presentations of images with detail. Two such closely timed stimuli can be perceived as superposed (Averbach and Sperling p200, 206 1961).

(b) The always present saccadic action of the eye in observations of the region of interest for an edge.

(c) The observer's method of spatially scanning an image to cover the space where lesion objects may be present.

Whereas persistence of vision and saccadic actions are common in normal vision (c) would favour experienced observers in searching for features.

The foregoing matters justify experimental testing and now leads us to Chapter 7 for experimental design.

A Note on $1/f$ Noise

The particular properties arising from component correlations of noise spoken of as "$1/f$" or "coloured noise" relate to the general case of noise with a power spectrum which declines with frequency as $1/f^{\alpha}$ where α has a value between 1 and 2. The following scale is worth noting for properties associated with α (from J.D. Barrow, "The Inventive Universe", 1995).

For $\alpha = 0$ white noise with autocorrelation zero. It is not possible to predict what the next amplitude will be.

$1 \leq \alpha \leq 2$ Produces "pink noise" which has some degree of correlations between its components over the whole spectral range. "An interesting case for possibilities" and often occurs in nature.

$\alpha > 2$ Produces "brown noise", unpleasant to the ear when accoustic and, likewise, "black noise" produces unusual low "growling" sounds, such as from earthquake disturbances.

It is possible to measure α from a limited segment of wave forms of the coloured noise using a simple graphical method for integration of two segments of the spectra (Crandell, 1994). Our test noise complies with the condition for "pink noise".

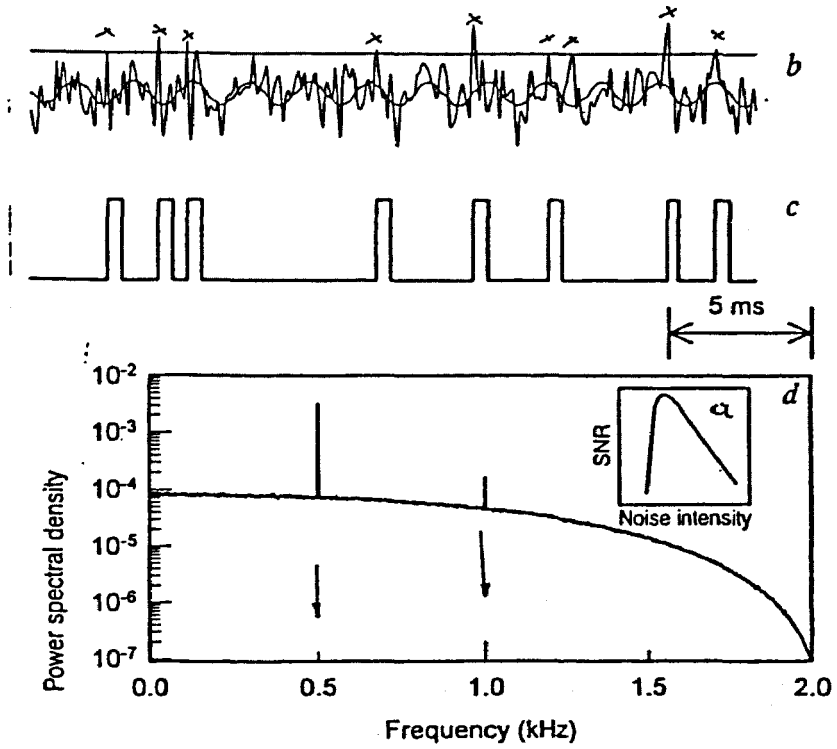

Fig 6.1 (Wiesenfeld and Moss, 1995)

(a) Inset, the characteristic signature of SR

(b) The simplest instance of stochastic resonance (SR) consists of a threshold (shown by the straight line) and a subthreshold sinusoidal signal with added gaussian noise. Each time the signal plus the noise increases across the threshold, a pulse of standard shape is written to the time series shown in c.d. Power spectrum of a long time series of the pulses shown in c has a broadband noise background whose amplitude at zero frequency is related to the mean pulse repetition rate and hence to the noise. The signal feature is the sharp peak located at the signal frequency (0.5 kHz in this case) riding on the noise background.

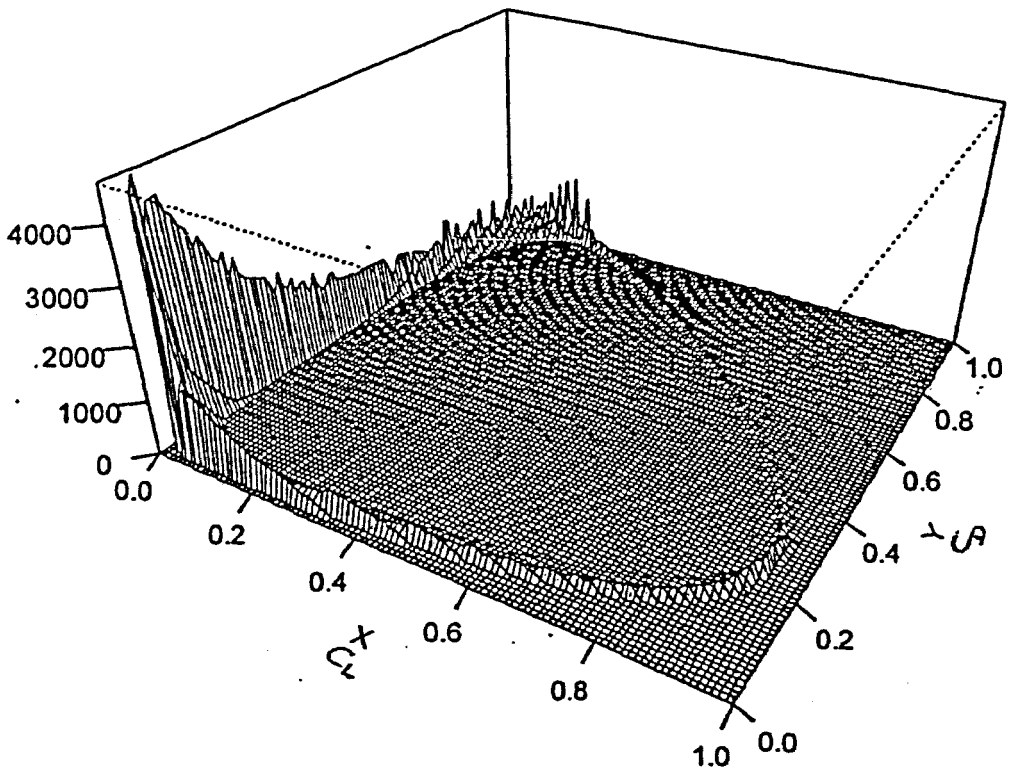

Fig 6.2a

Orbital plot of C_L and C_D responses (XY plane) and density of occurrences (vertical axis) with $1/f$ noise added to the interaction parameters in the L-V model in Chapter 5.

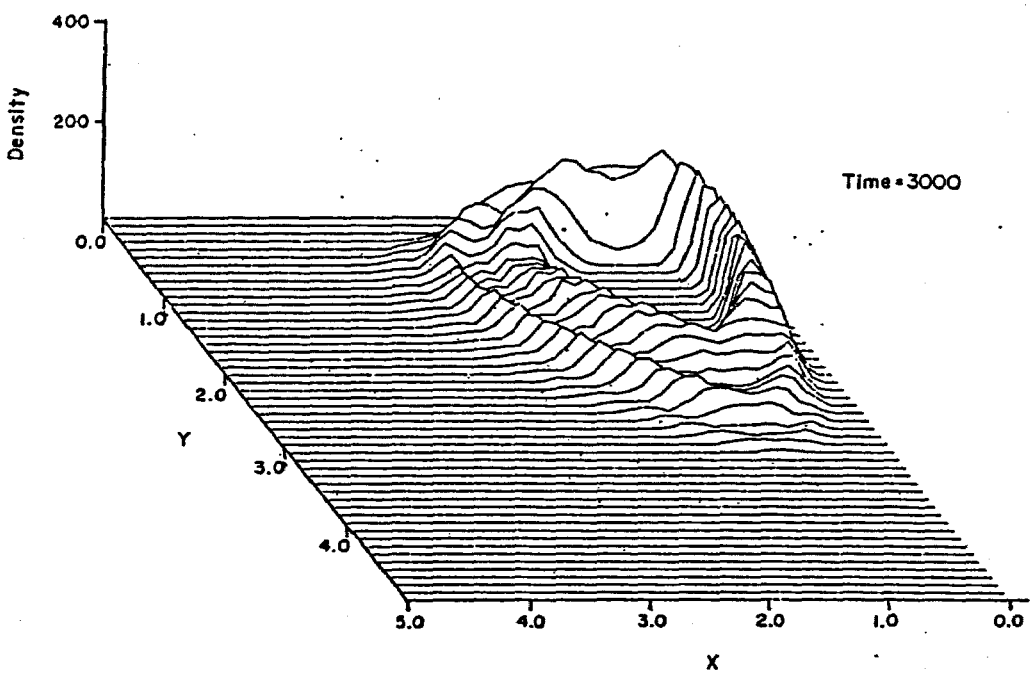

Fig 6.2b (Stucki 1979)

The trajectories passing through individual points in the state plane were cumulated during the simulation. This figure shows a typical resulting trajectory density profile obtained after 3000 time units units of simulation. The following parameter set was used for this simulation: $\sigma = 0.1, \alpha = 10.0, \epsilon_1 = \epsilon_2 = k_2 = 1$ **and initial conditions were** $x_0 = 0.2, y_0 = 1.0$.

$$\dot{x}_t = (\epsilon_1 + \varsigma_t) x_t - k_2 x_t y_t$$

$$\dot{y}_t = k_2 x_t y_t - \epsilon_2 y_t$$

ς_t = coloured noise, computational (p172 Stucki)

Chapter 7

Considerations for an Experimental Design

An Experimental Test for the Effect of Added Noise

Our simulation for C_L and C_D behaviour in our model with coloured noise indicates that an experimental system can be tested to induce resonance and improve perception of edges and detail in mammograms and that this could be done when viewed directly in real-time. We also note (Chesters, 1982) that "all attempts to enhance threshold detection where the noise and the signal arise at the same point, as for example in X-ray quantum limited images, have been broadly unsuccessful. The only gains have been convenience or aesthetic importance". However, "when the noise arises at a point after the signal, significant gains are possible". This applies to our provision for introducing noise in the experiments.

Lesions with Microcalcifications as Test Images

A suspect Region of Interest (ROI) in a mammogram can be digitised and processed off-line by high technology computer aided methods which mark locations on-screen for expert attention. However, there are some shortcomings in digitization in relation to detection of some small, but important microcalcifications, either in the ROI or possibly just outside it. A method to test if the proposed addition of $1/f$ noise can help an observer to perceive such detail during the real time screening process is desirable. We chose to test the method on lesions with microcalcifications viewed in real time, as in breast screening, without any image processing. (The principle involved will also apply to other lesions in mammograms).

Microcalcifications in general have sizes between $0.1-1.0\,\text{mm}$ implying that, if the mammogram is digitised, they will be correctly digitised when using a resolution of at least $50\mu\,\text{m}$. Mammograms, when digitised, may still show the presence of microcalcifications but the contrast between the microcalcifications and the surrounding

tissue is much lower at lower resolutions. In some cases, depending on resolution, the microcalcifications can blend into surrounding tissue due to the digitisation process and are not detectable in the digitised image (Brzakovic et al, 1993). Also poor microcalcification detail may sometimes be hard to differentiate calcifications from benign diseases or artifacts (Schmidt et al, 1999).

Generation of $1/f$ Type Noise for the Experiment

Figure 7.1 illustrates a known principle for generation of $1/f$ type noise:

Consider a set of independent white light inputs to a set of tuned wavelength filters, where this set of filters provides selective responses for each unit in the group and which decrease with frequency f over a desired spectral region. It is known (Crandell, 1994 pp153,284) that the combined output of such a system, even with a relatively small number of units, can provide an output with coloured $1/f$ noise with correlations of the spectral power.

Our particular implementation of the principle is shown in Fig 7.2a,b where a polaroid sheet is driven by a computer controlled servo to swing across the optic axis of the system as indicated (equipment photos are in Chapter 8). A collimated white light source illuminates the mammogram region mounted as shown and viewed by the observer through left and right eyepieces equipped with colour filters (L, blue range, R yellow range). Our wide band colour filters achieve the decreasing power spectra and correlations are achieved largely by the responses of the three types of cone cells L, M and S and the rod cell response between M and S cone responses. The spectral characteristics of the filters are shown in Fig 7.1 with three "tuned" peaks of decreasing amplitude as required over the spectral range of yellow/orange (600 nm) to blue/violet (400 nm). Each eyepiece also has a polaroid with its plane of polarisation set at approximately 90^0 to the other eyepiece. This combination allows different groups of wavelengths to be inputs for each eye dependent on the axis of orientation of the main polaroid when swinging. When the polaroid is moving in random motion steps across the optic axis, each eye is subjected to segments of random time sequences of differing

wavelength segments over its particular filter's spectral response. Each eye receives these independent inputs analogous to the basic "tuned filters" of Fig 7.1.

Our filters have declining transmission coefficients, T, in the ratio 10, 5, 2.7 (approximately) at the peak sensitivities of the overlapping responses of the three cone types L, M and S and the rod peak (498 nm) between the M and S cone responses (see Fig 3.1c in Chapter 3). As a result, their overall transmitted correlated spectral power declines in the form required. The T values given above compare with $1/f$ values proportional to 10, 7, 1.9 so a $1/f$ type noise will result when the initial Polaroid motion produces independent random inputs to the filters of each eye. ("$1/f$ type" noise properties apply for $1/f^{\alpha}$ when α has a value between 1 and 2, and in our application $\alpha \sim 1.3$).

Interaction at the Striate and extra Striate Visual Cortex

We have previously seen how the outputs from left and right eye, each having components for parvo (colour and fine spatial detail) and magno (orientation and low contrast sensitivity) paths, travel separately via ipsilateral and contralateral paths from each eye to the LGN and on to the striate visual cortex V1. The actual on-centre and off-centre signals C_L and C_D are both transmitted in the optic nerve channels at about 39 m/sec, from cat optic nerve fibre measurements (Granit, 1977).

The P pathway in the human visual system begins in the P type ganglion cells of the retina and ultimately divides to form a pathway for colour and a pathway for 'form' linked to colour (Fig 7.3a). From the P layers of the LGN, the signals are relayed to V1 layers 2 and 3 where they supply the metabolic cytochrome oxidase "blobs" (colour) and the "interblobs" (form) as shown (stained) in Fig 7.3c. These two subdivisions finally relay most of their information to area V4 indirectly for registering colour through the thick "stripes" and "interstripes" of area V2 (Zeki, 1994 p183). Within the cortex the signals M and P mix and the inputs to the specialised visual areas may utilise signals from either source.

In our experimental arrangement the C_D^V and C_L^V signals which produce spatial edge response combine in V1 in the presence of their $1/f$ noise components. The temporal noise covers the filters' spectral range 400 nm to 600nm and each eye receives separate temporal input segments over the swing times of the order 0.1 sec produced by the computer controlled polaroid system. This produces a time lag in the inputs generated from the difference between the pulse of the light input to the left and to the right eye. We make use of an observer's visual retention of at least 70 bits of information and which can be superimposed during 0.1 sec (Averbach and Sperling, 1961, p210).

The delay for superposition is within the swing times of the Polaroid. The information inputs from each eye from the discrete time segments are combined at V1 as a result of this process. This provides a correlation of the power spectra components which declines with increasing light frequency f. Coloured $1/f$ noise is thereby added to C_L^V and to C_D^V and the independent spectral inputs from the left and right eye interact according to the convolution process in our L-V model of Chapter 5.

The $1/f$ noise which is both temporal and wavelength dependent is independent of the static image noise in the mammogram image itself. Our noise excites colour sensitive cells in laminae 2, 4 and 6 in V1 and becomes endogenous noise for the observer via the infero temporal cortex and V1 afferent branch of the trigeminal nerve inputs to the reticular formation. From the medial reticular formation cells these sensory signals are transmitted to the LGN which has interaction exchange with V1. This is characteristic of stages and subdivisions within several pathways (Zeki, 1994 p306).

Experimental Design Implications for Tests With and Without Noise

(a) Static (Series A) and Harmonic (Series B) Polaroid Motion for "No Noise"

We used polaroids and eyepiece filters with random selections from the declining retinal sensitivity of the observer from yellow to blue to generate time dependent

spectral segments $\lambda(t)$ for each eye. In our first (Series A) tests the observer's results with "no noise", (static polaroid), were compared to those "with noise" added (dynamic polaroid). Series B tests used comparison of observer's results with noise added and those from a periodic motion of the polaroid at frequencies of the same order of magnitude as the variations in the noise-added case (around 8 to 10 Hz). The polarisation effect for the case of the periodic inputs to the left and right eye, on both sides of the polaroid motion across the optic axis, was symmetrical both in relative location to the image and for the swing time relative to the optic axis. Although different in spectral content, due to the polaroid eyepieces each with a filter, both of these inputs are cyclic and there is no stochastic component generated for a possible resonance effect.

(b) Assessment of Intermittent Light Pulse Effect from the Polaroid Motion

A flicker or intermittent intensity stimulation can increase the electrical activity in the visual tract by up to $10\mu V$ (see Fig 7.4b). Maxima for flicker occurs around 12 to 16 Hz and around 7 to 12 Hz for "intermittent stimulation". Irregular intensity flicker occurs in our random motion case but is not a basis for stochastic resonance. Also the magno signal stream, not the (spatial) parvo, is the one mainly concerned with flicker as well as form.

The effect of steady illumination and transient rate of change have quite different effects upon the activity of the primary visual pathway (Pinneo, 1971). Each produces, in its own way, a change in "brightness" but not stochastic resonance. Measurements made which are relevant to rates of change in illumination in our Series A and Series B tests have shown (Fig 7.4a) that the rate of change of increasing or decreasing light flux,. from the speed of polaroid crossings, does not affect the known (Pinneo, 1971) geniculate activity at our level of observer illumination (< 0.3 ft cdls/sec). Also we note that at 0.4 ft cdls/sec the evoked "on" response peak value is measured at only about $1\mu V$ rms. At low luminances flicker sensitivity has been found to be similar with and without noise (Rovano et

al 1999).

(c) **Contrast and Illumination**

In regard to contrast seen by an observer when illumination changes, Heeger and Tolhurst (1997) evaluated a model which can explain the known contrast normalisation, ie no change in contrast for changes in illumination. The V1 to LGN feedback loops used in Heeger's model are also implicit in our model formulation in Chapter 5 regarding LGN/V1 interchanges.

Series A and Series B Tests

The foregoing matters presented in this Chapter resulted in the design of the experimental design for Series A and B. In our initial tests Series A, the observer was required to rate the difference in clarity of microcalcification detail on a nominal scale of 1 (low quality) to 5 (high quality) for observations on randomised presentations with, and then without, noise added. Subsequently we decided that a less subjective method could be used for Series B to make the experiment "symmetrical" (Pelli and Farell, 1995) by having the Polaroid in motion for observations made both with and without noise but using a harmonic motion of comparable amplitude and timing in the latter case. Instead of ratings, the observer responses were simply to be a "forced choice" response: better, worse or no change. The advantages of "forced choice" in experiments such as ours is explained by Pelli and Farell (1995) and quantitatively by Schnitzler, (1973). The background image noise in the actual mammograms is the same in both modes of presentation for any particular image being viewed.

The presentation using harmonic polarised motion as the "no noise" alternative presentation in the Series B tests produces, in effect, a placebo. Supporting arguments are given below.

- **Changes in Eyepiece Light Intensity during Polaroid Motion**

  Photometric measurements of the light intensity levels at the eyepieces for both models of operation were used to calculate the incident light flux. This was done in order to correlate with published data (reproduced in Pinneo's (1971) paper) on the

effect of changes in intensity as the dynamic polaroid passes across the static polaroid in each eyepiece.

The rates of change of intensity used in our experiment are considerably less than the level which produces any noticeable increase in optic tract activity

Also, for visual sensation and visual acuity at levels of retinal illumination within which the observations were made, (about 3 trolands, ie approximately 0.01 lumens/m^2), published data shows that the effect of changes in illumination as the polaroid swings, corresponds to the almost flat linear range for visual acuity changes. (See right hand side of response data in Fig 7.5, Murch, 1973). In other words there is no difference to the observer's acuity between the two modes of observations in Series B tests due to changes in illumination. For Series A the changes in "brightness" due to the polaroid motion were of the order $20\mu V$ rms and $10\mu V$ rms. We note that spectrally opponent cells of the macaque can discriminate wavelengths independent of brightness (deValois et al, 1966). This benefit in human vision applies to both Series A and Series B tests. Sinusoidal stimulation of the optic tract of the cat (Saunders, 1977) also showed the importance of geniculate colour opponent neurons for colour discrimination (poor in cats). Our colour opponent usage was the same for both Series A and Series B tests.

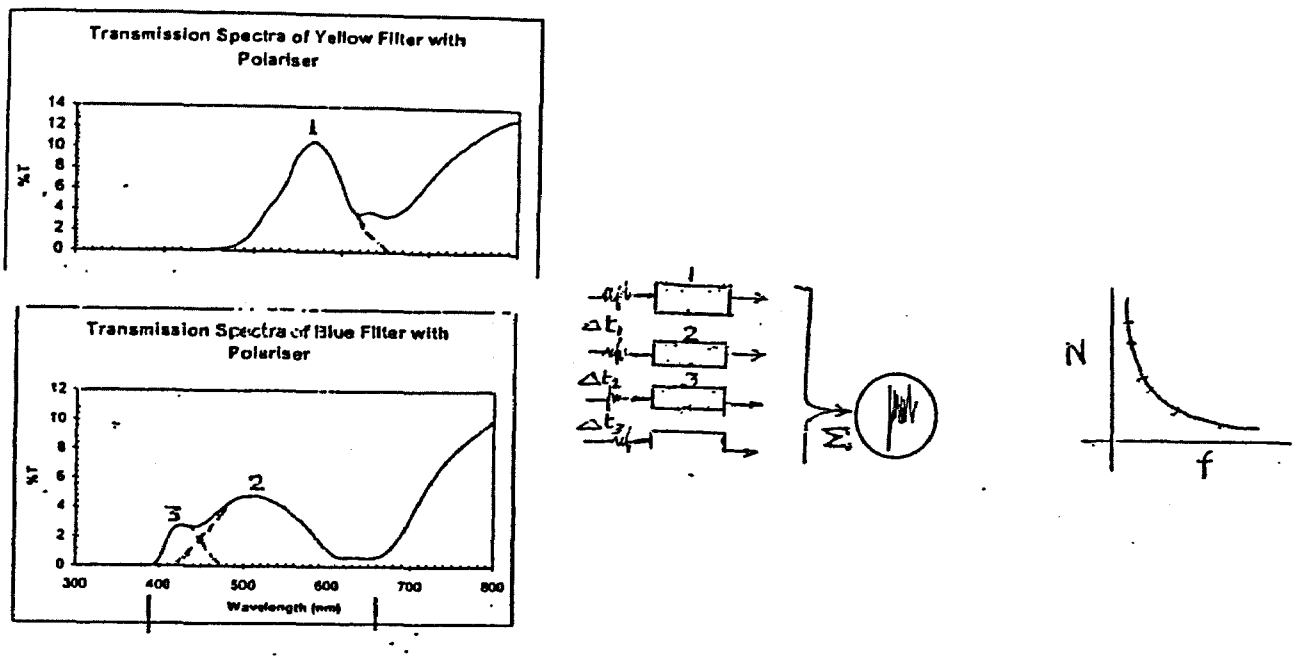

Fig 7.1 (Adapted from Crandell, 1994)

For a group of filters with Gaussian random variables from independent white noise sources and power spectra declining as 1/frequency)^2 the output has $1/f$ coloured noise $N(f)$. Only a relatively small number of filters is required (Crandell p159, 281). The optical analogy is used in a system with polaroid filters, retinal receptor responses and noise time segments from a random polaroid motion.

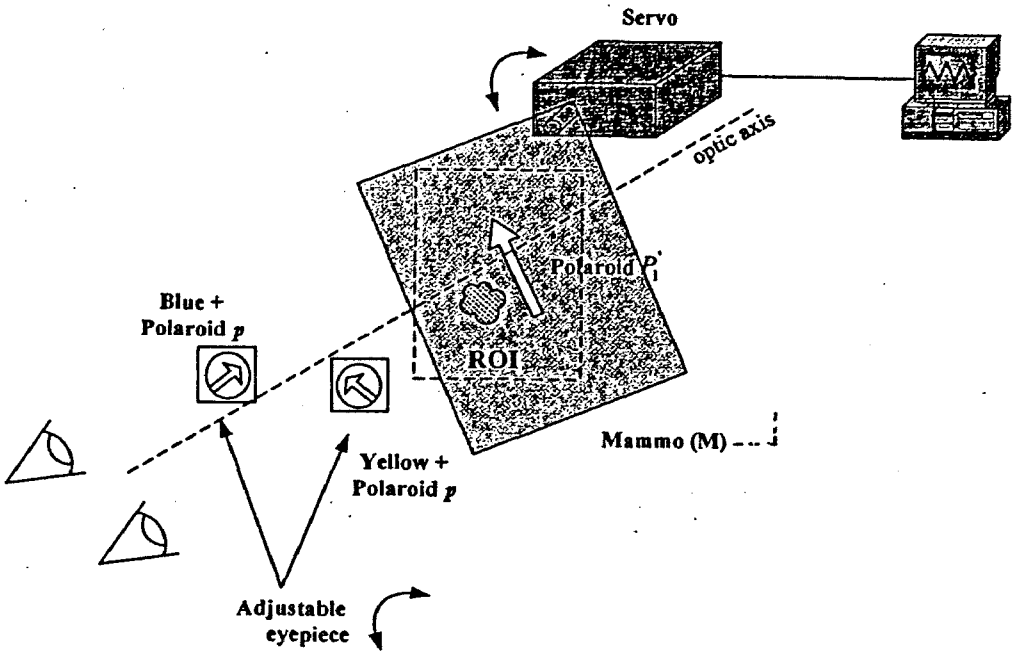

Fig 7.2a

Principle

- **As main polaroid swings "noisily", orientation of Polaroid eye pieces give "on"and "off" ("flashes") in a "noisy" manner.**
- **The percentage colour combination of blue and yellow to the eyes changes as the Polaroid swings.**
- ** **The colour input to the vision system is a noise input which the brain's visual cortex converts to a spatial signal.**
- **The combination of the spatial pattern from the ROI and this noise signal may offer a means of improving SNR and therefore image definition.**

*** Farley and Clark 1961 showed one-to-one correspondence for certain ranges of inputs.**

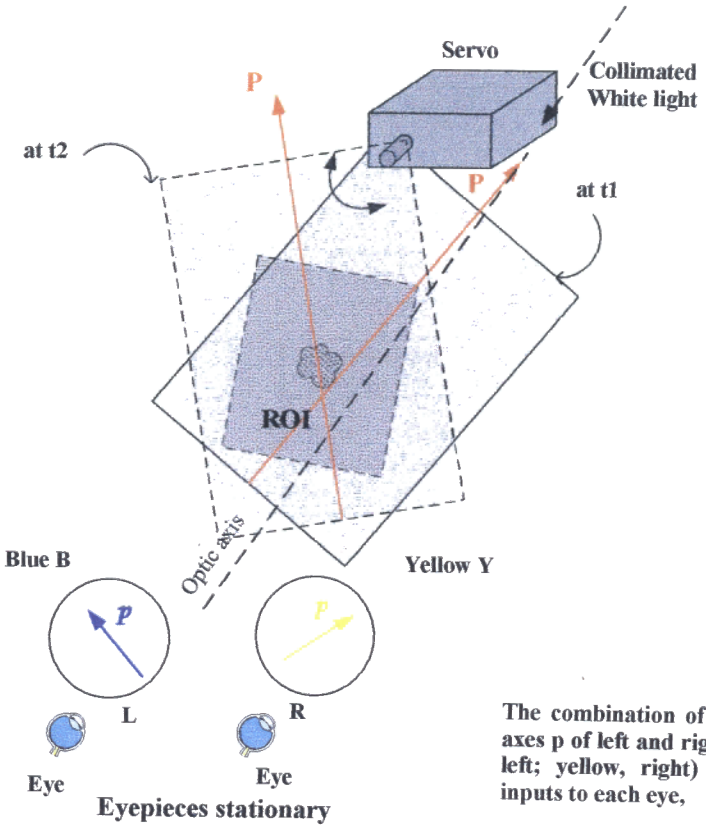

Fig 7.2b
The combination of motion of polaroid P and polarisation axes p of left and right eyepieces as shown with filters (blue, left; yellow, right) produces different temporal spectral inputs to each eye,

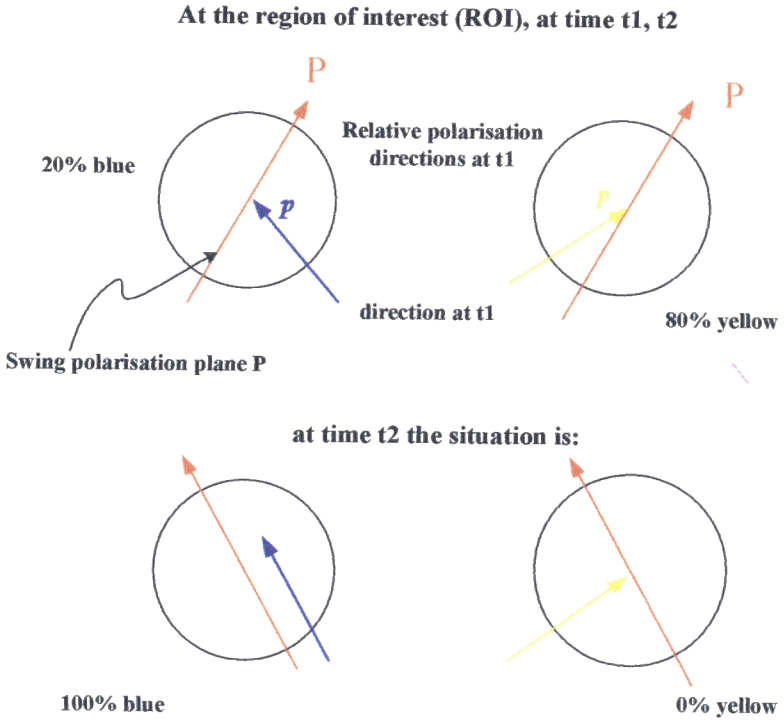

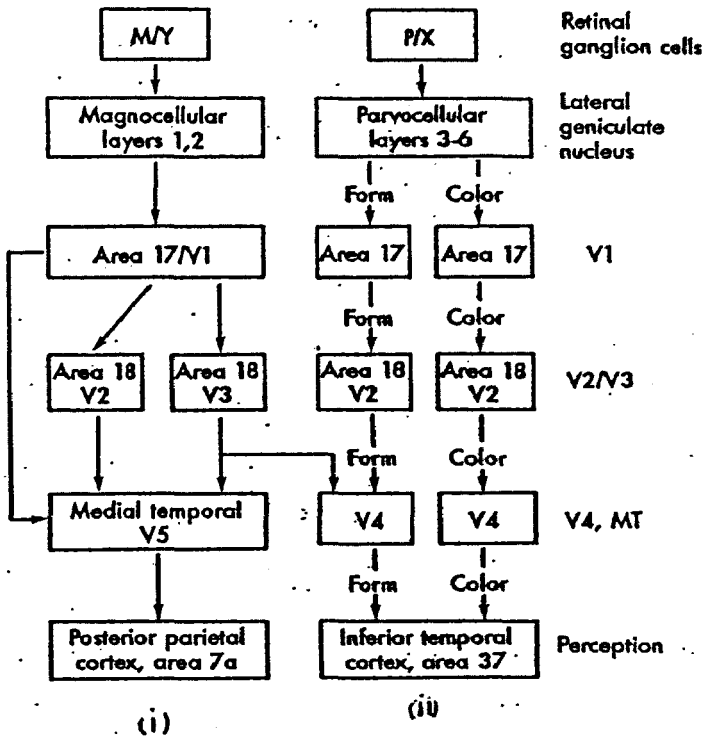

Fig 7.3a (Adapted from NeuroScience, Bear et al, 1990)
Magno(M) and Parvo(P) Pathways for form and colour

M and P cells coexist in retina, LGN, and V1 even though they process separate streams of information. The information carried by the M stream originates largely in rod cells and in the peripheral portions of the retinas and that the receptive fields involved are large. This information is used in determining *where relevant visual stimuli are located, and whether they are moving.*

The P stream, which originates mainly in cones and in the central area of the retina, codes for *form* and for *colour* (Fig 3a-ii). Starting in the lateral geniculate nucleus, form and colour information are carried by separate portions of the P stream. The portion that subserves form perception makes use of the small receptorfields and consequent high acuity of the P ganglion cells.

(The diagram includes the older Brodmann labelling of visual cortical regions as well as the V labelling).

The color-specific neurons of the primary visual cortex are particularly sensitive to the boundaries between different colors. Further color-specific cortical processing occurs mainly in area V4, to which the axons of neurons in V1 project. Area V4 has been shown to include nerve cells with a high degree of color specificity, which are activated by stimuli within a relatively narrow range of hues. The receptive fields of some of these neurons are subdivided into bands with different color specificity, so that color contrasts are particularly effective stimulus patterns.

(Grusser, 1987)

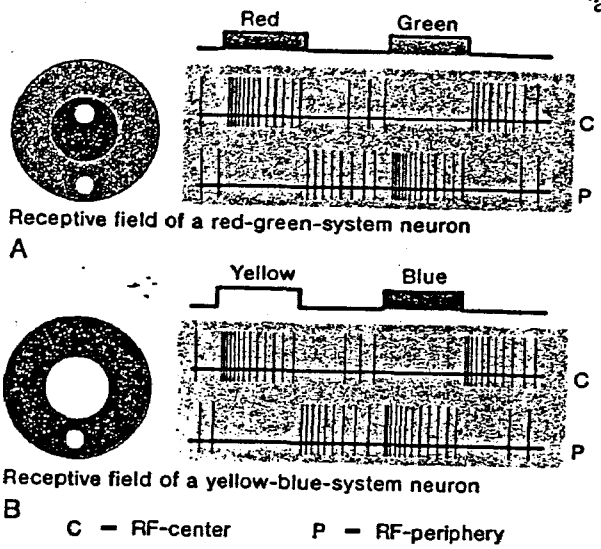

Fig 7.3b (Grusser and Grusser-Cornehls, 1987)
Simplified diagram of the spatial organisation of 2 receptive fields in either the ganglion-cell layer of the retina or the lateral geniculate nucleus of a mammal with colour vision.

A. Nerve cell of the red-green system.

B. Nerve cell of the yellow-blue system.

In colour-specific receptive fields there is an antagonistic organisation of RF-centre and RF-periphery.

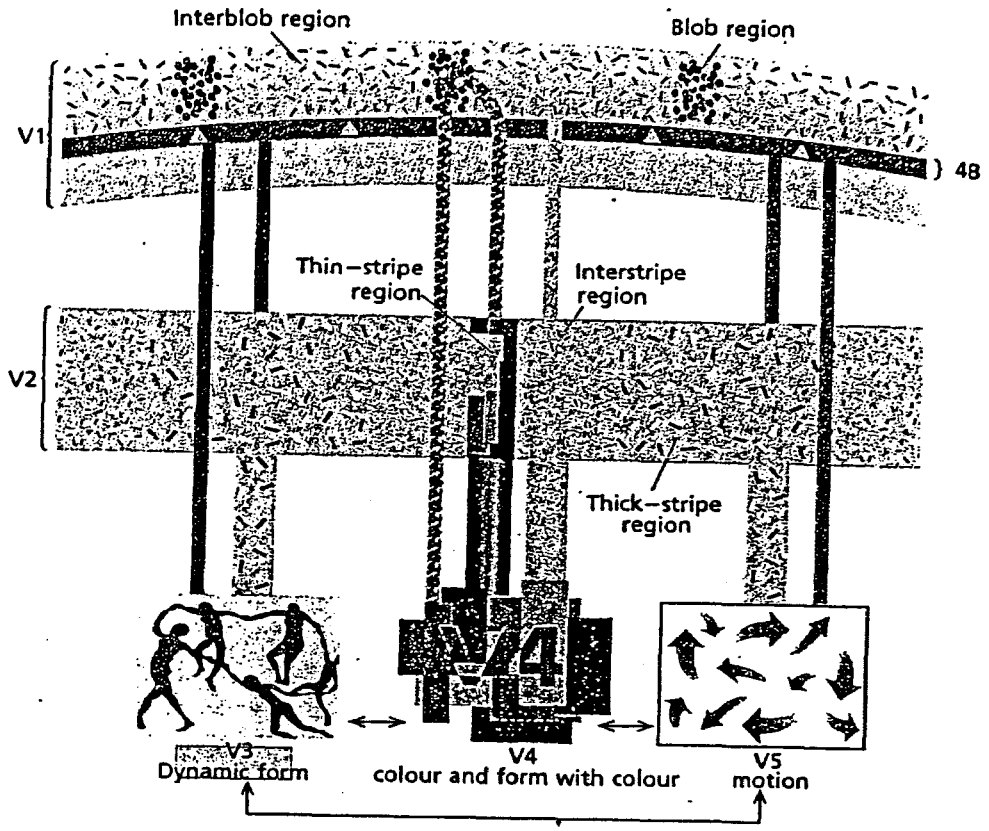

Fig 7.3c (Zeki, 1994)

Summary diagram of the four perceptual visual pathways and their anatomical connections, from V1 to the specialised visual areas of the prestriate cortex (Zeki, 1994)

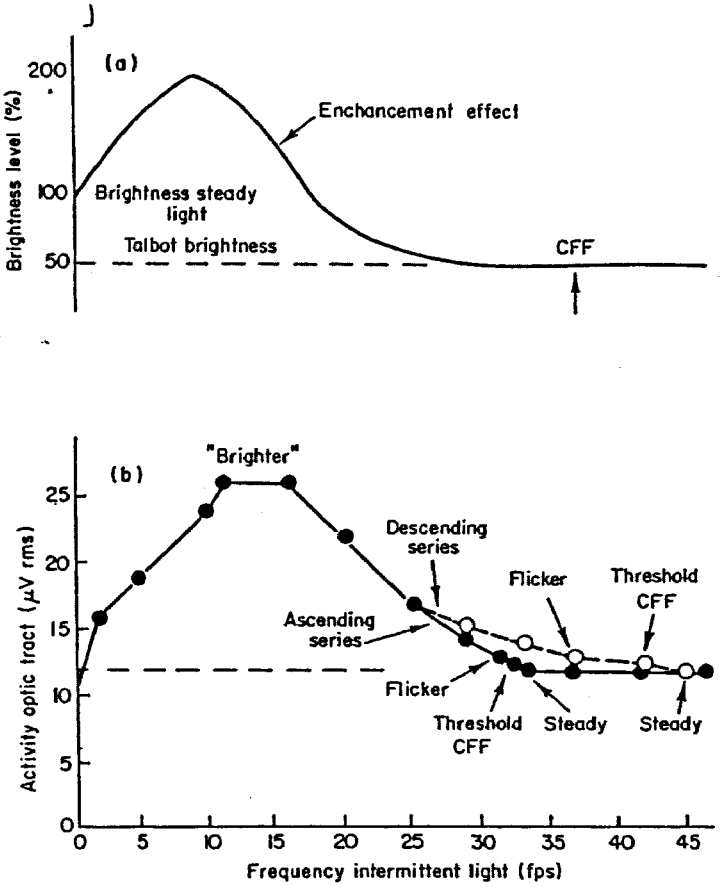

Fig 7.4a (Pinneo, 1971)

Comparison of activity of human "brightness" function (a) and average amount of human optic tract activity (b) as a function of frequency with intermittent light stimulation.

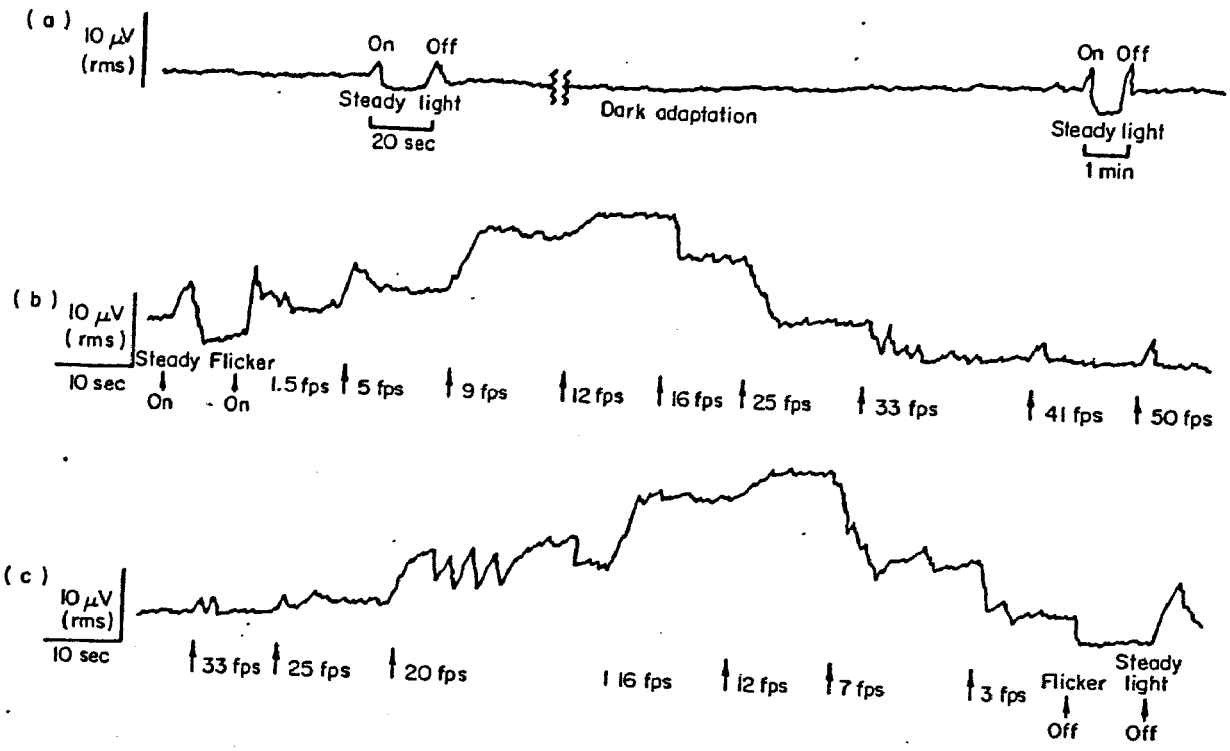

Fig 7.4b (Pinneo, 1971)

Direct recording of electrical activity of human optic tract during dark adaptation (a), increased frequencies of flicker (b), and decreased frequencies of flicker (c) with intermittent light stimulation.

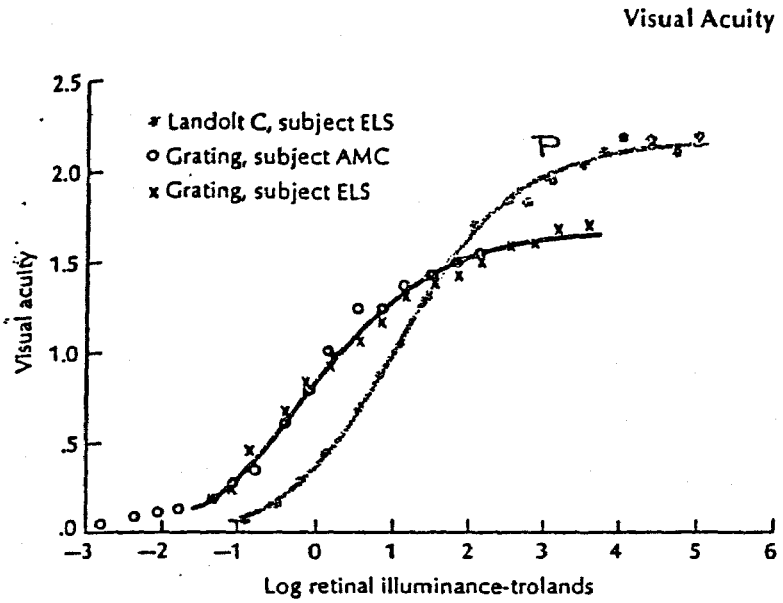

Fig 7.5 (Murch, 1973
Visual acuity for a grating and a Landolt C as a function of retinal illuminace (reproduced from Murch 1973).

Landolt "L", (orientation position)
Grating (resolution)

Chapter 8

Experimental Design, Observer Selection and Protocol

The null hypothesis is that the addition of coloured $1/f$ noise to the vision system does not improve an observer's ability to detect detail governed by edges in mammograms. Microcalcification deposits in a set of 30 images from mammograms were used. The observers were selected from a range of backgrounds in technical images of various types. Microcalcifications are generally easier to see than stellates but the details of their shapes, non-uniformity and spatial density of the particles are some of the key factors used for diagnosis by radiologists. We were not concerned with diagnosis but improvement in observation of such spatial detail of clusters by observers.

Sample Size to Detect a Difference

A method by Al-Bayyati (1970) provides a means for determining a sample size from each of two populations, where the variability of the assay is unknown, in order to detect a level of difference d (zero to 100 percent). A group of approximation values is shown in his Table 1 where, for example, we note that to be able to detect a difference of 30 percent at a significant level of 5 percent and probability of success in detection of 80 percent, a sample of 31 is required for a one-tail test. We used a sample size of 30 for each set of images with and without $1/f$ noise randomly added ie two populations, one "treated" with noise, the other not treated. The sample of 30 from each situation should allow a difference of 30 percent in the observation of an image to be detected at a level of success of 80 percent with and without $1/f$ noise added.

Two Randomised Sets of Observations for both Series A and Series B

We arranged for a group of five people covering a range, low to high level, of image experience to observe 30 cases in Series A and another group of five in Series B under two conditions of "no noise" and "with noise". The same experienced breast screening radiologist was included in both series. In order to be able to test intra-observer

variability in the presentations, a second set of the same 30 cases was randomised and observations made later by the same people tested under the same previous conditions.

The Information Given to Observers

Background information on mammography was provided to each observer in advance of their participation: (see Exhibit A and Exhibit B at the end of this chapter).

Examples shown to Observer prior to Viewing the Actual Cases

Examples of microcalcification deposits in a high quality reference book on the subject were shown to the observer who then viewed some similar mammogram regions of interest in our static equipment through the eyepieces. These included images which ranged from poor (rating 1), medium (rating 3) and high quality (rating 5) in clarity of detail and background. We did not discuss the technical detail of the equipment and asked the observer to "just rate what you see", 1 to 5 scale in Series A and, at the much later date Series B, "better", "no change", or "worse", ie forced choice alternatives, no ratings.

Selection of Observers for the Test of the Hypothesis

A set of 30 lesions with various types of image quality of microcalcification clusters were chosen for the tests. Five observers were chosen, male (4), female (1), ages 26 to 50, with experience levels ranging from one expert breast radiologist, to several with some experience with detailed images (but not mammograms), down to one with limited image experience of any type. The printed information sheet (Exhibit A) was initially provided to each person explaining what microcalcifications are and the need to observe clarity of detail and spatial extent of the lesion. A second sheet (Exhibit B) was given regarding the actual observation procedure.

The Rating System (Series A) and the Forced Choice System (Series B)

Two series of tests were organised. The first Series (A) requiring the observer to rate (1 to 5) the quality of detail observed in each of two modes of presentation (not stated what these were). "Just rate what you see for quality of detail".

After processing the results from Series A, the second series, Series (B) was subsequently organised. This Series was at a later date and was of improved design in presentation and more stringent. It required only a better, worse or no change response in the randomised presentations. A different group of observers was chosen except for the very experienced radiologist who was included in both groups.

Observation Conditions and Randomisation

Observations were made in exactly the same laboratory and room environment, lighting, temperature and seating comfort. The observer made a comparison of perception of fine detail in the same ROI when noise or no noise was added to the observer's vision. In Series A no noise presentation was with no Polaroid motion and in Series B the no noise presentation was via a symmetrical periodic motion of the Polaroid with a frequency of the order of average frequency of the noise fluctuations. The order in which these situations were presented in Series A and Series B tests was randomised, as was the actual sequence of cases in a subsequent run of the same set of images.

Series A Tests and the more Stringent Series B

Series A

Three hundred observations from five observers for each of 30 cases were presented twice at separated times after re-randomising the sequence.

Comparison was of ROI images with and without noise added by using the polaroid system with one polaroid in noise generated motion. Random presentation of ROI's and random application of the order of noise presentation were used for the sequence of 30 cases. Observer ratings were, as stated, from 1 to 5 according to clarity of detail.

Series B (and reason for follow-up from Series A)

This forced choice method reduced the possible subjective ratings in the Series A tests. In Series B the observers' observations were of random presentations of the ROI with either the harmonic disturbance or noise. This provided symmetry in the experimental

design. The observer responses for the forced choice method were: better, worse or no change as previously stated.

In both Series A and B observer could not see the computer screen, nor the operator actions. In addition the observers had no knowledge of how the system was designed nor its technical details.

Equipment Arrangement for the Observations

Equipment

With reference to the experimental arrangement up in Fig 8.1a:

lamp: 100W commercial incandescent tungsten filament broadband lamp providing white light

diffusing screen: finest quality draughtsman's transluscent sheet (University Coop Supplies, Sydney)

collimating lens: 10cm diameter, focal length 15cm providing collimated light to illuminate the mammogram region of interest

mammogram for study: a region of interest (ROI) containing microcalcifications was copied directly from a full mammogram on to a high quality transparency giving image quality equivalent to the film copies of the original mammogram. Thirty examples were chosen. Each region of interest was approximately within a 4cm diameter area

polaroid sheet P_1: a rectangular polaroid sheet (12cm x 17cm) was obtained from CSIRO Measurements Laboratory, Sydney. It provided approximately 30 percent linearly polarised light parallel to the axis and 10^{-4} percent of light perpendicular to the axis at 550 nm, and angle of field 60°. The sheet was

mounted securely on the spindle of a servo, the axis being at the centre of the top shorter side, 2cm from the edge. Fig 8.1c (photograph) shows the polaroid in position on the servo. The mammogram image was suspended from the clamp (shown empty) between the polaroid sheet and the collimator lens.

location of polaroid sheet P_1

see Fig 8.1b and legend

servo:

the servo drive was set up above the light path such that the polaroid sheet P_1 could be made to oscillate across the light path when the servo was driven by the program in the computer. The computer and servo were supplied by the School of Electrical Engineering at UTS

computer generated motion of P_1:

a PC type computer was mounted on a separate platform and provided a choice between 2 computer programs, one providing a noise output the other an amplitude modulated sinusoidal output for the servo for the Series B observations. The output could be switched from one to the other by a simple key stroke on the control panel (Fig 8.2) which displayed the parameters used and dynamic waveforms

viewing eyepieces:

2 eyepieces 2.5cm were mounted on the rear face of an internally blackened metal light box (25cm x 15cm x 10cm) the front of which was open to receive the light path. The eyepieces were set in mountings which allowed each eyepiece to be manually rotated. The polarisation axis was marked on the eyepiece in each case. Any small angle

adjustment by an observer could be noted, if used, from a circular scale on the eyepiece. Each eyepiece was fitted with a piece of polaroid of the same specification as that used for the oscillating polaroid sheet P_1. The right eyepiece was fitted with the yellow filter, the left eyepiece with the blue filter. The sheets used as filters were from commercially available coloured transparent sheets. The spectral transmission for the yellow and blue samples is shown in Fig 8.3.

check on field size for colour discrimination: From neurology we note that if the angle subtended by the image to the retinal field of the eye of the observer is less than half a degree of arc vision, there is a gradual loss of sensitivity to blue-yellow colour difference (Geisler and Banks, 1995). Measurements were made to check that in our equipment configuration the dimensions of the region of interest and geometry of the optics complied with the discrimination of colour.

experimental environment: the experiments were conducted in the air conditioned Biomedical Laboratory at UTS. The same ambient light condition was used for each observer and the views of the illuminated region of interest in the test cases were verified as acceptable for screening purposes by an experienced radiologist. Each observer was seated to provide comfortable viewing. The same conditions were maintained for each observer.

Interdependent Inspection of System and Methods for Observation and Recording

The equipment was inspected by Mr Paul Newman from Clinical Trials Unit NHMRC at the University of Sydney and previously Project Manager at the NSW Breast Cancer

Institute. The methods for observation and recording were explained. No changes were suggested.

Preliminary Minor Experiments for Observer Validations

Prior to the actual tests in Series A and Series B, two minor experiments were conducted to ensure that a cohort of observers could not hear any noise from the motion of the polaroid while using earplugs or head phones. Fig 8.4 illustrates the reasoning for provision of an acoustic environment for responses below the corresponding threshold for hearing. The auditory perception region corresponding to any sound in the motion of the polaroid is in the bottom left hand triangular region of Fig 8.4 below the auditory threshold curve.

The protocol for these tests were as follows:

- For Series B a cohort of persons, independent of the actual observers were selected who were willing to be tested acoustically to detect if they could hear any sound when the polaroid was swinging driven with noise present compared with when it was an amplitude modulated periodic motion. The observer was told to close his/her eyes and was equipped with a new set of earplugs or an industrial headphone protector as part of the tests. A random sequence for "on" or "off" was determined in advance for the operator. The test was conducted 4 times for each observer allowing 5 seconds rest with eyes open before going to the next test with eyes closed. The results indicated no acoustic awareness of the different motion.

  In the Series A tests the polaroid motion and polaroid eyepieces had intermittent illumination compared with the static, no noise conditions. Observers were not made aware of which condition was being presented and did not comment.

  For Series B, we tested for any difference noted by observers between a modulated sinusoidal swing of the polaroid P_1 and a random non periodic motion of the same sheet in the range of frequencies used. There was no comment regarding any

visual or acoustic difference by the observers.

The style of format for the presentations is shown in Table 1.

Protocol for Viewing and Operation of the Experimental System

1. A series of 30 ROI's from mammograms was used covering a range from low to high film quality. These covered a wide range of microcalcification types and distributions. The mammograms were supplied by Western Area Breast Screening Unit, Sydney.

2. Each observer was provided in advance with a written statement (see Exhibit A) describing the purpose of the experiment and the relevance of perception of detail used in screening. For the observations, the observer was given Exhibit B for practical requirements including any adjusting of the eyepieces to gain the best perception of detail. The order of mode operation of the polaroid was randomised in advance of the tests, the sequence being listed on a chart prior to the experiment.

3. A double blind approach was used in the tests. The operator whose task it was to mount the successive mammogram ROI's in random order was not shown the separate random sequence of presentation of the oscillation of the polaroid P_1. Likewise the computer operator was not made aware of the identity of the ROI case being presented. A period of approximately 30 seconds was allowed for the observer to view each case and time signalled to the observer by touching his/her arm after 20 seconds. The observer simply voiced his/her result (a rating in Series A or a better, worse, or no change in Series B).

Table 1
Style of Format for Presentations

Mode "with noise" or "not noise" Sequence of Presentation		Observer's decision for the better case
1st	**2nd**	
not noise	Noise	1
not noise	Noise	2
noise	not noise	1
noise	not noise	1
not noise	noise	no change
Noise	not noise	no change

Method of Scoring

Series A

The result was a rating 1 to 5 for the range of low to high quality of detail in both the 1st and 2nd presentations

Series B

better with noise (+1)
no change (0)
worse with noise (-1)

Additional Note on Eyepiece Adjustment for Best Perception

It is interesting to note that a slow rotation adjustment clockwise and/or anti-clockwise of one or both eyepieces appeared to have a "tuning" effect, more for some observers than others. It was a quite small but noticeable "jump" in image definition for some cases. This had also been noted by some helpers [3 out of 4] during the installation and preliminary test of the experimental equipment. It was similar to the manual tuning of a radio for best station reception. This may be related to the known, and only recently explained, "jump effect during slow transition through resonance" (Celet et al, 1998, Vilar and Rubi, 1997 and Thomas, 1992) in some mechanical and electronic examples in

the presence of noise. If so it would tend to add an additional support for the existence of a resonance effect in our experiment. It was not explored further for the present project beyond the possible connection to the reference papers cited.

EXHIBIT A

Mammography is recognised as the most effective method currently available for detecting breast malignancies and relies on experienced observers' interpretations of both "direct" and "indirect" signs. "Direct signs" include palpable mass, nipple discharge, nipple or skin retraction, erythema and dimpling. "Indirect signs" include the presence of characteristic calcifications. Subtle microcalcifications are often the first and sometimes the only radiographic findings in early, curable, breast cancers. It is important during visual inspections and subsequent diagnosis not to miss any detail in the microcalcification region. This is also important in the detection of "masses" (actual tumours). Mammograms (soft X-rays) provide very good spatial resolution but the regions of interest are part of a mixture of "shadows on shadows" characteristic of X-rays. In mammography we are interested in edges to show sizes and shapes and their spatial distribution in deposits of microcalcifications or boundary detail in the case of a suspect mass. An example of the relevance of edges and clarity of detail for microcalcifications is that when there are 15 or more microcalcifications per cm^2 the probability of indicating a suspicious case is considered high. This is only one of the features used but it is an important one. Characteristic shapes of cluster distributions are also important so the boundaries of the cluster in the region of interest (ROI) should be observed. In our experiment we require only an observation of clarity of detail, not the diagnostic significance.

NOTE FOR OBSERVERS
EXHIBIT B

The experiment is to determine whether 2 different types of motion of a polaroid sheet in a vision experiment produce any change in an observer's ability to clearly see the boundary of the region which has small "dots" of microcalcification deposits. It is a matter of clarity of the image of these features and deciding whether the first or second presentation gives the better result ie simply say "first" or "second" or "no change".

The scientific purpose is simply to find out if an effect exists or not. The results will be analysed statistically to determine this from a number of observers. The deposits in many images are not well defined, so do not expect sharp boundaries. We will show you some actual cases ranging from poor clarity to very good clarity to help you see what the range actually looks like, even though the cases you will see vary in structure and pattern.

To make your observation please rotate one eyepiece (the right hand one) slowly from its original position, over a small range and watch carefully for any position which you think is the best to observe the details of the features. It is best to go slowly past this position and rotate slowly back to get the best position (like tuning a radio to get the best reception). Then decide between "first", "second", or "no change". Only comment on what you see. Do not imagine. There will be a set of 30 images and you may take about 20 or 30 seconds to do each One. To help your concentration you will be offered a clean set of earplugs to block out any distraction. After completion we would ask you to take a break or return at another time to do a second set of observations.

Fig. 1a

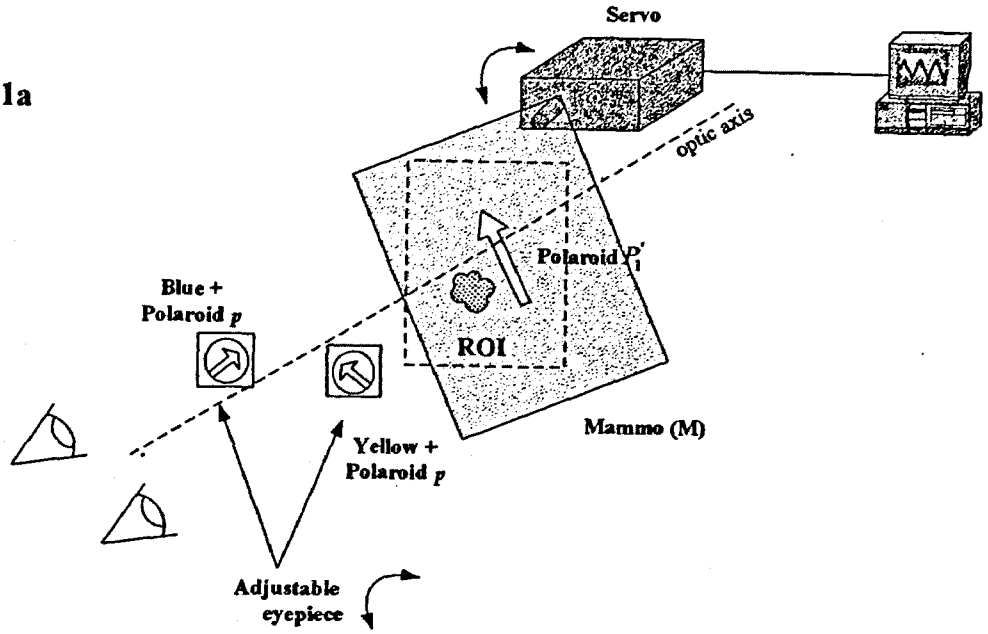

Fig. 1b

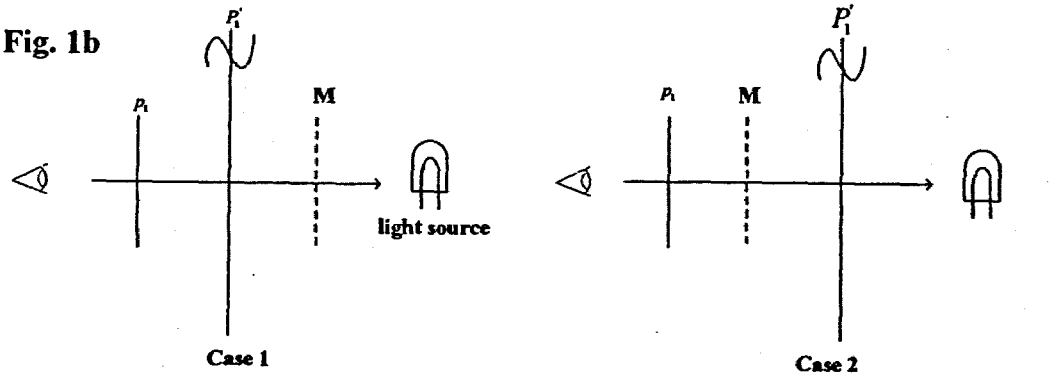

Polarisation and scatter from mammogram constant input to noise generator $p_1 P_1'$

Polarisation and scatter from mammogram vary as polarisation axis of P_1'

Figs 8.1a and 8.1b

Although both cases produce noise, the Case 2 adds a small varying polarisation and scatter contribution from the ROI microcalcifications as the polaroid oscillates in random back and forth to produce a noise effect.

This would result in a departure from the L-V differential equations in the theory of retinal vision when viewing features in mammograms in translucent light. The function used for the noise would have to include some characteristics of the ROI microcalcifications.

Case 1 has the scatter and polarization from the microcalcifications constant before that light is incident on the oscillating polaroid system. Therefore it does not contribute to the system in a time varying manner as would occur in Case 2. Therefore the noise process generated by the polaroids does not directly involve any time varying feature from the light from the microcalcifications.

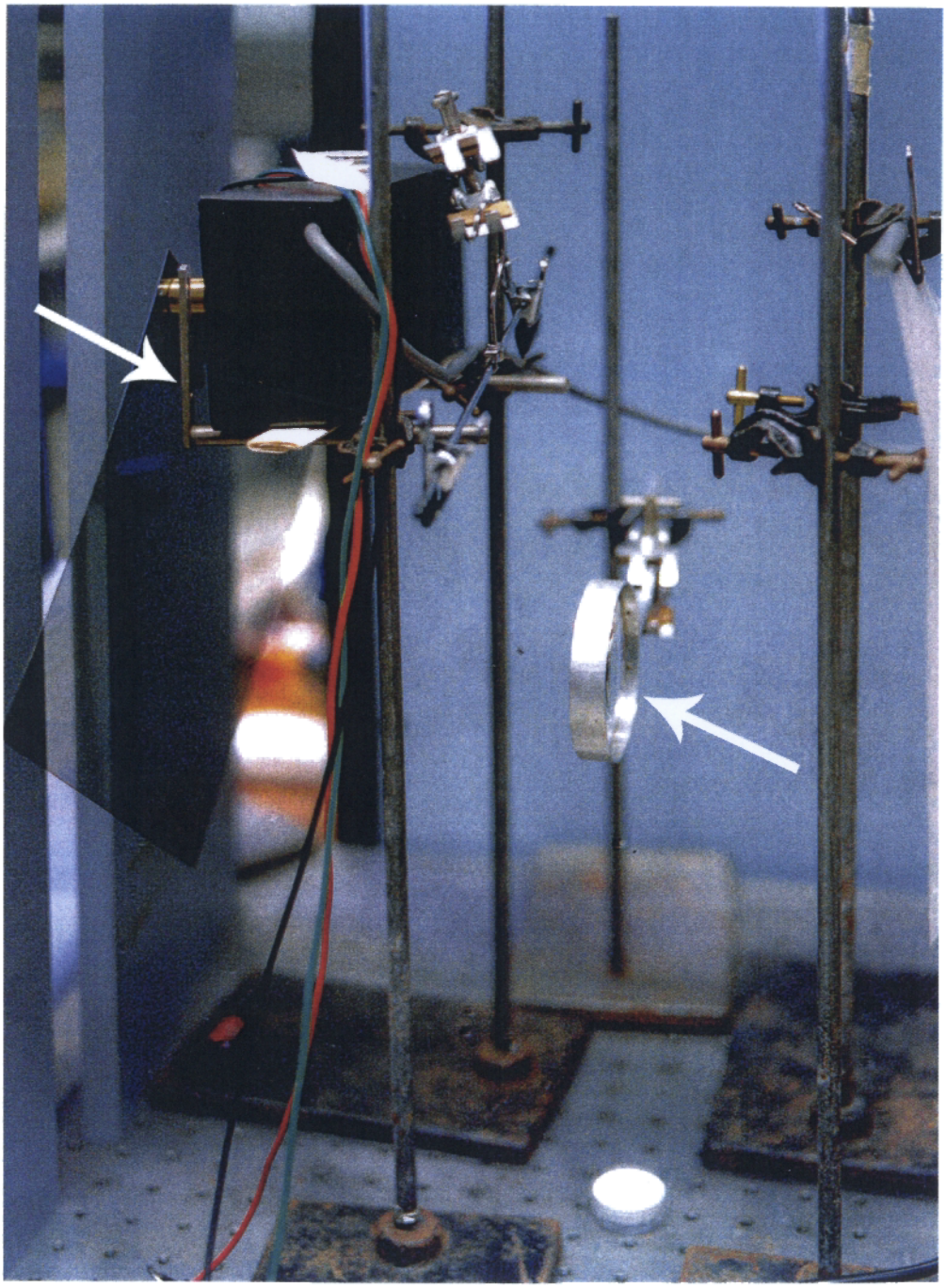

Fig 8.1c
Servo mount with polaroid sheet mounted on a stand (left),
Collimation lens (centre).

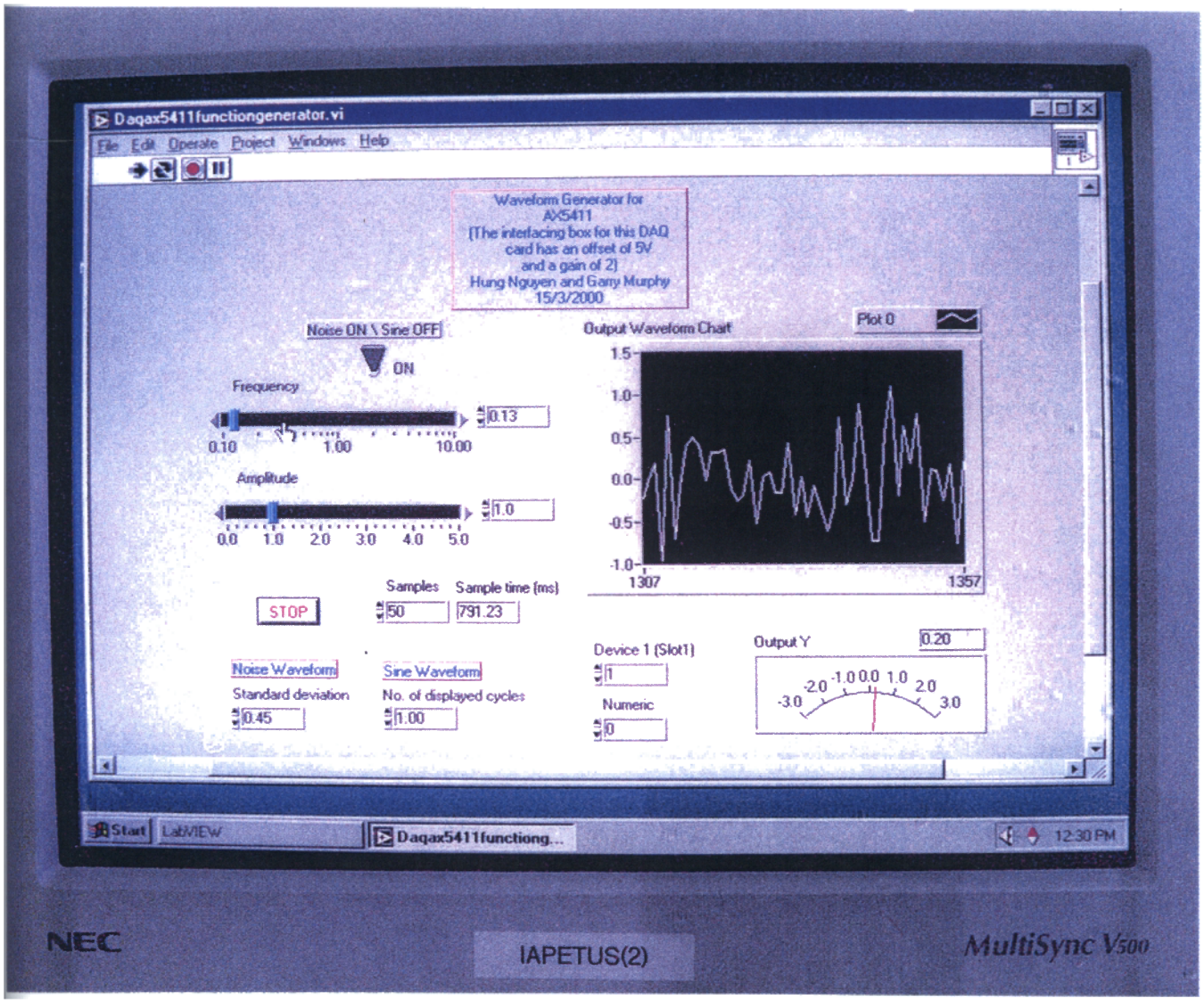

Fig 8.2
Computer Screen Control Panel for dynamic polaroid motion

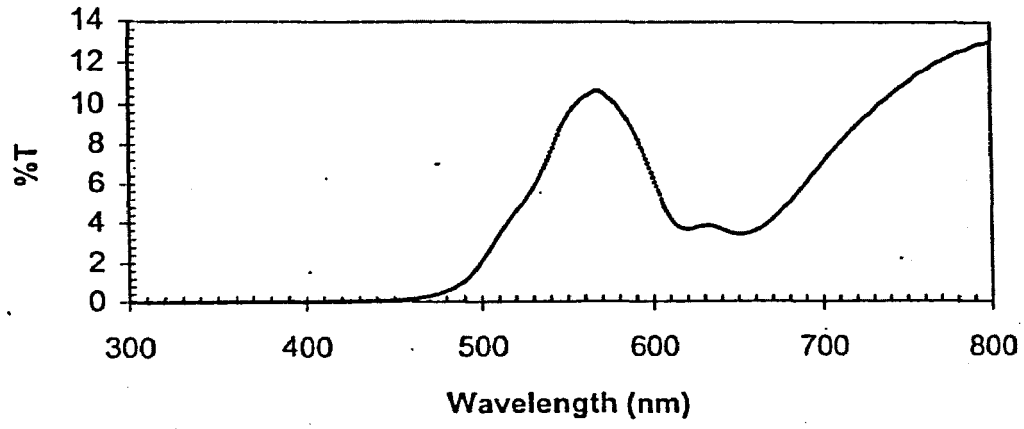

Fig 8.3a
Transmission Spectra of Yellow Filter with Polariser

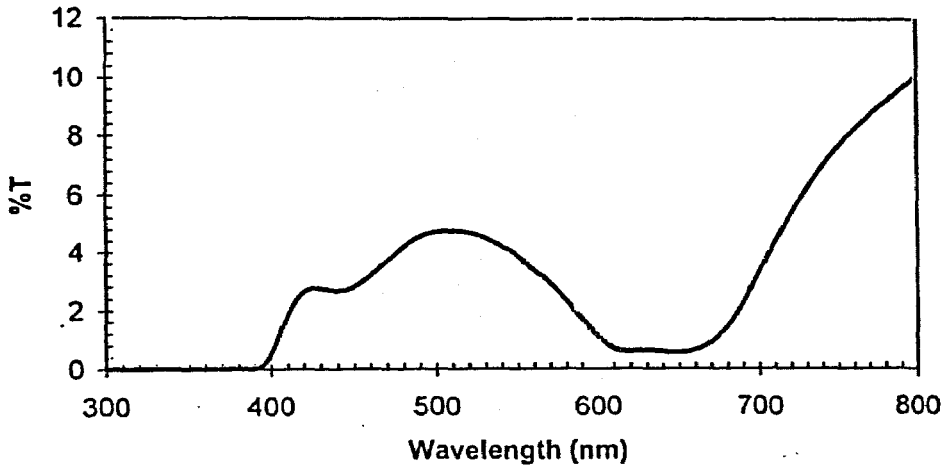

Figure 8.3b
Transmission Spectra of Blue Filter with Polariser

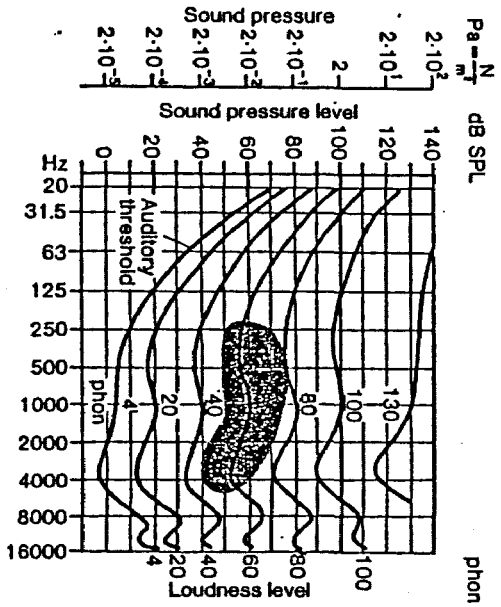

Fig 8.4 (Grusser and Grusser-Cornehls, 1987)
Curves of equal loudness (isophones) according to the standard DIN 45630. The ordinates on the left give the equivalent values of sound pressure and sound pressure level. The shading indicates the speech region.

Chapter 9

Results of the Tests and Implications for Observer Performance

Statistical tests were applied to the observations with the assistance and advice of Dr W.T. Hung, an experienced statistician

Data – Each observer trial consisted of 30 images "with" and "without" $1/f$ noise applied from a randomised sequence of mammographic regions of interest. The observer decided whether the detail perceived "with noise" or "without" was better, worse or no change.

Five observers, were utilized in Series A and a different five in Series B (except for an expert radiologist common to both). As stated previously, they viewed a randomised set of the 30 images and then after a time lapse, a second re-randomised set of the same images. The sequence of "with noise" or "without noise" treatment was also re-randomised.

One-tail and two-tail tests

As noted in Chapter 7, a sample of 30 cases was used on the basis of a one-tail test (Al-Bayyati, 1971). "One-tail tests are more sensitive (more "powerful" statistically) for disclosure of a difference. When, from previous experience or on the theoretical grounds, the nature of an assumed difference between two parameters is known or thought to be known, then a one-tail test should be made after deciding on the assumed direction of the test" (Diem and Seldrup, 1982). A further comment from Diem and Seldrup, is that "the tendency in medical and biological investigations is to use too small a significance probability".

The reason for conducting most experimental tests is that the investigator has reason to believe that the alternative hypothesis is true, ie that there is reason to believe that there is

an effect", as in our case. The biophysical motivation for our hypothesis of a favourable effect from $1/f$ noise has been given in previous chapters from published papers on noise and on L-V differential equations. In our experiment we also note that there appears to be no reason ever reported that $1/f$ noise would make perception worse than when it is absent. Also we noted in Chapter 7 that the harmonic perturbation used in the alternative presentation to observers is a placebo effect.

Independent Observers – The trials were undertaken at different times and with observers independent of each other. The observers were chosen from different background experiences in image work. There was no communication between observers during all of the tests and all observers were from different work backgrounds.

Significance – The p value is used for significance of the null hypothesis using the Tests given below.

The Sign Test for Paired Differences

This used the Binomial Distribution for Confidence Limits when $+1, 0, -1$ signs are assigned to better, no change, or worse. In such cases the null hypothesis is that the differences do not on the average differ from zero, or rather that the numbers of differences respectively smaller than and larger than zero are the same. The median is therefore zero. The number of differences which are smaller or greater than zero, are counted. The number of differences is checked against significance levels for the same value from Tables of the Binomial Distribution. (The McNemar and the Stuart-Maxwell tests for paired differences with alternative forced choices were also considered but were inappropriate due to the requirements for two independent sets of data).

Results of the 600 observations

Series A Series A observers used ratings 1 to 5 (common in radiology work) of their perception of detail in 30 microcalcifications of interest done in 2 sets of readings of the 30 after re-randomisation. A rating of the effect on observed detail with noise added to the vision

system as compared with no noise added was made for each image presented.

Sign Test
For significance

The 1st set results of 30 observations made by the 5 observers gave $p < 0.05$

The 2nd set results of 30 observations made by the 5 observers gave $p < 0.05$.

The intra observer variability test results were also very good. The results of Series A indicate significance for the hypothesis $(p<0.05)$. However, it was decided that the subjective rating by observers was a weakness. Also the comparisons from the use of a dynamic and static polaroid operation was not a 'symmetrical" experimental design.

Series B

The Series B tests used a more stringent condition for observers ('better', 'worse' or 'no change') with "forced choice" to eliminate, or at least reduce, any subjectivity using ratings. In addition the test was symmetric with a harmonic motion of the polaroid (no noise) and the random polaroid motion to provide $1/f$ noise input to the observer.

As in the Series A tests, the Series B observers were each given the same basic information on what was required in observing any difference in detail quality in an ROI but not given any indication of the random order of presentation of the cases nor of the type of visual perturbation applied.

Series B Sign Test Results

At the $p<0.05$ level of significance 5 out of 10 (5 observers, 2 sets each) were significant. At $p<0.1$ level, 7 out of 10 were significant. Two observers who were the most experienced with images among the group gave $p=0.07$.

The p results for the expert radiologist were always smaller than any of the others. The results for the observer with no experience with any images gave the worst results. When the inexperienced person was excluded all 4 observers gave $p<0.07$ for the second set. (The improvement was from 3 observers out of 5). However the results for the first set remained unchanged.

Intra-Observer and Inter-Observer Variability in Series B

Tests were made of intra-observer and inter-observer variability. Series A showed good results. In Series B all 5 observers had good agreement between their first and second sets of readings for the 30 cases. The inter-observer results required a more careful analysis and interpretation. The analysis of results (Shoukric and Pause, 1999 and Landis and Koch, 1977) indicated poor inter-observer agreement which probably is consistent with their level of background experience but restricted us from combining their results in the tests.

Comments on Significance and p - Values

Mr Paul Newman of the NHMRC Clinical Trials Unit for Breast Cancer who had inspected the equipment and methodology as well as the data sheets, commented as follows:

- Series A indicates significance $(p \leq 0.05)$
- Series B (more stringent test) would traditionally indicate "a trend toward significance $(p \leq 0.1)$"

He also pointed out that $p \leq 0.07$ attained for observers in our test are becoming acceptable for experiments in biology and neurology due to the difficult nature and biological/neurological uncertainties in many experiments (including ours). Also a senior statistician at the Trials Unit who had also seen the data from our test Series, said that in comparing two sets of results at .05 and .07 level, the result at the .07 level would not be discarded subject to the magnitude of the actual number of cases recorded showing a positive effect as seen in Table 2 below:

From the 300 observations (5 x 2 sets of 30) in Series B

$\frac{178}{300}$ preferred 'added noise' as seen in Table 2

Table 2

(1) *better with noise*	(0) *no change*	(2) *better without Noise*
Count: 178 59.34%	67 22.33%	55 18.33

A recent journal article from the Royal Statistical Society also debates the taking of $p < 0.05$ as an irrevocable level in significance (Reese, 2004). The following is from the Encyclopedia of Statistical Science (Wiley Interscience, 1986). "The p value is well-defined, with a specific probability interpretation. It is not arbitrary, as a preselected significance level usually is in practice, and it is objective. An investigator who can report only a p value conveys the maximum amount of information contained in the sample and permits all readers to choose essentially their own level of significance and make their own individual decision about the null hypothesis. This is especially important when there is no justifiable reason for choosing one particular level of significance".

Conclusion from Analysis of Test Results

The foregoing results give reason to claim with a reasonable level of confidence that a hypothesised favourable effect from $1/f$ noise does exist for edge detection and is more likely to be registered by observers with experience. However, for acceptance in clinical practice in screening it is suggested that a future series of tests would be desirable with experienced radiologists rather than observers with different backgrounds. This would then also allow the tests to include detection of stealthy stellates which can have weak boundary edges.

Discussion

The primary vision cortex model presented included important effects which are observer-dependent such as the interaction with the infer temporal cortex (related to threshold detection) and reticular formation (for alertness and attention) plus interactions with higher level cortical functions giving input to V1 laminae. We note the coefficients c_1 and c_2 in the L-V differential equations 5.6 and 5.7 for both C_L and C_D for the selective inhibition of unwanted detail. This depends on experience and attention in feature extraction from images (Heslenfeld et al, 1997) and therefore implies that an experienced radiologist would be associated with results different from an inexperienced observer. Persons experienced in particular types of image observations are often considered to have "templates" in memory which can be assessed in feature recognition (Kent, 1981 and Windsor, 1988).

It should also be noted that in our experiment improvement in edge detection from the addition of $1/f$ noise is a spatio-temporal effect, not a static one. That is to say, it occurs during the orbital cycle of the solutions of the L-V equations and at the particular spatial region with small values where the fovea should be used by the observer. Therefore better results would be expected from an organised visual search of the image rather than a static viewing where details are simply expected to appear without a search.

It was not practical to give the observers training in image searching and, for those seeing regions of mammograms for the first time, knowing "what to look for" was probably a difficult concept despite a brief talk and a written guide to microcalcifications.

A test was made (by Dr P. Petocz, Department of Mathematical Sciences, UTS) to assess if a tiring effect was present or not for the observers by listing the order within a trial. The result showed that the order within a trial did not give significant difference for the result, so no tiring effect was indicated. It can also be noted that there was only a marginal preference by observers for noise presented first (91/170) or presented second (87/130) as seen from the Table below.

Table 3

Order for 'noise added'	No change 0	better 1	worse 2	All
2nd	22	87	21	130
1st	45	91	34	170
All	67	178	55	300

There are about 100 million rod receptors in the retina and about 5 million cones. The cones are densely populated in the fovea for detail detection. As pointed out by Kent (1981) the brain somehow produces a complete analysis of their patterns for illumination about 10 times each second. To do such analysis by examining all possible permutations of the millions of pieces of information and decoding it against some test of known codes would be too great a task even for the brain so it actually goes to some extremes to reduce the data. "The first step is to make decisions about what not to look at" including suppression of unwanted information. This also involves the complementary but opposite actions used by neurons of the vision system. Other advantages in human visual processing arise from the micro architecture of receptor fields in the retina as researched by Sheridan in computational vision (Sheridan, 1997).

A further comment is needed on the observer-related effect on parameters in the models for C_L and C_D arising from the observer's acutance and acuity which affect the basic formulations for gradients in the models:

Acuity, in human vision, is defined as the reciprocal of resolving power expressed in minutes of arc. If the eye can resolve 1 minute of arc the acuity has the value 1. Under less optimum conditions of seeing, acuity may range down to below 0.1 (L.M. Biberman, 1973) p23.

Acutance is a measure of the sharpness of an edge expressed in terms of the mean square of the gradient of luminuous flux (or image density in a film image) with distance from the edge. Acutance and resolving power in acuity are often closely related but this need not be the case. Acutance, A, has been often used as a measure of image quality but it is known that the expression $A\left[1-\exp\left(-kR^2\right)\right]$ is well correlated with *subjective* impressions of image sharpness. k is a constant and R is resolving power (Higgins and Wolfe, 1955). This aspect of observer dependence is probably also a contributor to the difference in edge detection performance of our observers who come from different levels of experience in viewing image detail in their everyday work

The foregoing discussion adds emphasis to the need for training of breast radiologists for "organised searching" when reading mammograms. Statistics on the variability in performance of breast radiologists in a USA study have been quite surprising (Beam et al, 1996) including detection variability of up to 11%. Our project shows that experience in active searching, not passive "looking", can assist in edge detection in mammography. In following up reasons for the difference in observer performance in other similar type of applications the summary of findings by H. Self and his associates (Biberman, 1973) is quite revealing in regard to likely application for visual searching processes. It is reproduced as an Exhibit on page 138.

EXHIBIT

Observer's Procedures, Training and Time Requirements. Self makes some observations based upon the yet unpublished results of some research by him and his associates.

"1. When a target is not quickly found, searchers tend to 'over-search' (repeatedly search) likely areas and completely avoid areas dismissed as either unsuitable or as suitable but not containing the target. Frequently targets in contextually unlikely places are not found for minutes even though of adequate size, resolution, and contrast for quick recognition when examined.

"2. Despite instructions and training, few observers systematically search a scene until after initial rapid scene-appropriate search fails to find a target. Clearly, search is neither purely systematic nor purely random.

"3. Observers sometimes forget which areas have been searched and assume that they have searched an area when they have not. This leads to large time scores when the target is there.

"4. Other things being equal, target objects closer to the center of the picture tend to be found quicker.

"5. Numerous moving image studies show that subjects under high pressure do hurry to find targets much quicker than those under little or no pressure.

"6. Some observers quickly find targets that others with equal training find only after extended search time or do not find at all. Chance factors, such as looking at the right place early in search, are clearly important. However, some subjects are consistently as much as two to three times faster than others over dozens of targets and scenes, and across studies.

"7. Averaged across many subjects, identically-appearing target images vary drastically in the time required to detect and to recognize them in different backgrounds (scenes). In other words, there is a strong target–background interaction.

"8. When briefing target pictures are rotated relative to the target in the scene, or are of a different size or lightness, target detection and recognition are slower."

Finally Self presented the following conclusions:

"Upon close examination it is seen that many variables or factors influence detection and recognition of objects. The effects become especially apparent when the time to view an image is limited. Even the common image quality measures in use today turn out to be complex in application and in specification of the obtained values. For example, it was pointed out that, at different points in the image and in different directions at any given point, obtained image resolution varies. In making predictions of observer performance, it is clear that the effects of even the simple quality aspects depend upon the state of adaptation, visual capabilities, training, instructions, motivation, etc., of the observers. Even observer search patterns are important. Clues from briefing and/or the image context can make a very large difference in performance. Similarly, time to find targets or the probability of finding them within specified time limits is greatly influenced by 'image complexity' variables, several of which are included in the term 'context.' The influence of target–background interaction effects is clearly established."

Chapter 10

Conclusion

The primary objective of the thesis project was to formulate a functional model for edge detection in the primary vision system from the retina to the visual cortex V1 and apply this with a new method for incorporating $1/f$ noise to achieve improved edge detection particularly in mammograms. The model also has potential for other applications. The principles of the project have been validated and several new methods have been developed in specific areas of early vision in utilising $1/f$ coloured noise. Although an extensive research literature exists on all aspects of vision, an integrated formal model from retina to V1 has been elusive. Seminal mathematical papers on edge detection have been criticised by neurologists for lack of appreciation of the functional neurology (Zeki, 1994). We endeavoured to provide this neurological requirement in formulating our model.

Production of a Functional Model in Early Vision

The thesis presents a new type of model based on the two key entities of on-centre and off-centre responses C_L and C_D of groups of neurons in vision. Such groups have been shown to exhibit single cell behaviour (Siegel, 1990). Our model for the retinal responses resulted in differential equations of the Lotka Volterra (L-V) type and shows good agreement with published measurements of ganglion responses (Baylor and Fuortes, 1970). The L-V properties replicate behaviour of the neuron potential from which spike response signals result in the optic nerve.

The neurological function for visual acuity and acutance in V1 depend on the spatial gradients of C_L and C_D at the locations of zero crossings (light $\leftrightarrow$ dark) and Logan (1977) has shown the important and surprising result that the information carried by responses at the zero crossings is sufficient to define the edge response. We utilise this result for our model to obtain the differential equations for edge responses. The zero crossings correspond to the points of inflexion of our C_L and C_D functions at V1. The

resulting differential equations are also of the L-V type but the interaction terms are more selectively complex than at the retina. This is due to the complexity of the functions involving inter- and intra-signalling in the six laminae of V1.

The known requirement for speed of transmission of vision information from V1 to higher cortical levels means that any extensive iterative computational processes are not realistic.

Retinotopic Property in Vision

Our result of the L-V behaviour at both the retina and V1 agrees with the known retinotopic image property giving a changed, but conformal, preservation of the original image. We are not aware of other modelling of early vision which demonstrates this property quantitatively.

Extending Information Theory for Simpler Formulation on a Functional Basis

The foregoing modelling from retina to V1 for edge detection was made possible by the fact that C_L, C_D and the mathematical operations on them, conform with the requirements for "information content" from Shannon's Information Theory, as extended for *functional* operations in microbiology by Rescigno and Maccacaro, (1961). This allowed us to avoid circuit-type modelling and the need to include microcircuits. The approach can be considered as a neurological modelling analogy of the type of experimental approach of Hubel and Wiesel which became the basis of much mainstream vision research since the 1970's.

Capitalising on L-V Properties for Resonances

The responses of our edge detection differential equations when $1/f$ coloured noise was included in interaction terms in the L-V model, showed correlated power spectra improvement when C_L and C_D had small, approximately equal, values. This provides a selective advantage for improving weak images. An experimental system to produce $1/f$ noise was devised based on the spectral properties of human vision from

yellow/orange to blue/violet where the rod and cone retinal responses provide a suitably declining and correlated spectral power over a wide spectral range (600 to 400 nm). The inputs to an observer's left and right eye were kept separate by a novel method involving a dynamic noisy polaroid motion and polaroid eyepieces with colour filters. This allowed noisy segmented outputs of C_L and C_D from the optic nerves of each eye to interact at V1, within the time of retention of vision. The $1/f$ noise was effectively introduced *endogenously* in our differential equations although the noise was introduced directly to each eyepiece. The above process results in the effect actually taking place in the interaction term in the L-V equations at V1.

Experimental Verification

As a result of two separate experimental designs for observations, 600 observations were made with and without $1/f$ noise incorporated by five observers in two Series (A and B) using 30 mammogram images with microcalcifications. The results of the first (Series A) set of observations showed significance for stochastic resonance in image detail $(p<0.05)$. The more stringent test (Series B) showed significance at the $p<0.1$ level. The more experienced observers had results at the $p\sim0.07$ level in Series B. Reasons for the difference between well experienced and not so experienced observers arise, we believe, from the search method required for examining the image, especially since observation of the occurrence of resonances requires a spatial search rather than an overall impression, according to our modelling results.

Differences between our Noise Processes and those in Recent Publications in other Areas

A very recent L-V type model in an application for stability and extinctions in population dynamics of two competing species in ecology (Valenti et al, 2004), uses a noisy interaction term in the presence of a periodic driving function and added Gaussian noise. Their modelling results included a stochastic resonance (SR) occurrence apparently due to a statistical synchronisation of the noise with the periodic driving function. The results

appear related to neurological concepts of Frohlich involving a periodic forcing function and modeled by Kaiser (1984).

Our edge detection model with stochastic resonance results also has a noisy interaction term but with $1/f$ type noise and without any driving force in the interaction formulation and the resonance arises in a different manner to Valenti et al. Our $1/f$ noise is from computer generated responses at discrete wavelengths in stochastic selections made periodically across the mammalian visual sensitivity response curve. There are spectral power correlations of retinal cones and rods responses in the spectral range 400 to 600 nm where the response curve is of the required form, declining with increasing frequency of light. The foregoing is utilised in a new method for generating $1/f$ type noise endogenously in the vision system and does not require solving any associated stochastic differential equations. It has been used successfully to produce SR in our experiments and should be applicable in other situations in practice, as will be mentioned in the subsection to follow.

A recent experiment with observer tests by Kitajo et al (2003) registered SR giving an improved range of perception of a periodic screen intensity (not edge detection) of a patch of computer screen. Gaussian noise was added to only one eye in an innovative experimental design to enable noise interaction in the cortex. This does not involve the processes of edge detection but it does support our model which has resonances in the striate cortex.

Future Developments and Research

- **Breast Screening**

  Whereas image processing is helpful "off-line" the initial mammographic screening sessions are still dependent on the radiologist's observations and visual searching in real-time. Our methodology uses a specialised arrangement of equipment for visual input to enable the brain to do its own improved image processing in real-time. The equipment can be simplified by new technology, as mentioned below.

The possible application of our method in real-time breast screening could use the method presented in the thesis for improving edge detection for stealthy stellate tumours, in addition to its use for microcalcifications. The model can be developed further for blurred or fuzzy edges. New technology for equipment design could be provided but the principle would be the same. It could be initially tested by computer by generating $1/f$ noise in responses for 3D orbital plots on screen, as used in the thesis. This should indicate if such tumours could be revealed even if they are below the visual threshold.

- **Lung Cancer Screening**

  The confusion which can sometimes arise between nodules and possible calcifications in lung cancer screening (Giger et al 1990) is a matter already referred to us by a leading radiologist as a possible application to reduce false positive detection.

- **Equipment Simplification using New Technology Materials**

  The developments which can provide selective spectral properties of new hollow core photonics band-gap crystal fibres suggests an alternative method for generating $1/f$ noise and applying it with appropriate optics in the manner indicated in the thesis. Electronic switching would be practical as part of the system design to replace the dynamic polaroid. The current cost of materials is high but the advantages may be significant in important applications such as in screening.

  A further example is for improved vehicle driver recognition of objects in poor visibility as a safety application also using photonic materials in our edge detection methodology. These are design tasks currently being examined by the writer.

In conclusion, we have developed a new functional model in vision which indicates that stochastic resonance for improved detection can be achieved from $1/f$ noise. Subsequent experiments have shown that this effect exists and that the method used can be applied in many areas for improved edge detection.

RELATIONSHIP OF THE APPENDICES IN THE DEVELOPMENT OF THE THESIS

Appendix A
Aspects of the Origin and Size Distribution of Breast Microcalcifications

Microcalcifications were the objects chosen for detection in the project. So this Appendix was the result of the writer's investigation with Professor H. Nguyen (Nguyen and Thornton, 1998) on the origin of the difference in size and spatial density distribution for microcalcifications and margins associated with malignant and benign lesion cells. Those sizes and distributions are two of the main characteristics for diagnostic indications during screening. Even if a detail has sufficient size and contrast in a lesion with microcalcifications, it may not be interpreted correctly if the spatial margins are indistinct (Lanyi, 1998).

The origin of the precipitation process was an early part of the writer's project. In the 1998 paper, we proposed the loss of contact inhibition in cancer cells reduces the "coherence length" to the order of intra-cell dimensions for small size precipitations of calcium hydroxyapatite whereas benign inter-cell communication provides for longer coherence lengths and can result in larger size precipitations. .Factors such as debris and impurities are involved in individual shape irregularities which are not very diagnostic.

Appendix B
Neurons and Neural Signals

This Appendix resulted from need to summarise the nature and properties of neurons particularly the interconnection processes in neural signalling in groups of neurons for a variety of processes utilized in the vision system. Crick (1994) has pointed out the abilities often ascribed to single neurons is actually the result of connections between a group of neurons.

Appendix C
Information on Magnocellular (M) and Parvocellular (P) Channels

This Appendix provides physiological detail of the type of cells in the early vision pathway which provide the on-centre and off-centre responses used for edge detection and the two pathways (Magno M and Parvo P) for spatial size, detail, form and colour.

Appendix D The Reticular Formation and its Input

This is a brief description of this important structure within the brainstem as an integrative region for regulation and control of sensory signals for alertness and attention. Among many other activities it is involved in an observer's visual searching for and observing details in images such as in mammograms.

Appendix E
Neurophysical Comments on Extracts of Farley and Clark's Experiments with a Neuron-like Net of Computer Elements

Farley and Clark in the 1960's demonstrated that a neuron-like net of computer elements can transform timed stimuli (ie a time-channel pattern such as in neuron signalling) into spatial patterns. Their experiments included visual displays. If the inputs are not too great, the transformation can be unique with a one-to-one correspondence between time channel configurations and subsequent spatial configurations as in our modelling of edge responses of neurons. There has been further support since their original experiments, including related results in a review article 2002 (Syme, 2002).

Appendix F
Directing and Focussing Attention to Locations in the Visual Field

This brief extract from Kent (1981) shows how the infero temporal cortex (ITC) is involved in an inhibition process in visual concentration for detail in an image and which can exclude unwanted surrounding information. It is relevant to an observer's experience and ability in searching for features in a complex image such as a mammogram. The process is included in our model via a spatial frequency parameter in the interaction terms of the L-V differential equations arising in the striate cortex.

Appendix A

Aspects of the Origin and Size Distribution of Breast Microcalcifications (Elysia Thornton and H.T. Nguyen, 1998)

The occurrence and characteristics of size and distribution of microcalcifications as byproduct indicators of a tumour arise from particular properties and the biophysics and biochemistry of transforming cells.

The diagnostic feature of non-uniformity of shape has been explained and illustrated in Chapter 1. There are however a number of unresolved questions on exactly how microcalcifications are formed and why different cluster sizes arise between malignant and benign lesions. These have been found to be characteristic in cancer screening by mammography. Their spatial extent is also important when a malignant tumour is to be excised.

Physico Chemical Composition of Microcalcifications

A spectrometric microanalysis of microcalcifications from a breast carcinoma indicated the following composition:

$Ca_3(PO_4)_2$	55.0%
$CaCO_3$	9.7%
$Mg_3(PO_4)_2 \cdot H_2O$	13.3%
Protein (albumin)	22.0%

A diffraction spectrometric examination of microcalcifications at the University of Technology Sydney (UTS), Department of Physics had been made previously for us on microcalcifications extracted from an excised lesion provided by Wesley Hospital Breast

Clinic and identified the calcium hydroxyapapite $Ca_5(PO_4)_3OH$ which was associated with microphotographs of the excised tissue.

In broad terms, breast microcalcifications associated with malignant lesions are smaller, more likely to be in clusters and display and non-uniformity of size and shape when compared to those associated with benign lesions. If there are more than 15/cm^2 clustered in the local tissue, the indication is that of a malignant tumour.

Origin of Microcalcifications as By-Products of a Lesion

Tumours mainly form from the rapidly dividing cells of the epithelial lining of the milk ducts or lobules (see main text). As the number of cells in a duct increases the duct elongates, becomes tortuous and folds upon itself. The resulting sharp angulations of the wall can become necrotic and calcify. In benign necrosis there will most often be larger flecks of necrotic material in comparison to the smaller flecks arising from malignant autolysis. Whereas this concept appears reasonable in the specific situation just described it now appears an oversimplification in the fundamental process of calcium salt deposits arising from both malignant and benign cells.

Further examination of the biophysical conditions of the rapid initiation of internal dielectric zones with different pH values and conductivity in malignant and benign cells can throw light on other important processes which may be involved as given below. The importance of the electrical properties of cells in the precipitation of calcium has been shown in experiments by Nordenstrom (1983).

1. The process of coherence is required for calcium hydroxyapapite precipitation. (This may possibly explain how other abnormal states which can occur in other parts of the breast (non ductal) can result in calcium hydroxyapapite deposits not necessarily dependent on necrosis and for which a reason is not known at present).

2. The electrochemistry control on the susceptible "transcription complex" of the Britten-Davidson theory of gene regulation (Britten and Davidson, 1969) can be disrupted in dielectric zones of different pH with their associated conductivity. Disruption of intracellular signalling by the changes in conductivity could affect the mitochondria's role in apoptosis, which is now known.
3. The very early rise of cytosolic ionic calcium which, coupled with the increased permeability of the membrane of a malignant cell, can be available for small calcium deposits under the influence of the loss of cell to cell communication giving only short "coherence lengths" between the cell's differing dielectric zones separating internal membranes (Thornton, 1984).
4. Calcifications associated with breast cancer when examined microscopically are usually dystrophic, ie they have suffered faulty development compared with normal crystal formation. They are deposited because the tissue is abnormal rather than being deposited as a result of elevated levels of calcium or phosphate in the blood (Bassett, L.W. 1992).

It is suggested that the involvement of the loss of contact inhibition by malignant cells compared with benign in relation to microcalcification cluster size can be considered as follows. Consider the two groups of Fig A.1 operating far from equilibrium states, one group being tumorous cells. Each group is embedded in a tissue of normal cells. As with all living cells the biophysics is that of a non linear system.

In Fig A.1 the malignant cells have "loss of contact inhibition" or often called "control inhibition", ie loss of communication for growth control between individual cells. However, within each cell there is exchange of biochemistry between the cell and the external environment as well as between pH zones between internal membranes. The latter may provide a range of small coherence lengths for possible calcium deposits.

The interchange of biomolecular material in normal or benign cells giving growth control can be brought about (Prigonine and Nicols, 1977) from very long range forces

$(\sim 10^{-6} m)$ which are highly specific. An organelle or cell could recognise another at a distance and be attracted or repelled depending on the phase of vibration in the membranes as originally established in 1968 Frohlich (update review Frohlich, 1983). Malignant cells have lost the communication facility of contact inhibition whereas benign cells retain the facility, giving long range correlations. The longer coherence lengths may give opportunities for large clusters of calcium deposits.

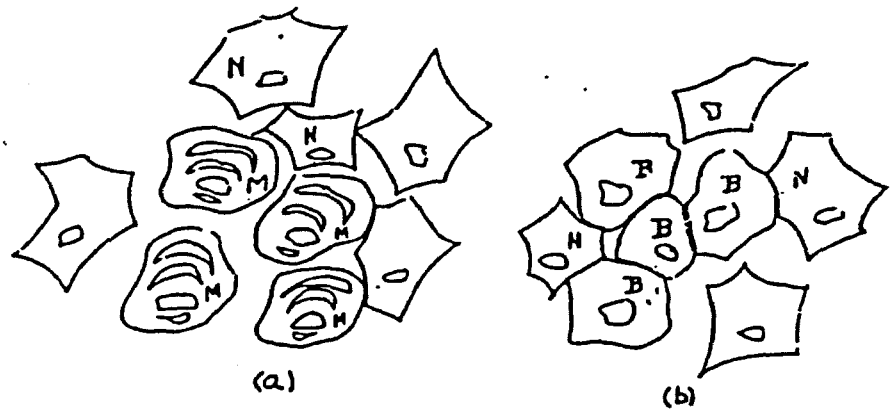

Fig A.1 (Thornton and Nguyen, 1998)

(a) Normal cells surrounding part of a tumour with malignant cells (with internal dielectric zones established) communications and control inhibited between malignant cells (contact inhibition) so biotransfers in the tumour are intra cellular between zones of malignant cells in the tumour (plus possible exchanges with normal cells).

(b) Normal cells surrounding benign cells which may have internal dielectric zones but not the mestastable state of cancer cells. Biotransfers are possible between all neighbours if in contact. Control and communication is not inhibited and pathways can be both internal and at the external cellular level for cells in contact.

Appendix B

Neurons and Neural Signals
Adapted from Adaptive Information Processing (Sampson 1976) and subsidiary references

Although there is no such thing as a "typical neuron," Fig B.1 portrays some of the physical features common to many of the forms taken by this cell type. Dendrites are processes specialised for reception of incoming signals. Dendritic processes may be numerous and highly branched but frequently do not extend any great distance away from the cell. The cell body or soma is where incoming information comes together. The axon is a process specialised for transmission of information from the cell to other neurons. The region where axon and soma cell/body come together is called the axon hillock.

The over generalisation inherent in this simple picture of the neuron must be stressed. There are, for example, neurons with no distinguishable axons, neurons with only a single process and a wide range of specialised shapes whose significance is not fully understood.

One neuron influences the activity of another through a specialised structure called a synapse. One common form of synapse in shown in Fig B.2. The presynaptic neuron and the postsynaptic neuron do not actually make physical contact at the synapse. There is a narrow (about $10^{-4}\ \mu$) synaptic cleft separating the two membranes. The presynaptic membrane is part of a terminal specialisation of the presynaptic neuron's axon, called an end-foot or synaptic knob. The postsynaptic membrane is a specialised region of the postsynaptic neuron's dendritic (or somatic) membrane. Synapses can be classified as axodendritic or axosomatic (or even axoaxonic, though these are rare) according to the location of the postsynaptic membrane on the postsynaptic neuron. Up to several thousand synapses may impinge on a single neuron, creating neural networks of incredible complexity.

Information processing events within a neuron are of a fundamentally electrochemical nature. By contrast, transmission of information across a synapse is a purely chemical phenomenon. The synaptic vesicles shown in the presynaptic terminal in Fig B.2 are spherical storage depots, each containing a few thousand molecules of a chemical called a transmitter substance. Signals arriving at the synaptic terminal trigger the release of the contents of the vesicles. The transmitter molecules then diffuse across the synaptic cleft and make contact with specialised receptor sites in the postsynaptic membrane. Although these receptors are poorly understood, the contact is assumed to alter the properties of the postsynaptic membrane. All neural signals are based on changes in membrane properties which give rise to ionic flows that temporarily modify the membrane potential.

Potential changes caused by "transmitter substance" acting on the postsynaptic membrane take one of two forms, depending on the type of receptors in the membrane. At excitatory synapses there is a sudden influx of Na^+ ions, reducing the potential and depolarising the membrane excitatory post synaptic potential (EPSP) lasts for several msec., as the membrane potential gradually returns to its equilibrium value. At inhibitory synapses a combination of Cl^- influx and K^+ eflux hyperpolarises the membrane, producing an inhibitory postsynaptic potential (IPSP) with a time course much like that of the EPSP. The magnitude of postsynaptic potential changes varies from a few mV to as much as 30 or 40 mV, depending on the amount of transmitter present. Graphs of EPSPs and IPSPs are shown in Fig B.3.

It is not strictly accurate to speak of excitatory and inhibitory synapses, only of excitatory and inhibitory effects at synapses. Although rare in higher animals, synapses have been identified in invertebrates where a single identified transmitter substance mediates either an excitatory or an inhibitory effect, depending on the frequency of the presynaptic signal. This finding implies the existence of a least two classes of postsynaptic receptors at such a synapse. The true complexity and information processing power of the postsynaptic membrane will probably not be fully appreciated for some time.

At a given time postsynaptic potentials of both types may be present at hundreds or even thousands of synapses on a single neuron. These potentials passively spread along the dendritic and somatic membrane (losing amplitude in the process) and interact with each other. Thus the effects of an EPSP can be virtually eliminated by a nearby IPSP of sufficient strength (spatial summation). And two potentials of the same sign will enhance each other if they occur closely spaced in time at a single synapse (temporal summation). As a consequence of all these interactions the somatic membrane is constantly monitoring the integrated net effect of all PSPs impinging on the neuron in the recent past. If this net effect is depolarising (it need not be), and if the magnitude of this depolarisation measured at the axon hillock exceeds a value known as the neuron's threshold, then a signal will be sent down the axon. Threshold potentials are usually reached with about 10 to 20mV of depolarisation but may vary considerably from neuron to neuron and over time for a given neuron.

The electrical signals which travel in axons are impulse or spike-like in character and are called action potentials. A typical action potential is diagrammed in Fig B.4. The rising or depolarising phase is a consequence of massive influx of Na^+; recovery is accomplished by extrusion of K^+. This is clearly a situation that cannot by itself go on for long, lest the axon become saturated with Na^+ and lose all its K^+. Compensation is provided by an active transport mechanism which is constantly working in the background. The so-called "Sodium Potassium Ion Pump" carries Na^+ out of the cell and K^+ back in. Despite the pump's presence however, a period of intense activity can create a sufficient ionic imbalance to interfere temporarily with an axon's activity.

Although it somewhat resembles a large EPSP, the action potential is a fundamentally different electrochemical event. First of all, action potentials are of essentially fixed amplitude, usually reaching a value of 5 to 10 mV positive, whereas PSPs are of variable size. Thus information cannot be carried in the amplitude of an action potential. A second difference is related to propagation. Where PSPs spread passively across the cell membrane, suffering a decrement in amplitude in the process, action potentials propagate nondecrementally; retaining their initial amplitude all the way down the axon. The speed

of this propagation ranges up to a few metres/second, being faster in axons of larger diameter.

Action potential propagation is really a wave phenomenon; nothing physical moves down the axon. Thus an action potential occurring at a given point on an axon provides (through passive spread) suprathreshold depolarisation of the axon tissue immediately in front of it, generating a new action potential at that point. This is why propagation is nondecremental. Although the tissue immediately behind the wave front (where the action potential has "just been") also received such stimulation, action potentials still travel only in the "forward" direction. Such unidirectional propagation is achieved because the threshold becomes effectively infinite during the rising and about the first half of the falling phase of an action potential. No further spikes can be induced during this absolute refractory period (abbreviated as ARP in Fig B.4). Since the tissue just behind the wave front will be in this absolutely refractory state, unidirectional conduction of impulses is assured.

After the end of the ARP there is another period during which the threshold is elevated but returning to its normal ("resting") value. During this relative refractory period (RRP), a larger depolarisation is required to evoke an action potential, the requirement being largest at the beginning of the RRP.

Let us now return to the axon hillock and imagine a situation in which a depolarisation just equal to the resting threshold is maintained there. An action potential will be generated in the axon only after its predecessor's RRP has elapsed, giving a "firing frequency" of no more than a few hundred impulses per second. If we now increase the sustained depolaristion in the hillock to a level somewhat above threshold, action potentials will be initiated near the ends of RRPs, giving a somewhat greater frequency of firing. Finally, let us increase the depolarisation to a level so high that action potentials will be initiated at the ends of ARPs. This situation will produce the maximum firing rate.

It is now clear how the neuron encodes information about stimulus magnitude in action potentials of uniform size. Encoding of information in the frequencies of pulses is pulse frequency modulation (PFM). This discussion should not be taken as ruling out even more sophisticated encodings at given times or places in the nervous system. But it is clear that all such encodings will be based on the PFM principle of variation in the temporal distribution of pulses.

We should note the important roles in neural function we have just discovered for each of the refractory periods. Although the ARP and RRP could be regarded as unfortunate limitations placed on neural information transmission by the "weaknesses" of biological tissue, we have seen that the former assures unidirectional conduction and the latter provides for PFM encoding. These two properties are at the core of a neuron's information transmission abilities.

Interconnection Processes of Neurons

A digitally based neuron model is shown in Fig B.5 (Windsor 1988) together with a representation of its essential constituents for interconnections. In the classic model for their function, proposed in 1943 by McCullough and Pitts, neurons are either 'on' (shown black) or 'off' (shown white). When on, the neuron fires and its output nerve, or axon, conveys a steady stream of action pulses to many other neurons (denoted by the hatching along the axon paths in the figures). The key to neuron abilities lies in the host of interconnections, or synapses, which link the ends of the output axons of one set of neurons to the input nerves, or dendrites, of another set, so forming a very complex network. The synapse strength varies chemically according to the firing rate of both the incoming axon and the neuron. Although synapse strength, like axon firing rate, actually varies smoothly over a range of values, in the Fig B.5 model its strength is defined digitally. It switches itself on and begins firing if the sum exceeds some threshold value (say 1·5 being half the maximum possible input of 3, chosen above). For example, in the Figure it is represented by the number of arrowheads. Each neuron is continually at work: it takes the products of the input signals from other neurons (1 or 0) with the corresponding synapse strengths (0, 1, 2 or 3) etc and sums over all the connections. It

switches itself off if the sum is below the threshold. All the neurons in the network are assumed to be continually updating their decisions in parallel but unsynchronised with each other.

Excitatory (positive) and inhibitory (negative) neurons (and synapses) occur and are essential components of this model. In nature's most elegant design rules Na^+ ions are transmitted through the selective ion channels in the synapses of excitatory neurons and K^+ ions through those in inhibitory neurons. An inhibitory neuron is switched off when the summed input is above a threshold but switches on otherwise.

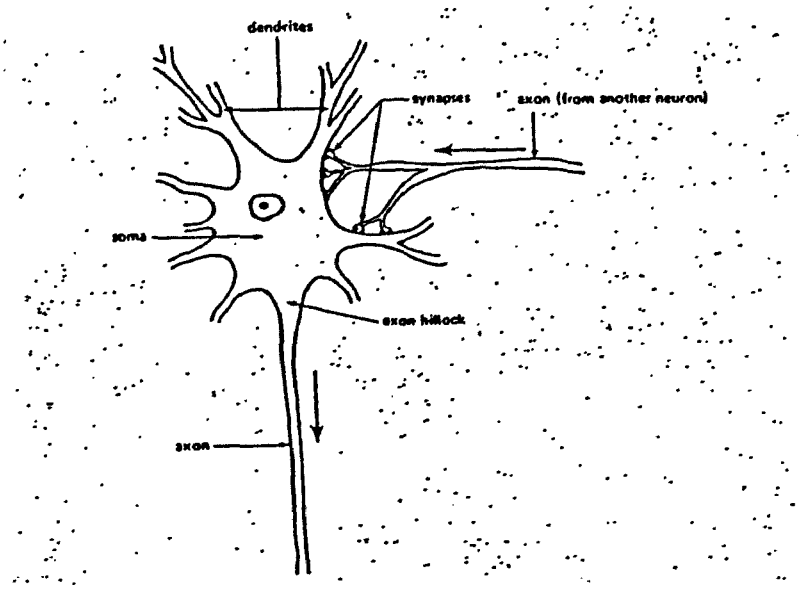

Fig B.1 (Samson, 1976 for Figs B.1-4)
(Common features of neurons, with arrows showing informationflos

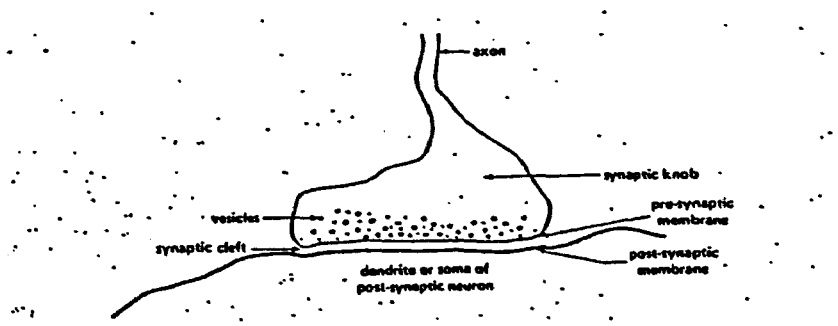

Fig B.2
One form of (chemical) synapse

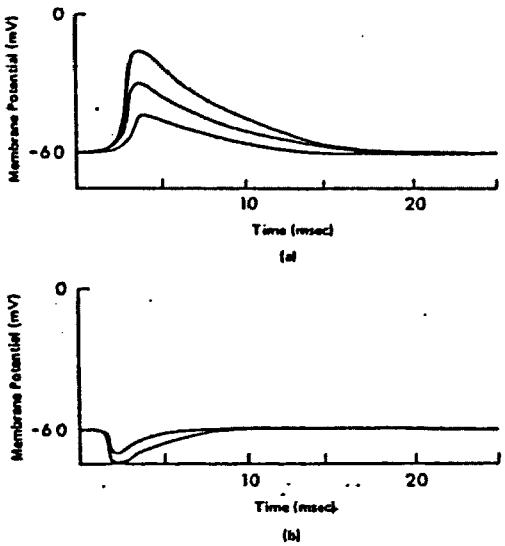

Fig B.3
Typical postsynaptic potentials.
(a) EPSPs, (b) IPSPs

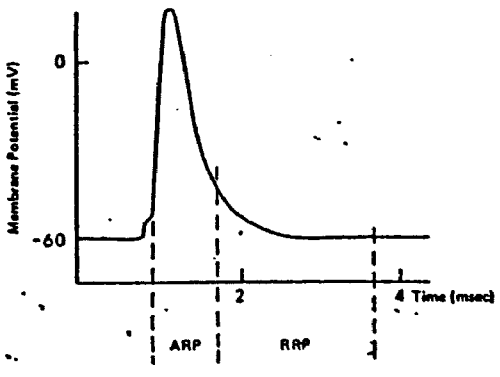

Fig B.4
An action potential

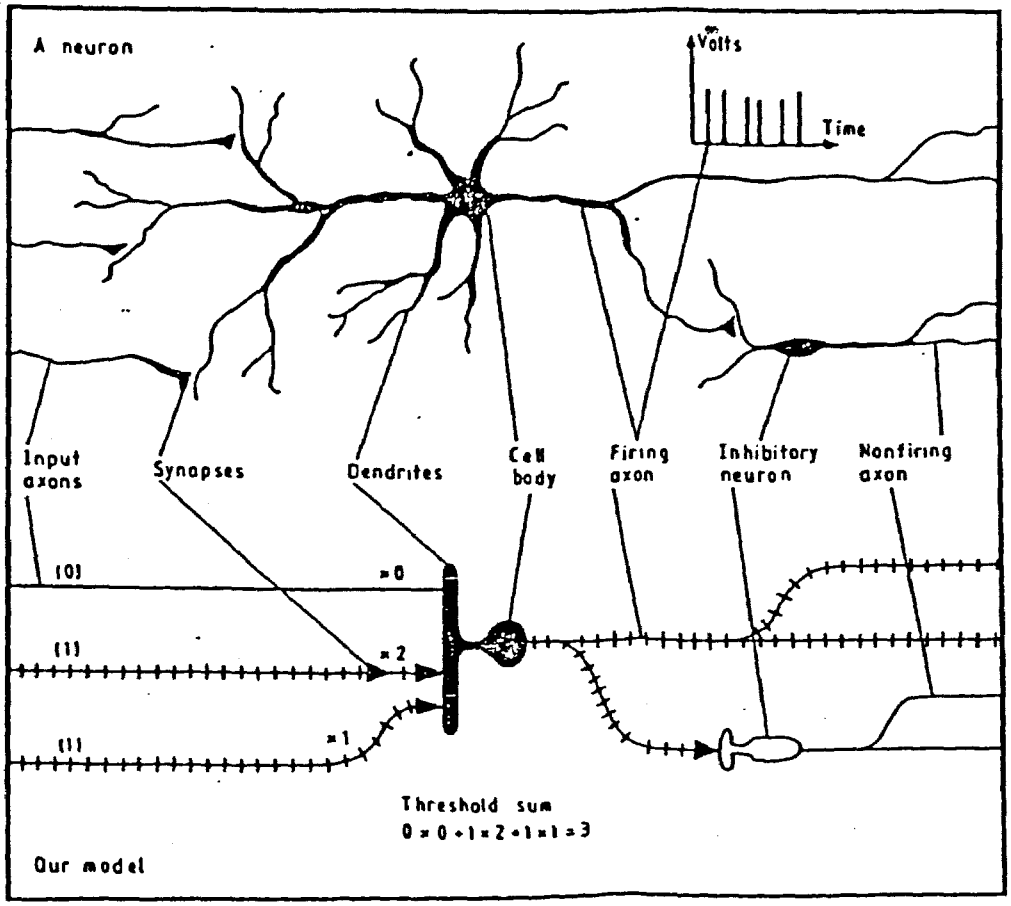

Fig B.5 (Windsor, 1988)
The Neuron and our Schematic Model for it.

The cell body is a miniature computer which receives on its input surface (the extensive branching dendrites) chemical signals from the output nerves (axons) of other neurons. These are modulated by the strength of the connections (synapses) between them. These synapse strengths, represented digitally by the number of arrows, are the means by which memory is stored. Excitatory neurons switch on and begin firing only if the sum of the input signals (1 or 0) times their synapse strengths (0, 1 or 2 etc) is greater than some defined threshold. A firing neuron sends action pulses insert) to other neurons in the network.

Appendix C

The Signal Pathways for Left and Right Eye and Further Information on M and P Channels

Chapter 4 examined the retinal processing and Chapter 5 outlined the transmission process of action potentials from the retinal ganglions, via the optic nerve, to the LGN for both the left and the right eye. We now extend our earlier chapters' description in more detail. (Also see Watson, 2000). At the optic chiasma at the base of the skull, the nerve fibres from the nasal half of each retina cross to the opposite side as shown in the main text. The fibres from the temporal half of each retina continue ipsilaterally, together with the crossed axons from the contralateral optic nerve, as the optic tract. The optic tract leads to the first central stations of the visual pathway – the lateral geniculate nuclei (LGN), the superior colliculi, the nucleus of the optic tract, nuclei of the accessory optic tract, the pretectal region of the brainstem and the hypothalamus.

The most important and massive projection of the retina in humans is that linking it to the LGN but it also has important inputs from the reticulate formation in the brainstem. The LGN itself consists of 2 magnocellular and 4 parvocellular layers. The uncrossed axons of the ipsilateral optic nerve terminate in three of these layers, and the crossed axons of the contralateral optical nerve terminate in the other three. The axons of most of the geniculate cells then pass over the optic radiation to the nerve cells of the primary visual cortex (area 17 or V1 of the occipital cerebral cortex. Area 17 is the older terminology). Area V1 is connected to the secondary visual cortex (area V2), the tertiary visual cortex (areas V3, V3a) and the visual integration regions in the occipitoparietal or occipitotemporal cerebral cortex. However the areas beyond V1 are still not fully understood.

The retino-geniculate projection which terminates in the dorsal part of the LGNd is the most prominent visual pathway in primates. Together with the subsequent geniculate-

striate projection to the primary vision striate cortex (area V1) in the occipital lobe and its cortical elaborations, it is the most studied visual "system" in all of neuroscience. Two of the many researchers, Hubel and Wiesel, were awarded the Nobel Prize in medicine for their many years' work in unravelling much of the neurology – but much of vision is still uncertain.

The two main types of 'on-ganglion' and 'off ganglion' cells described so far are called "simple" cells. There are other neurons in the primary and secondary visual cortex called "complex" cells which are larger and have on-responses and off-responses from every part of their receptive field, not just the concentric arrangement of the "simple cells". They can receive inputs from "simple cells" and can be responsive to lines of specific orientation.

Historically, on-centre and off-centre cells in the retina were divided into two groups; linear (X) and non-linear (Y). These two classes of cells form different systems and these systems were additionally sub-divided (at the LGN) into parallel M and P channels tuned to detect objects of different sizes. Colour was not an important variable at that time (1960's) using experiments with cats.

Since that time the magno and parvo pathways are known in more detail summarised by Zeki (1994) as follows. "The output from the P layers of the LGN is relayed to layers 2 and 3, where it divides to constitute two pathways. One of these feeds the blob cells and is therefore concerned with colour, while the other feeds the interblob cells and is therefore concerned with form. By contrast, the output from the M layers is relayed to layer 4B of area V1, and also divides into two components. One component feeds the orientation- plus direction-selective cells of layer 4B and is therefore concerned with motion, while the other feeds the orientation-selective cells of the same layer and is therefore concerned with form". The temporal and spatial frequency properties of the two channels is shown in Fig C.1 (Milner and Goodale 1995). The properties can be accessed cooperatively by V1 processes as pointed out by Zeki (1993).

Our experimental test system uses particular features (Merigan and Maunsell, 1993) for separate colour inputs to each eye. One class of primate ganglion cells the so-called $P\alpha$, responds transiently to visual stimulation, and have rapidly conducting axons. The second class of primate ganglion cells the $P\beta$, have medium-sized to small cell bodies and have small receptive fields. They respond in a sustained fashion to visual stimulation and have somewhat slower conduction velocities. In contrast to the $P\alpha$ cells, the receptive field centre of most $P\beta$ cells receives input from only one or two cone types. Since complementary spectral information is received from the surround regions within the receptive field of these $P\beta$ neurons, they are frequently characterised as forming a 'colour-opponent' channel. This is used in the vision system to produce the advantage of narrow wavelength selectivity. Output from one set of cones (eg for long wavelengths) is opposed by another output (eg for middle wavelengths) so that a cell may give an on response to long wavelengths and off-response to middle wavelengths.

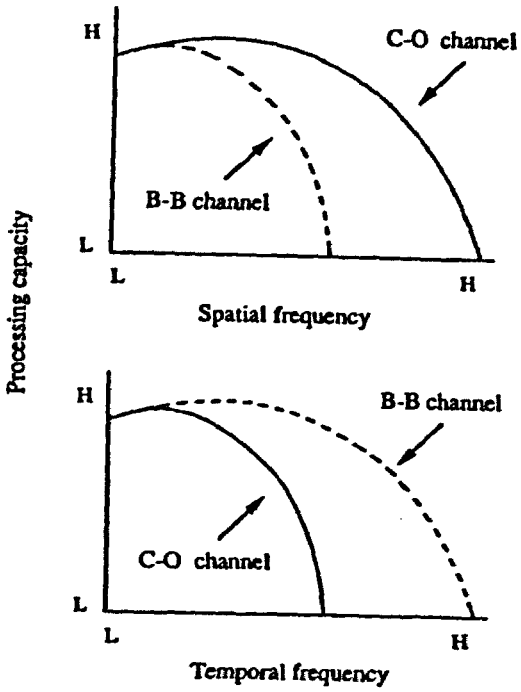

Fig C.1 (Milner and Goodale, 1995)

Schematic diagram showing differences in the processing capacity for the parvocellular (colour-opponent of C-O) and magnocellular (broadband or B-B) channels for spatially and temporally modulated stimuli. In the spatial domain, the processing capacity of the broadband channel drops off more rapidly than the colour-opponent channel with increasing spatial frequency (that is, fine-grain structure). In the temporal domain, the opposite is the case and the processing capacity of the colour-opponent channel drops off more rapidly than the broadband channel.

Appendix D

The Reticular Formation and its Input

The reticular formation, an elongated structure within the brainstem, is an important integration region of the non-specific system. There are many afferent and efferent connections of this region as shown in Figs D.1,a,b,c, for regulation and control of alertness and attention.

The Reticular Activity System continually monitors the input of all of the sensory systems, more for quantity and changes in activity than for detailed analysis, and controls the degree of activation of various portions of the higher centres on this basis. Thus, it can immediately arouse the brain when a novel or significant change in stimulus is encountered and alert the whole system to a state of attention.

Intuitively, we know the difference between feeling highly alert and feeling awake but inattentive and relaxed. These states reflect different levels of operation of the forebrain under control of the reticular formation. The general modulating inputs from the reticular formation are diffusely connected through the forebrain and serve to bias the cells there towards or away from the firing level. This not only has implications for the rate of activity in these cells but also influences the nature of the processing they perform, because the "analogue" and "digital" factors in the cell's input are interactive. Thus, not only the level of activity and speed of processing, but also the nature of processing, is affected in ways appropriate to the degree of attention required by a particular situation. Carefully searching a mammogram is one such situation requiring attention and therefore involves reticular formation activity.

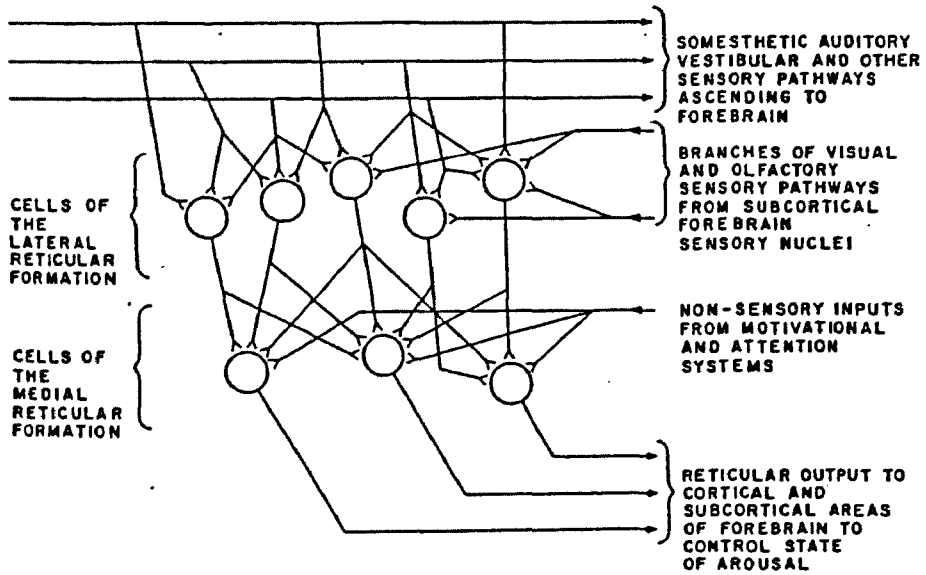

Fig D.1a (Kent, 1981)

The basic connections of the "reticular activating system". Three classes of inputs can result in activation of the cortex. These are the branches from the external sensory inputs entering the lateral reticular formation, the inputs from motivational systems in response of organismic need states, and the inputs from "attention" systems that allow higher cortical processes to regulate the level of non-specific cortical arousal.

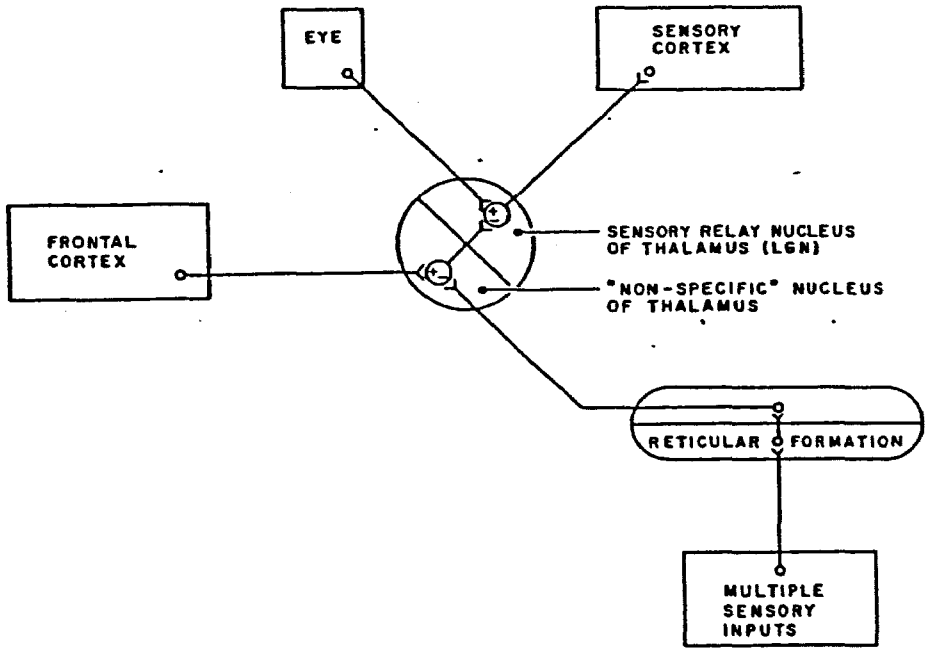

Fig D.1b (Kent, 1981)

The basis mechanism of the control of attention. Nonspecific activation by the reticular activating system can be opposed in specific fashion by the frontal cortex at the level of the "non-specific nuclei of the thalamus, resulting in a selective pattern of cortical activation. The mechanism is shown here for the simple case of regulation over an external input channel. The same basic mechanism can operate to govern the operation of cortical areas involved in high-level operations.

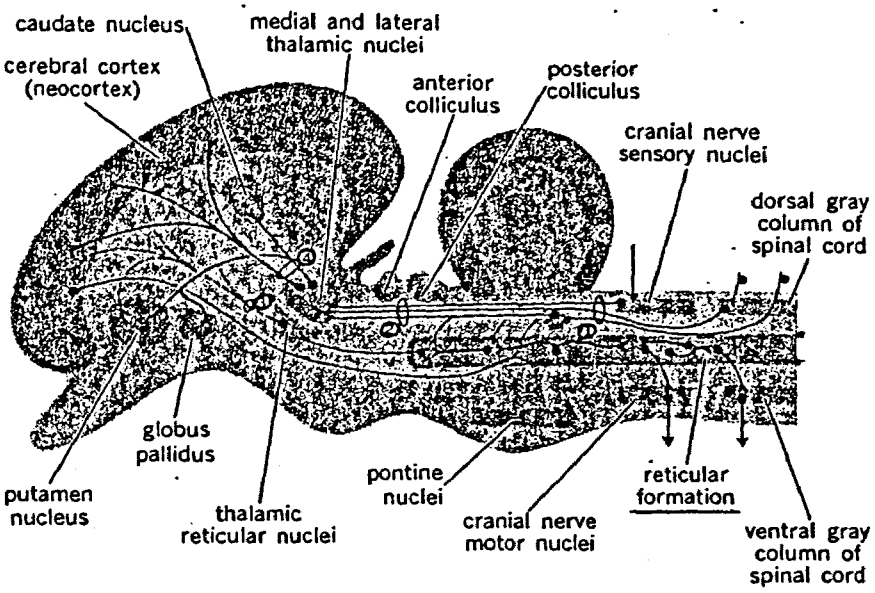

Fig D.1c (McGraw Hill Encyclopaedia of Science and Technology, Vol. 9, 1970) Sagittal section of brainstem showing location of reticular formation and related connections

Appendix E

Neurophysical Comments on Extracts of Farley and Clark Experiments with a Neuron-like Net of Computer Elements

The following are extracts from Farley and Clark's early experiments with nets of neuron-like computer elements.

Farley and Clark (1961) found "that a net of these elements has the property of transforming timed stimuli (time-channel pattern) into spatial patterns of active elements and, if a suitable time is chosen, that the transformation may be unique and there can be a one-to-one correspondence between input time-channel configurations and space configurations, provided the class of inputs is not too large". Following from this, "elements activated by non-linear interaction may be of particular use in classification and study of such systems is of interest because perception consists essentially in the classification of inputs." We note a recent review and results (Figure E.1) which are related to this matter (Syme et al, 2002).

"Considerable interest attaches to how the behaviour of these nets of neuron-like computer elements may vary when the thresholds of groups of cells were changed", as stated by Farley and Clark. Some examples of this kind are shown in Figures 4, 5 and 6 of their paper. Their 1960's findings seem to be of relevance to the much later advent of stochastic resonance when we note their further comments. "When the average threshold in an area is raised, activity tends to avoid it and when the average is lowered, activity tends to be attracted into the area. If a suitable mechanism were available for manipulating thresholds, it could have the effect of 'channeling' or otherwise controlling the pathways and time of cell firings. For example, motor activity consists primarily in the firing of cells representing muscle-fibre groups and muscle groups in specified orders with specified timing, so that such a mechanism could control muscle contractions. The controlled cells need not be adjacent; a certain fraction of cells in an area could be used to control the average activity or output." This may also relate to the recently reported stochastic resonance effect in the cortex (Kitajo et al, 2003) giving a motor muscle

response (button press) to record an observer's threshold limit for a progressively reduced periodic intensity of a patch area of a computer screen (Kitajo et al, 2003). This does not apply to edge detection.

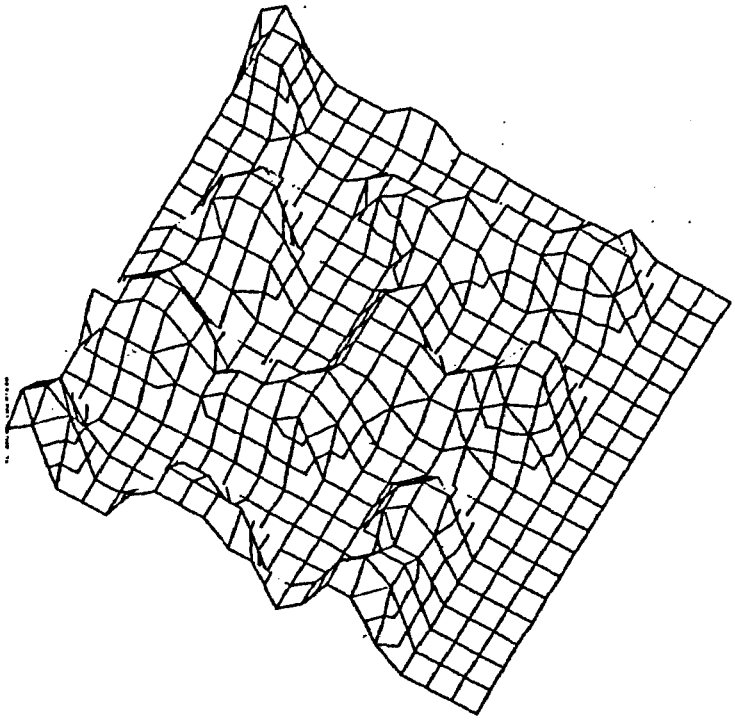

Fig E.1 (Syme et al, 2002)

A computer simulation of a single-layer network of 400 "pyramidal cells" that have been connected in a manner that reflects how they are connected in the cortex. Each node on the 20 x 20 grid represents one of the cells, while the z-axis indicates how many times the cell fires in response to a particular input. This particular network has been "trained" to recognise a pattern by repeatedly presenting it with the pattern. When the network is exposed to a pattern typical of that category, it responds "dynamically" – in other words the cells fire for a few times and then stop. This model was run until all the cells stopped firing – about 30 ms. The firings settle into "clusters" of activity, with the same distribution of clusters always obtained when the network is exposed to a training pattern. In other words, the network recognises and responds to an external input rather like the way humans perceive sights, sounds and smells. Such behaviour has been recorded by neurobiologists, with particular strong responses during odour perception.

Appendix F

Directing and Focusing Attention to Locations in the Visual Field

(Kent p109, 1981) summarises the above process as follows. It is important to note how the observer is involved in our particular application in viewing a region of interest in a mammogram.

"Given the findings which implicate the subcortical system in the analysis of visual location, suggests the availability of an apparatus for directing the object identifying apparatus to any particular location in the visual field. The geometry of the connections suggests that this must be occurring by an inhibitory input (probably a pre-synaptic one) to the fibres reaching the infero temporal cortex (ITC) from earlier cortical stages. The ones arising from unwanted locations in the spatially-mapped earlier stages would be inhibited and the ones reaching the ITC neurons from the location of interest would be free to enter feature recognition data. This mechanism is reminiscent of the "focusing" of attention in which concentration on a particular small detail can effectively eliminate perception of other portions of the visual scene, so long as they do not trigger the automatic attention and orienting mechanisms."

"One suspects that this input from the subcortical systems usually operates more or less automatically; perhaps this process is directed by inputs from retinally mapped cortical regions, which act as feedforward to the "dynamic tuning" feedback method of perceptual model building . The ITC has reciprocal connections with the forward parts of the prefrontal lobe of the cortex which are to be involved in voluntary attention processes, and it may be that conscious direction of visual attention operates through this mechanism, as well as by bringing the object to the center of the visual field. It has been established that the location of attention can be dissociated voluntarily from the locus of visual gaze direction. However, the two usually operate synergistically, so that attended objects will be studied with the optimum acuity."

REFERENCES

Al-Bayyati, H.A., A rule of thumb for determining a sample size in comparing two proportions, Technometrics, 13, No. 3, pp675-677, 1971.

Arnold L., Horsthemke W. and Stucki J.W., The influence of external real and white noise on the Lotka-Volterra model, Biom. Jl, 21, pp451-471, 1979.

Averbach E. and Sperling G., Short term storage of information in vision, Information Theory ed Colin Cherry, Butterworths, pp196-211, 1961.

Barrow J.D., The Inventive Universe, Penguin, p222, 1995.

Bassett, L.W., Mammographic analysis of calcifications in breast imaging: current status and future directions, Radiological Clinic of North America, 30, pp93-105, 1992.

Bassett Lawrence W., Jahanshahi Reza, Gold Richard H. and Fu Yao S. Film-screen mammography, An Atlas of Instructional Cases, Martin Dunitz, London, 1991.

Baylor D. and Fuortes M., Electrical responses of single cones in the retina of the turtle, Jl. Physiology (London), 207, p77, 1970.

Beam C., Layde P. and Sallison D., Variability in interpretation of screening mammograms by US radiologists: finding from a national sample, Archiv. Internal Medicine, 156, pp209-213, 1996.

Bear M., Connors B. and Paradiso M., Neuroscience exploring the brain, Lippincott, Williams and Wilkins, 1990.

Bennett C.H. and Shor P.W. Quantum channel capacities, Science, 303, p1784, 2004.

Biberman L. M. ed., Image Quality in Perception of Displayed Information, Chapter 2, pp11-86, Plenum Press, 1973.

Boynton Geoffrey M., Demb Johathan B., Glover Gary H. and Heeger David J., Neuronal basis of contrast discrimination, Vision Research, 39, pp257-269, 1999. Also see Watson (1994) for computational modelling.

Britten R. and Davidson E., Gene regulation for higher cells; A theory. Science, 165, p139, 1969

Brzakovic D., Brzakovic P. and Neskovic, M., An approach to automated screening of mammograms, SPIE, 1905, p690, 1993.

Carandini M., Heeger D. J. and Senn W., A synaptic explanation of suppression in visual cortex, The Journal of Neuroscience, 22, November 15, pp1053-10065, 2002.

Celet J.C., Dangoisse D. and Glorieux P., Slowly passing through resonance depends on noise, Physical Review Letters, 81, (5), pp975-978, The American Physical Society, pp975-978, 1998.

Chesters M.S. Perception and Evaluation of Images, Chapter 7, Scientific Basis of Medical Imaging, P.N.T. Wells Ed., Churchill Livingstone, 1982.

Chialvo D. R. and Apkarian, Modulated noisy biological dynamics: three examples, Journal of Statistical Physics, 79 , (112), 1993.

Cook N. D., The Brain Code, Mechanisms of Information Transfer and the Role of the Corpus Callosum, p114, Methuen, 1986.

Cornsweet T. N., Visual Perception, Academic Press, 1970.

Crandell R. E., Projects in Scientific Computation, Section 5 and 6, Springer-Verlag, 1994.

Crick F., The Astonishing Hypothesis, The Scientific Search for the Soul, Simon & Schuster, 1994.

Cuenod M. and Durling A. A Discrete-Time Approach for System Analysis, Chapter 2. Academic Press, New York and London, 1969.

DeValois R., Abramov I. and Mead W., Single cell analysis of wavelength discrimination at the lateral geniculate nucleus in the macaque, Jl. Opt. Soc.Am, 58,p 415 and 56, 966, 1966.

Diem K. and Seldrup J., Geigy Scientific Tables, 2, 8th Edition, Statistical Methods, p193, 1982.

Farley B.G. and Clark W.A, Activity in Networks of Neuron-Like Elements in Information Theory, pp242-251. ed Colin Cherry, Butterworths, pp242-251, 1961.

Forgus R. H., Perception, The Basic Process in Cognitive Development, McGraw-Hill Book Company, 1966.

Frohlich H., Coherent excitation in active biological systems in Modern Bio-electric Chemistry, Gutmann and Keyzer Eds, Plenum N.Y. pp241-261, 1985.

Geisler W. S. and Banks M. S., Visual Performance in Handbook of Optics, Volume 1, Fundamentals, Techniques and Design, Second Edition, Chapter 25, PP25.1-25.55, McGraw-Hill, Inc., 1995.

Giger M. L., Ahn N., Doi K., MacMahon H. and Metz C. E., Computerised detection of pulmonary nodules in digital chest images: use of morphological filters in reducing false-positive detections, Med. Phys. 17(5), pp861-865, 1990.

Gotelli N. J. and Murray T., Ecology, Second Edition, Sinauer Associates, Inc. Publishers, Sunderland, Massachusetts, USA, 1998.

Granit R., The Purposive Brain, The MIT Press, 1977

Gross M., Visual Computing, Springer Verlag, 1994

Grusser O.-J. and Grusser-Cornehls U., The Sense of Sight, Human Physiology, Second Completely Revised Edition,Springer-Verlag, pp237-276, 1987.

Heeger D., Normalisation of cell responses in cat striate cortex, Visual Neuroscience, 9, pp181-197,1992.

Heslenfeld D., Kenemans J., Kok A. and Molenaar P., Feature processing and attention in the human visual system: an overview, Biological Psychology, 45, pp183-215, 1997.

Higgins G. and Wolf R., The relation of definition to sharpness and resolving power as a photographic system, Jl. Opt. Soc. Amer., 45 pp121-129, 1955.

Hubel D. and Wiesel T., The Ferrier Lecture: Functional architecture of macaque monkey visual cortex, Proc. Roy. Soc. London, B198, pp1-59, 1984.

Kaiser F., Entrainment, quasiperiodicity, chaos, collapse: bifurcation routes of externally driven self-sustained oscillating systems in Nonlinear Electrodynamics in Biological Systems (Conference Proceedings), 393, Plenum Press, 1985

Keirnan J.A., The Human Nervous System – An Anatomical Viewpoint, 7th Edition, Lippincott-Ranon, 1998.

Kent E. W., The Brains of Men and Machines, University of Illinois Chicago, Illinois, BYTE/McGraw-Hill, 1981.

Kitajo K., Nozaki D., Ward L. M. and Yamamoto Y., Behavioral stochastic resonance within the human brain, Physical Review Letters, 90, (21), pp218103-1-218103-4, 2003.

Kulikowski J., Neural Stages of Visual Signal Processing, Search and the Human Observer (Ed. Clare J. and Sinclair), Taylor and Francis Ltd, 1979.

Landis J. and Koch G., The measurement of observer agreement for categorical data, Biometrics 33, pp159-174, 1977.

Lanyi M., Diagnosis and Differential Diagnosis of Breast Calcifications, Springer-Verlag, 1988.

Legge G., Kersten D. and Burgess A., Contrast discrimination in noise, Jl. Opt. Soc. Amer., 4, pp391-463, 1987.

Logan B., Information in the zero crossings of bandpass signals, Bell Sys. Tech. J., 56, (4), pp487-510, 1977.

MacLeod K., Backer A. Laurnet G., Who reads temporal information contained across synchronized and oscillatory spike trains? Nature, 395, pp693-698, 15 October, 1998.

Marr D. and Hildreth E., Theory of edge detection, Proc. Roy. .Soc. London, B207, pp187-217, 1980.

Marr D., Vision, A Computational Investigation into the Human Representation and Processing of Visual Information, W.H. Freeman and Company, 1982.

Martin K., A.C. Microcircuits in visual cortex, Current Opinion in Neurobiology, 12, pp 418-425, 2002.

Merigan W. and Maunsell J., How parallel are the primate pathways? Annual Review of Neuroscience, 16, pp369-402, 1993.

Milner A. D. and Goodale M. A., Visual Brain in Action, Oxford University Press, 1995.

Mitiades G. and Thomas E., Pulsating laser oscillations depend on extremely-small-amplitude noise, Physical Review A., 45, (9), pp6636-6642, The American Physical Society, pp6636-6642. 1992

Murch G. M., Visual and Auditory Perception, The Bobbs-Merrill Company, Inc. Indianapolis, p83, 1973.

Murray J.D., Mathematical Biology, Springer-Verlag, 1995.

Neri P. and Heeger D., Spatio-temporal mechanisms for detecting and identifying image features in human vision, Nature Neuroscience, 5, p812, 2002.

Nestares O. and Heeger D. J., Modeling the apparent frequency-specific suppression in simple cell responses, Vision Res., 37, (11), pp1535-1543, 1997.

Nishikawa R. M., Detection of microcalcifications, Image-Processing Techniques for Tumor Detection ed Robin N. Strickland, Marcel Dekker, pp131-153, 2002.

Nordenstrom B.E., Biologically Closed Electrical Circuits, pp8, 26, 77, Nordic Publications, 1983.

Pelli D. and Farell B., Psychophysical Methods Ch. 29.9 Handbook of Optics; Fundamentals, Techniques and Design 1., Ed., L.M. Bassett et al, McGraw-Hill, 1995.

Pinneo, L.R., Visual Prosthesis by Electrical Stimulation of Primary Visual Pathways, Visual Prosthesis, The Interdisciplinary Dialogue, pp109-127, (ed Sterling, et al), Academic Press, 1971.

Prigogine I. and Nicols G., Self Organisation in Non Equilibrium Systems, Wiley - Interscience, New York, 1977.

Reese, R. A., Does significance matter? Significance, Royal Statistical Society, pp39-40, 2004.

Rescigno A. and Maccacaro, G.A., The Information Content of Biological Classifications, Information Theory ed Colin Cherry, Butterworths, p437-446, 1961.

Rovano J., Raninen A. and Donner K., The effects of temporal noise and retinal illuminance on foveal flicker sensitivity, Vision Research 39, pp533-550, 1999.

Sampson J. R., Adaptive Information Processing, An Introductory Survey, Springer-Verlag, Chapter 8, 1976.

Saunders R. McD., The spectral responsiveness and the temporal frequency response (TFR) of cat optic tract and lateral geniculate neurons: sinusoidal stimulation studies, Vision Research, 17, pp285-292, Pergammon Press, 1977.

Schmidt F., Sorantin E., Szepesvarig C., Graif E., Becker M., Mayer H. and Hartwagner K., An automatic method for the identification and interpretation of clustered microcalcifications in mammograms, Phys. Med. and Biol., 44, pp1231-1243, 1999.

Schnitzer A., Analysis of noise-required contrast and modulation in image – detecting and display systems in The Perception of Displayed Information, Ed. W. Wolfe, Plenum, 1973.

Shams L. and von der Malsburg C., The role of complex cells in object recognition, Vision Research 42, pp2547-2554, 2002

Sharon D. and Grinvald A., Dynamics and consistency in cortical spatio-temporal patterns of orientation processing, Science, 295, pp512-515, 2002.

Sheridan P., Spiral architecture for machine vision", PhD Thesis, School of Computing Science, University of Technology Sydney, 1997.

Shoukric M. and Pause C.A., Statistical Methods for Health Sciences, CRC Press, 1999.

Sickles E. A., Breast calcifications: mammographic evaluation, Radiology, 160, pp289-293 1986.

Siegel R.M., Non-linear dynamical system theory and primary visual cortical processing, Physica, D42, p385, 1990.

Sirovitch L., Everson R., Kaplan E., Knight B., O'Brien E. and Orbach D., Modelling the functional organisation of the visual cortex, Physica, D96, pp355-366, 1996.

Stucki, J. W. Stability analysis of biochemical systems – a practical guide, Progress in Biophysics and Molecular Biology, 33, Pergamon Press Ltd., Headington Hill Hall, pp99-147, 1979.

Syme S., Oppwod R., Mallot H., Mason S. and Zrenner E., Mimicking the brain, Physics World, 15, p31, February, 2002.

Thornton B.S., Inversion of Raman spectra related to energy control, Physics Letters, 106A, pp 198-202, 1984.

Thornton E, Initial presentation and literature review for PhD presentation Seminar, Faculty of Science, University of Technology, Sydney, April 4, 1998.

Thornton E. and Nguyen H., A proposed physico-chemistry model for a key diagnostic feature of breast microcalcifications used in mammography, BIOPS 98 Conference, Sofia, Bulgaria, 7, 29-45, 1998.

Thornton E., Factors in the use of breast screening for effective secondary presentation, Jl. Proc. Roy. Soc NSW, 134, pp89-99, 2001.

Valenti D., Fiasconaro A. and Spagholo B., Stochastic resonance and noise delayed extinction in a model of two competing species, Physica A 331, pp477-486, 2004.

Vilar J.M.G. and Rubi J.M., Effect of the output of the system in signal detection", Physical Review E, 56, (1), The American Physical Society, p32, July 1997.

Watson A. B., Neural contrast sensitivity, Computational Models of Visual Processing (ed Michael S. Landy and J. Anthony Movshon), Chapter 7, A Bradford Book, The MIT Press, 1994.

Watson J. D..G., The Human Visual System, Brain Mapping: The Systems, Academic Press pp263-289, 2000.

Wiesenfeld K. and Moss F., Stochastic resonance and the benefits of noise, Nature, 373, pp33-36, 1995.

Williamson R. E., Introduction to differential equations and dynamical systems, McGraw-Hill, International Edition, 1997.

Wilson H. R., Levi D., Maffei L., Rovame J. and DeValois R., The perception of form, retina to striate cortex, Visual Perception: The Neurophysiological Foundation, pp231-272, 1990.

Windsor C., Recalling memories, Phys. Bulletin, 39, pp16-18 1988.

Young J., A Model of the Brain, Clarendon Press, Oxford, 1961.

Young, J.Z. Programs of the Brain, Chapter 12, Oxford University Press, pp117-131, 1978.

Zeki Z. and Shipp S., The functional logic of cortical connections, Nature, 835, pp311-317, 1988.

Zeki Zemir, A Vision of the Brain, Blackwell Scientific Publications, Oxford, 1993.

Zhou X. and Gordon R., Detection of early breast cancer: an overview and future prospects, Biomedical Engineering, Critical Review, 17, (3), pp203-255, 1989.

Zimmerman M., The somatovisceral sensory system, Chapter 9, Human Physiology, Springer-Verlag, 1987.